Draft version March 1, 2022
Typeset using LaTeX **twocolumn** style in AASTeX631

Transit Hunt for Young and Maturing Exoplanets (THYME) VIII: a Pleiades-age association harboring two transiting planetary systems from *Kepler*

Madyson G. Barber,[1,*] Andrew W. Mann,[1] Jonathan L. Bush,[1] Benjamin M. Tofflemire,[2,†] Adam L. Kraus,[2] Daniel M. Krolikowski,[2] Andrew Vanderburg,[3] Matthew J. Fields,[1] Elisabeth R. Newton,[4] Dylan A. Owens,[5,1] and Pa Chia Thao[1,‡]

[1] *Department of Physics and Astronomy, The University of North Carolina at Chapel Hill, Chapel Hill, NC 27599, USA*
[2] *Department of Astronomy, The University of Texas at Austin, Austin, TX 78712, USA*
[3] *Department of Physics and Kavli Institute for Astrophysics and Space Research, Massachusetts Institute of Technology, Cambridge, MA 02139, USA*
[4] *Department of Physics and Astronomy, Dartmouth College, Hanover, NH 03755, USA*
[5] *Gemini Observatory, NSF's NOIRLab, 670 N. A'ohoku Place Hilo, Hawaii, 96720, USA*

ABSTRACT

Young planets provide a window into the early stages and evolution of planetary systems. Ideal planets for such research are in coeval associations, where the parent population can precisely determine their ages. We describe a young association (MELANGE-3) in the *Kepler* field, which harbors two transiting planetary systems (KOI-3876 and Kepler-970). We identify MELANGE-3 by searching for kinematic and spatial overdensities around *Kepler* planet hosts with high levels of lithium. To determine the age and membership of MELANGE-3, we combine new high-resolution spectra with archival light curves, velocities, and astrometry of stars near KOI-3876 spatially and kinematically. We use the resulting rotation sequence, lithium levels, and color-magnitude diagram of candidate members to confirm the presence of a coeval 105±10 Myr population. MELANGE-3 may be part of the recently identified Theia 316 stream. For the two exoplanet systems, we revise the stellar and planetary parameters, taking into account the newly-determined age. Fitting the 4.5 yr *Kepler* light curves, we find that KOI-3876 b is a $2.0 \pm 0.1 R_\oplus$ planet on a 19.58-day orbit, while Kepler-970 b is a $2.8 \pm 0.2 R_\oplus$ planet on a 16.73-day orbit. KOI-3876 was previously flagged as an eclipsing binary, which we rule out using radial velocities from APOGEE and statistically validate the signal as planetary in origin. Given its overlap with the *Kepler* field, MELANGE-3 is valuable for studies of spot evolution on year timescales, and both planets contribute to the growing work on transiting planets in young stellar associations.

Keywords: exoplanets, exoplanet evolution, young star clusters- moving clusters, planets and satellites: individual (KOI3876)

1. INTRODUCTION

Stellar clusters and associations serve as critical benchmarks for stellar and planetary astrophysics. Stars in such groups formed from the same interstellar cloud, and hence share a common (or similar) age, abundance pattern, and formation environment. The commonality makes it significantly easier to assign properties to the whole population, providing age estimates that are more precise and accurate than when the same techniques are used outside clusters (e.g., Gyrochronology; Barnes 2007; van Saders et al. 2016) and which can be applied to stars where ages are especially challenging to determine (e.g., M dwarfs; Kiman et al. 2021). Such coeval associations are therefore ideal for studying how stellar and planetary properties evolve with time (e.g., Krumholz et al. 2019; Bouma et al. 2019; Newton et al. 2021).

Corresponding author: Madyson G. Barber
madysonb@live.unc.edu

* UNC Chancellor's Science Scholar
† 51 Pegasi b Fellow
‡ NSF Graduate Research Fellow
Jack Kent Cooke Foundation Graduate Scholar

Associations within the *Kepler* field have been especially valuable for stellar and planetary astrophysics. The 4.5 yr baseline, and exquisite photometry enable precise measurements of rotation periods, even at older ages (e.g., Angus et al. 2015; Aigrain et al. 2015), providing some of the best constraints on the rotation evolution of stars past 1 Gyr (Meibom et al. 2011; Curtis et al. 2019). The four *Kepler* clusters (NGC 6866, NGC 6811, NGC 6819, and NGC 6791) have also provided a wealth of information about stellar mass-loss (Miglio et al. 2012), post-main-sequence stellar evolution (Corsaro et al. 2012), and the occurrence of planets inside clusters (Meibom et al. 2013).

The four original clusters in the *Kepler* field are all at distances of more than 1 kpc and ages $\gtrsim$500 Myr (Batalha et al. 2010). While these older ages (compared to nearby young groups) fill an important niche in stellar spin down and post-main-sequence evolution, their distance from the Sun makes it challenging to study the low-mass members and search for small planets in the clusters.

The *K*2 and *TESS* mission covered many younger and more nearby clusters and star-forming regions (Ricker et al. 2014; Van Cleve et al. 2016). This lead to a wide range of surveys on stellar rotation (e.g., Rebull et al. 2017; Douglas et al. 2019), eclipsing binaries (e.g., Kraus et al. 2015; David et al. 2019a), and planetary systems (e.g., Gaidos et al. 2017; David et al. 2019b). The latter included two major surveys, Zodiacal Exoplanets in Time (ZEIT; Mann et al. 2016a) focusing on planets in clusters observed with *K*2, and the *TESS* Hunt for Young and Maturing Exoplanets (THYME; Newton et al. 2019), focusing on similarly young stars observed with *TESS*. Such surveys have dramatically increased the number of known planets in young associations. However, the reliance on *K*2 and *TESS* data meant the overwhelming majority of stars had only 27 or 80 days of monitoring, limiting the precision and orbital period window. Associations in the *Kepler* prime field would have the full $\simeq$4.5 yr baseline.

The availability of precise parallaxes and proper motions for millions of stars from *Gaia* (Gaia Collaboration et al. 2016, 2021) has enabled the discovery of new coeval stellar associations (e.g., Meingast et al. 2019; Kerr et al. 2021), including the 40 Myr δ Lyr cluster that overlaps with the *Kepler* field (Bouma et al. 2021). The `FriendFinder` code[1] (Tofflemire et al. 2021) was designed to take advantage of *Gaia* data, by searching for potential co-moving 'friends' around a user-identified young star. This method has already been useful in finding the 250 Myr MELANGE-1 (Tofflemire et al. 2021) and MELANGE-2 (Newton et al., submitted) associations, and age-dating a planet in the Musca region of Lower-Centaurus-Crux (Mann et al. 2021).

To find undiscovered associations with transiting planets, we ran `FriendFinder` on *Kepler* Objects of Interest (KOI) with lithium levels indicating an age younger than Hyades (Berger et al. 2018). The most promising association was a group of stars nearby KOI-3876: the candidate members showed a color-magnitude diagram (CMD) and lithium levels consistent with the Pleiades.

Here, we demonstrate that MELANGE-3 is a coeval, 105 Myr-old group, 300 pc from the Sun, that harbors two transiting planetary systems (KOI-3876 b and Kepler-970 b). In Section 2, we detail our initial selection of potential members of MELANGE-3. We describe the range of archival and new data taken for candidate members of MELANGE-3 in Section 3. In Section 4, we show that MELANGE-3 is a coeval population and derive its overall properties and basic membership. Our effort to recover known and find new planets in MELANGE-3 is described in Section 5. This includes the identification of another member with a confirmed planet (Kepler-970). We describe the parameters of KOI-3876 and Kepler-970 in Section 6, and we derive the properties of the two identified planets in the association, KOI-3876 b and Kepler-970 b, in Section 7. The latter signal is already confirmed, and we statistically validate the former as planetary in Section 7.1. We summarize our findings in Section 8 and briefly discuss the future utility of an association overlapping the *Kepler* field.

2. TARGET SELECTION

To identify known planets in previously undiscovered young associations, we ran the `FriendFinder` code (Tofflemire et al. 2021) on KOIs that appear to be young based on their lithium absorption as reported by Berger et al. (2018); this initial seed list included KOI-3876. The `FriendFinder` algorithm used *Gaia* EDR3 positions, parallaxes, and proper motions to identify stars with similar (reprojected) sky-plane tangential velocity and XYZ position to a selected input source. This required an absolute radial velocity for KOI-3876, for which we used the value from APOGEE ($v_{\rm rad} = -26.79$km s^{-1}; Jönsson et al. 2020).

The lithium absorption levels suggested an age for KOI-3876 close to the Pleiades (Bouvier et al. 2018). Unbound or weakly bound associations >100 Myr should have been significantly dispersed as they orbit through the Galaxy (Krumholz et al. 2019), so we used

[1] https://github.com/adamkraus/Comove

a generous selection. We included any star with a parallax uncertainty $\sigma_{plx} < 0.5$ mas, a tangential velocity $v_{\tan} < 5$km s^{-1} from KOI-3876 and a physical separation S < 50 pc from KOI-3876. This yielded 1007 candidates.

Our selection assumed the group is circular and centered around KOI-3876, neither of which is likely to be true. However, our aim was not to make a perfectly clean list or a complete list of members. Rather, we aim to select a generous list that contains enough members to derive an age for the planet hosts. If the population extends beyond the edge of our search region, a future census can aim for greater spatial completeness.

The spread of the candidate member color-magnitude diagram (CMD) indicated significant contamination from field stars (Figure 1). However, the CMD also harbors a sequence of the closest stars (in tangential velocity) consistent with the Pleiades single-star sequence, matching the age suggested by the Li levels in the spectrum of KOI-3876.

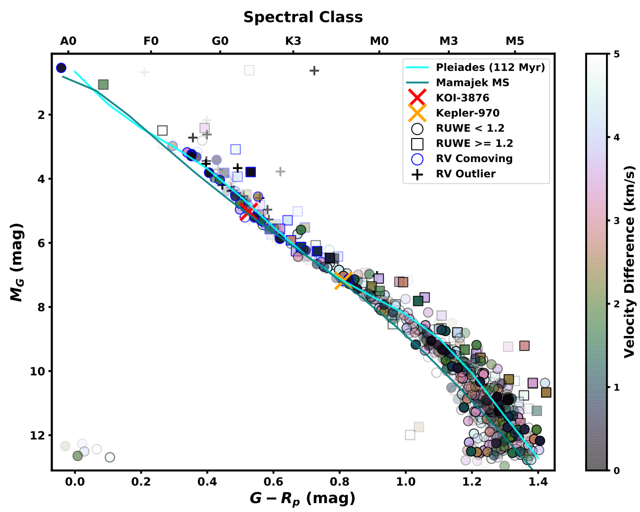

Figure 1. *Gaia* color-magnitude diagram of all stars within 5 km s^{-1} in tangential velocity and 50 pc of KOI-3876, excluding those with high contaminated photometry (Riello et al. 2021). Points are color-coded by the difference between their expected and observed tangential velocity assuming a perfect *UVW* match to KOI-3876 and assigned transparency based on their three-dimensional distance from KOI-3876. Stars with radial velocities consistent with KOI-3876 are marked with blue circles and those with discrepant velocities are changed to plus signs (and excluded from the color-coding). Approximate main- and Pleiades- single-star sequences are shown as colored lines (Pecaut & Mamajek 2013; Lodieu et al. 2019).

3. OBSERVATIONS

3.1. *Optical spectra from McDonald 2.7 m Coudé*

We observed KOI-3876 and 22 association candidates (Section 2) with the Coudé spectrograph on the Harlan J. Smith 2.7m telescope at the McDonald Observatory. The Robert G. Tull Coudé is a cross-dispersed echelle spectrograph, delivering a $R \sim 60,000$ spectral resolution from 3400–10000 Å using the 1.″2 slit (Tull et al. 1995). Observations were taken over three nights from two observing runs, on 2021 July 9 and 2021 August 26 and 27.

The sample was selected to include association candidates that could be observed with the Coudé in modest exposure times ($G < 13$), and spectral types later than mid-F ($B_p - R_P > 0.55$), where we expect lithium absorption to be a sensitive age diagnostic.

We reduced all spectra with a custom python implementation of the standard IRAF procedures. Wavelength calibration made use of ThAr lamp spectra taken at the beginning, middle, and end of each night. The signal-to-noise of our spectra ranged between 14 and 60 per resolution element.

To assess whether association candidates are comoving in three dimensions, we measure radial velocities using spectral-line broadening functions (BFs). The BF is a linear inversion of an observed spectrum with a narrow-lined template and represents the average stellar absorption-line profile. This profile (the BF) can be fitted with a rotationally-broadened line profile to measure the stellar radial velocity and $v \sin i_*$. We compute BFs for 34 spectral orders between 4300 and 9800 Å that is free of telluric contamination using the `saphires` python package (Tofflemire et al. 2019). BFs from individual orders are combined into a single, high SNR BF and fit with a rotationally broadened profile (Gray 1992). Narrow-lined templates, specific to each star, are taken from the Husser et al. (2013) PHOENIX model suite at the $T_{\rm eff}$ closest to that provided by the *TESS* Input Catalog (v8.0; Stassun et al. 2019). Radial-velocity errors depend on the S/N and rotational broadening but are generally on the order of 0.1 km s^{-1}. Measurements from the Coudé spectra are provided in Table 5.

3.2. *Archival Velocities*

In order of preference, we drew radial velocities for candidate MELANGE-3 members from the second *Gaia* data release (DR2; Katz et al. 2019), the sixteenth APOGEE data release (DR16; Jönsson et al. 2020), and the fifth LAMOST data release (DR5; Luo et al. 2015, 2019). Velocities from our spectra (Section 3.1) were given the highest priority. In the instance where a star had multiple velocities from the same source, we used the weighted mean and error. We did not combine multiple velocities from different sources. We applied an offset to the LAMOST velocities of $+4.54$ km s^{-1} based on the comparison from Anguiano et al. (2018). There may be additional zero-point differences between the velocity sources, but these are likely smaller than the internal velocity spread within the group.

In total, we adopted *Gaia* RVs for 56 stars, APOGEE RVs for 5 stars, and LAMOST RVs for 25 stars. This was in addition to velocities from our Coude spectra for 22 candidate member stars and KOI-3876. The adopted velocities are given in Table 5.

3.3. *Kepler and TESS light curves*

3.3.1. *Light curves for transit search and characterization*

We searched for *Kepler* photometry for all 1007 candidates within the Mikulski Archive for Space Telescopes (MAST). A total of 84 targets had *Kepler* data, the majority of which had data from all quarters (Q0-Q17). We restricted our analysis to long-cadence data (30 m), as short-cadence was not available for any of the candidate planet hosts and short cadence data is not needed for our transit search or rotation estimates.

Where available, we used the Pre-search Data Conditioning Simple Aperture Photometry (PDCSAP; Stumpe et al. 2012; Smith et al. 2012). This included KOI-3876 in both *Kepler* and *TESS* data, all candidate members with *Kepler* light curves, and the 15 targets with 2-minute cadence photometry from *TESS*. For the 41 with 30-minute cadence TESS data, we used the Quick-Look Pipeline light curves (Huang et al. 2020) for our planet search. Table 5 lists which stars have *Kepler* and/or *TESS* photometry that was used for our planet search. More details on our transit search can be found in Section 5.

The remaining 885 sources had no pre-extracted *TESS* or *Kepler* light curves. We did not extract additional curves from the full-frame *TESS* images for our planet search or characterization. The association is more than 300 pc away; most of the remaining stars were too faint (QLP limit of $T < 13.5$ Huang et al. 2020), to extract a light curve precise enough for our planet search. However, many such systems are still useful for measuring rotation periods, as we discuss in the next section.

3.3.2. *Stellar rotation periods*

To assess the membership and age of the candidate association we collected stellar rotation periods from the literature, which we supplemented with our measurements from *Kepler* and *TESS* light curves. First, candidate members were cross-matched against Nielsen et al. (2013), McQuillan et al. (2013, 2014), and Santos et al. (2019, 2021) to identify literature rotation periods. We matched candidate members to the *Kepler* Input Catalog (KIC; Brown et al. 2011) using the `astroquery` package, selecting the KIC match by smallest on-sky separation. If a KIC ID was not returned from this search, we manually identified KIC IDs using the *Kepler* Target Search portal. We identified 56 candidate members with available literature rotations, all but five of which have rotation measurements in multiple catalogs. For candidates that appear in only one catalog, we adopt the single measurement value. In cases where a star had measurements from more than one source, we adopt the average of the measurements as the rotation period. Only one object, KIC 3743810, had a conflicting rotation period between catalog sources. Based on a visual examination of this object's *Kepler* PDCSAP light curve, we selected the value from Nielsen et al. (2013).

For stars without literature rotation periods, we performed our analysis on *Kepler* and *TESS* data. Priority was given to *Kepler* PDCSAP data followed by *TESS* full-frame images (FFI). For each star with available *Kepler* data, we searched each single-quarter *Kepler* light curve for rotation periods between $0.1 - 50$ days using the Lomb-Scargle algorithm (Horne & Baliunas 1986). We selected the initial rotation from the quarter returning the rotation period with the highest periodogram power. To confirm these measurements, we phase-folded the single-quarter light curves to the candidate period and examined the signals' consistency across quarters. We performed an eye-check in the style of Rampalli et al. (2021), labeling obvious rotations as Q0, questionable rotations as Q1, spurious detections as Q2, and non-detections as Q3. In total, we identified usable rotations of quality Q0 or Q1 in 11 out of 15 of the stars with *Kepler* data and no literature rotation period. As a check, we also ran a handful of stars with literature rotation periods, and found agreement to be excellent in all cases.

For the rest of the 933 candidates without rotations found in the literature or through our *Kepler* light curve measurements, we searched for signatures of rotation in CPM light curves extracted from the *TESS* Full Frame Image data. We did not use the QLP curves, as we found they did not preserve the stellar rotation signal reliably. Instead, we generated *TESS* light curves from the FFI cutouts. We first created raw flux light curves from the FFI cutouts centered on each candidate. Then, we generated a Causal Pixel Model (CPM) of the telescope systematics using the `unpopular` package (Hattori et al. 2021) for each individual star. We subtracted the CPM systematics from the initial light curves. For 26 targets, we failed to extract a usable CPM curve;

8 because of no clear matching TIC ID and 18 because the CPM extraction process failed. After searching each single-sector light curve of each star for rotation periods from 0.1 − 30 days using the Lomb-Scargle algorithm, we repeated the same rotation selection and quality check procedure as outlined for the *Kepler* data. We found 64 quality Q0 or Q1 rotations from the 907 *TESS* CPM-subtracted light curves available.

In total, we were able to assign rotation periods to 131 candidate members, all of which are reported in Table 5; 67 periods were determined based on *Kepler* data, 11 newly calculated and 56 from literature, and 64 were calculated from *TESS* data.

Based on variations in the extracted rotation period between *TESS* sectors and/or *Kepler* quarters, we estimate rotation period errors to be ≃10% for our measurements. This is larger than the expected errors just considering signal-to-noise and Lomb-Scargle errors from bootstrapping, likely due to differential rotation and spots appearing and disappearing on the surface of the star (Rampalli et al. 2021).

3.4. *Archival photometry and astrometry*

We download positions, parallaxes, proper motions, and B_P, R_P and G photometry for all candidate members of MELANGE-3 using the third *Gaia* Early Data Release (EDR3; Gaia Collaboration et al. 2021). For KOI-3876 and Kepler-970 (see Section 5), we also retrieved photometry from the Two-Micron All-Sky Survey (2MASS; Skrutskie et al. 2006), the Wide-field Infrared Survey Explorer (WISE; Cutri & et al. 2014), and the AAVSO All-Sky Photometric Survey (APASS; Henden et al. 2016). Photometry for KOI-3876 and Kepler-970 are listed in Table 3.

4. THE MELANGE-3 ASSOCIATION

Our goal for the rest of this section is to demonstrate that the friends of KOI-3876 represent a coeval population and to determine the age and kinematic properties of the association. We refer to this group as MELANGE-3 (Membership and Evolution by Leveraging Adjacent Neighbors in a Genuine Ensemble), following the naming convention in Tofflemire et al. (2021), although it is likely that MELANGE-3 is a component of the larger Theia 316 string (see Section 4.7).

As we detail below, we found that MELANGE-3 members closely match those of the Pleiades in Lithium equivalent widths (Section 4.2), rotation (Section 4.3), and CMD. We combined these to estimate that MELANGE-3 is 105 ± 10 Myr. From a subset of high-probability members, we derived the Galactic position (XYZ) and kinematic (UVW) parameters (Section 4.5).

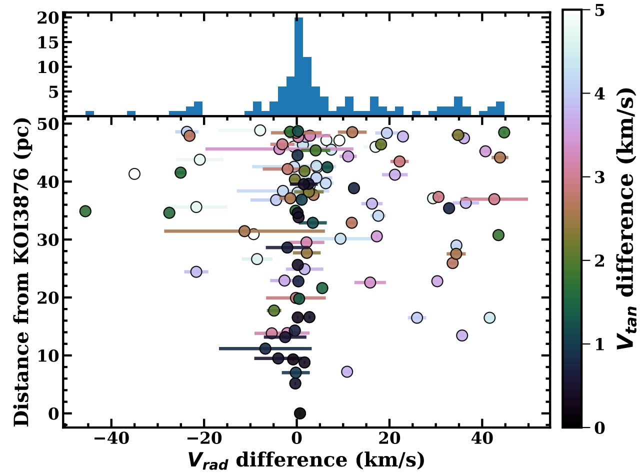

Figure 2. Distance from KOI-3876 as a function of the difference between the observed and predicted radial velocity of candidate members of MELANGE-3, color-coded by the tangential velocity offset from KOI-3876. The top panel shows a histogram of the radial velocity difference. The predicted velocities were calculated assuming each candidate has an identical UVW to KOI-3876. We do not expect all true members to be exactly consistent with zero velocity difference: KOI-3876 is not necessarily at the kinematic center of the group, the group has some intrinsic velocity spread, and some stars may be tight binaries. The over-density of points near-zero velocity difference is strong evidence that the association is real and extends to at least to 50 pc from KOI-3876.

Using stellar rotation periods and radial velocities, we estimated that 50-60% of the original MELANGE-3 candidate list are real members (Section 4.6).

4.1. *Radial Velocities*

`FriendFinder` generated a predicted radial velocity for each candidate member under the assumption that every member star has an identical UVW to KOI-3876 (i.e., re-projecting the UVW of KOI-3876 to the position of each star). Since radial velocities were not used in the target selection (only XYZ and tangential velocities), the difference between the predicted and measured velocities can be used to test if the stars are truly comoving. We show this comparison for candidate members of MELANGE-3 in Figure 2, taking into consideration the three-dimensional and tangential velocity offsets.

The radial velocities of candidate members are heavily clustered within ≃ 2 km s^{-1} of the predicted values. The over-density is also highest for stars closer to KOI-3876 in tangential velocity and position. Based on the Besançon Galactic model (Czekaj et al. 2014), typical thin disk stars with similar XYZ to KOI-3876 will have a velocity spread of ≃ 40km s^{-1} and centered more than 30km s^{-1} from the locus seen in Figure 2. Thus, the probability of such a buildup by chance is negligibly small. Interestingly, there is still an overdensity of stars with consistent radial velocities even 50 pc from KOI-3876. This suggests that the true population is much larger.

The distribution in Figure 2 also highlights a challenge: there is a large population of stars with radial velocities well outside the central locus. Such contaminants include stars near KOI-3876 and Kepler-970 in position and tangential velocity. Further, the overdensity in velocity space is not necessarily coeval; overdensities in kinematic space can occur for other reasons, such as dynamical perturbations from the Galactic bar (Bovy & Hogg 2010).

4.2. *Lithium*

Lithium is quickly burned in the cores of stars. As a result, surface lithium is slowly depleted over time in low-mass stars, yielding a mass-dependent lithium sequence that shifts with age (e.g., Jeffries et al. 2017; Cummings et al. 2017). We can therefore confirm that MELANGE-3 is a coeval population and estimate its age by comparing the lithium levels as a function of color to measurements from other known clusters.

We estimated the equivalent width (EW) of the Li 6708 Å line for 23 stars (including KOI-3876) using the Coude spectra described in Section 3.1. Using our measured radial and rotation velocities from the BF analysis, we shifted each spectrum to zero velocity and compared it to a rotationally broadened template of the same $T_{\rm eff}$. We then interactively defined regions of continuum between 6685 and 6730 Å, and the bounds of the EW integration. We measured the EW[Li] and its uncertainty using a bootstrap approach. The continuum was first fit using `emcee`. After completion, 1000 random draws from the fit posterior were used to normalize the spectrum; for each realization, the Li absorption line was numerically integrated 10 times where the integration bounds were varied randomly from a normal distribution with the width of a resolution element. This procedure resulted in 10,000 EW[Li] measurements, and we took the median and standard deviation as our final measurement and its uncertainty, respectively.

Past detections of Li with the same observational setup and our typical spectrum SNR indicate we were sensitive to Li down to equivalent widths of 20mÅ or better, so we report this as our upper limit when no line is detected. One star (Gaia EDR3 2052858307226740352) had a $v \sin i_* >$ 50km s^{-1}, which made the extraction of the Li line unreliable. So, we instead reported a $<$ 70mÅ upper limit for this source

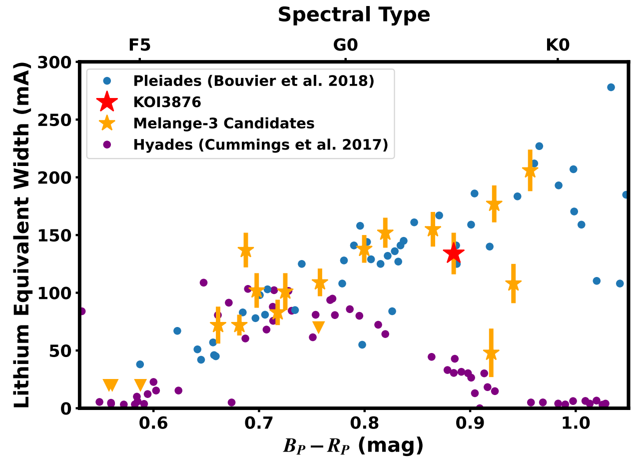

Figure 3. Lithium equivalent width as a function of *Gaia* $B_P - R_P$ color for candidate friends of KOI-3876 (MELANGE-3; orange), KOI-3876 (red), and members of the 125 Myr Pleiades from Bouvier et al. (2018) and ≃700 Myr Hyades (Cummings et al. 2017). Triangles indicate upper limits. We have excluded MELANGE-3 candidates with velocities inconsistent with membership (as defined in Section 4.6). The MELANGE-3 sequence is consistent with that from Pleiades members; only one star has an anomalously low Li (Gaia EDR3 2044150037698600448) compared to the Pleiades sequence. The high levels of Lithium seen in the mid-G dwarfs alone demonstrate that MELANGE-3 is much younger than Hyades. Kepler-970 has weak lithium (EqW$<$ 40mÅ), but at $B_P - R_P = 1.5$, we expect it to be depleted at this age; we left it off the edge of the figure.

based on earlier detections on similarly broadened spectra.

For KOI-3876, we estimated a EW[Li]$= 134 \pm 18$mÅ. This is marginally higher than (but consistent with) the value from Berger et al. (2018) (EW[Li]$= 120 \pm 7$mÅ). We attribute this difference to Berger et al. (2018)'s removal of the Fe line at 6707.44Å. We did not attempt to correct for this contamination or from broad molecular contamination in the cooler stars. Fe line contamination sets a (systematic) limit on the precision of our equivalent widths at the ≃10% level, comparable to the measurement errors. The difference was small compared to the offset in Li levels between clusters. We used our Li measurements for all targets for consistency.

Two spectra (Gaia EDR3 2101333021814076800 and 2048317736525727488) had two clear sets of lines, indicating double-lined spectroscopic binaries (SB2s). For our Li measurements, we measured each line individually with a manually-applied velocity offset and combined the two equivalent widths.

In Figure 3, we compared the Li sequence for MELANGE-3 to that from the ≃112 Myr Pleiades (Bouvier et al. 2018) and the 650-700 Myr Hyades (Cummings et al. 2017). The MELANGE-3 sequence is nearly identical to that from the Pleiades. The Li sequences of nearby clusters from `BAFFLES` (Stanford-Moore et al. 2020) suggested an age between 85 Myr and 200 Myr This age range is conservative, as the bounds can only be set using the set of clusters with ages and extant lithium sequence measurements.

4.3. *Rotation*

We used the rotation periods from Section 3.3.2 to better assess the age and membership of MELANGE-3. Coeval members should follow a rotation sequence in color (a gyrochrone; Barnes 2003, 2007), which we show in Figure 4. The distribution is consistent with that from the Pleiades, further validating the Li-based age.

To determine the number of stars with rotation periods consistent with the Pleiades, we used a three-step cut. The first cut required stars with a $Bp - Rp < 0.7$ to have a rotation period $\leq$ 3 days. The second cut required stars with $0.7 \leq Bp - Rp < 1.0$ to have a rotation period $\leq$ 7.5 days. The third cut required stars with $Bp - Rp \geq 1.0$ to have a rotation period $\leq$ 10 days. We note that these cuts are somewhat qualitative but designed to capture $> 95\%$ of the Pleiades rotators (see Figure 4) and remove most field stars. These cuts yielded 92 stars consistent with the Pleiades rotation sequence. Most of the slower rotators are likely to be field interlopers, as they are (statistically) further from KOI-3876 in both three-dimensional distance and tangential velocity. MELANGE-3 stars rotating faster than the Plieades slow rotator sequence are considered association members, as the Pleiades contains fast rotators and many of the fast rotators may be binary members (Rebull et al. 2016a; Douglas et al. 2019).

Of 1007 initial candidates, finding Pleiades-like rotation periods for just 92 stars initially appeared to be an unexpectedly low success rate. However, for the overwhelming majority of the 876 stars with a light curve but no rotation period, no period could have been measured even if one was present (mostly due to intrinsic faintness). For example, of the 925 stars with a matching TIC ID, but no rotation period from *Kepler* data, 751 were either too faint ($T \gtrsim 15$) or too contaminated by nearby stars to extract a usable CPM curve. Thus, the difference is mostly due to how much deeper *Gaia* can retrieve precise astrometry for stars far fainter than for which *TESS* can provide rotation periods.

4.4. *Isochronal age*

We estimated the age of MELANGE-3 by comparing the CMD to the PARSEC (v1.2S) models (Bressan et al. 2012). We used a mixture model, as detailed in Mann et al. (2021)[2], based on the method outlined in Hogg et al. (2010), and wrapped in the `emcee` Markov-Chain Monte-Carlo sampling algorithm (Foreman-Mackey et al. 2013). To briefly summarize, we fit the population with the combination of two models. The first described the single-star member sequence drawn from PARSEC models. The second is an outlier population, which may contain a mix of populations (e.g., binaries, field interlopers, and stars with erroneous parallaxes or photometry). The fit included six free parameters: the association age (τ), the average reddening across the association ($E(B-V)$), the amplitude of the outlier population (P_B), the offset of the outlier population from the main population CMD (Y_B [mags]), the variance of the outliers around the mean (V_B [mags]), and a term to capture missing uncertainties or differential reddening across the association (f [mags]).

Reddening was limited to < 0.2 mag based on the three-dimensional extinction map from Green et al. (2019). All other parameters evolved under uniform priors, bounded only by physical limits. To ensure uniform sampling in age, we re-sampled the model grid in equal steps around the expected age (50-300 Myr). Using the raw grid did not significantly change the results.

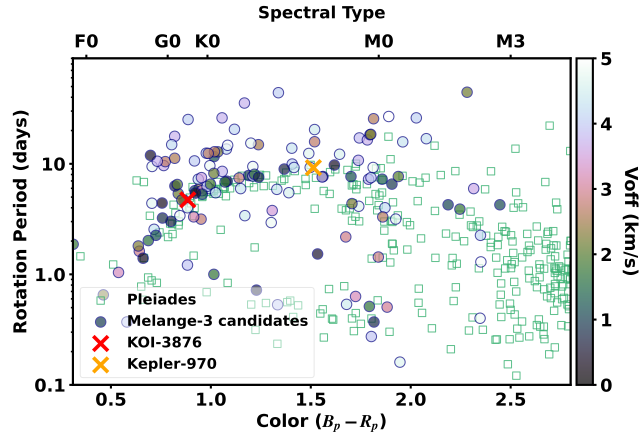

Figure 4. Rotation periods of candidate members of MELANGE-3 (dark circles) as a function of *Gaia* $B_P - R_P$ color. Only stars with literature measurements or Q0 or Q1 rotations are shown. For reference, we show rotation periods from $\simeq$110 Myr Pleiades (green squares; Rebull et al. 2016b). Stars are color-coded by their tangential velocity difference compared to KOI-3876. The stars on the Pleiades gyrochrone are also generally closer to KOI-3876 in tangential velocity. Because of the distance to the cluster, we have few rotation periods past M1.

[2] https://github.com/awmann/mixtureages

Gaia photometry was available for all candidate members and was generally far more precise than other available photometry. Many stars were also resolved as binaries (or the target and a background star) in *Gaia*, but seen as a single source in 2MASS and KIC photometry (Brown et al. 2011). We therefore restricted our analysis to *Gaia* magnitudes.

While the mixture model can handle high contamination rates by making P_B larger, tests suggest that when $P_B \gtrsim 0.4$, the model often calls stars in the main population outliers, instead of fitting the background population as the true one (yielding a field age). As we show in Section 4.6, the background contamination rate is likely $\gtrsim 0.4$. Further, for the isochrone analysis, there will be additional true members that should be treated as outliers due to binarity, poor photometry, or poor parallaxes. As a result, in addition to limiting the sources to objects within the colors and magnitudes bounded by the model grid, we applied the following restrictions to the input data:

- a renormalised Unit Weight Error (RUWE; Gaia Collaboration et al. 2021) < 1.3,
- $1.0+0.015(B_P-R_P)^2 <$ `phot_bp_rp_excess_factor` $< 1.3 + 0.06 * (B_P - R_P)^2$,
- physical separation within 40 pc of KOI-3876,
- tangential velocity within 4 km s^{-1} of KOI-3876, and
- a radial velocity within 3σ of the group or no radial velocity.

These cuts were designed to mitigate, but not completely remove, issues of binarity, data quality, non-member interlopers, as well as limitations of the models. The mixture model approach means they do not need to completely remove bad data or non-members. Taken individually, none of these had a significant impact on the derived age except the `phot_bp_rp_excess_factor` criteria. Stars with flux contamination tended to have CMD positions far *below* the main-sequence, likely due to poor or non-detections in B_P reported as detections near the limits. After all cuts were made, we were left with 205 stars.

As we show in Figure 5, the resulting fit yielded an age of 106^{+7}_{-6} Myr. As a test of the systematic errors, we ran the same fit using models from the Dartmouth Stellar Evolution Program (DSEP, Dotter et al. 2008). Using the DSEP models with magnetic enhancement described in Feiden & Chaboyer (2012) gave a similar age of 101±7 Myr. DSEP models without magnetic enhancement gave a younger age of 96±10 Myr, although

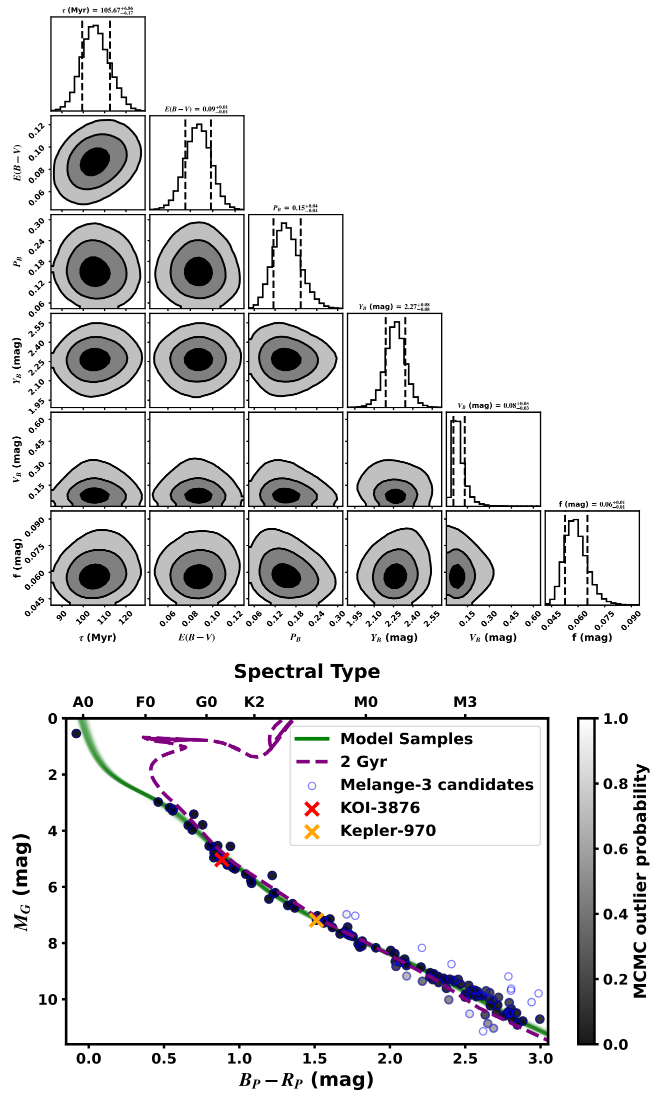

Figure 5. Comparison of the PARSEC model isochrones to candidate members of MELANGE-3. The top shows the corner plot of our MCMC mixture model comparison, with contours corresponding to 1σ, 2σ, and 3σ. The bottom plot shows the *Gaia* G versus $B_P - R_P$ CMD of stars included in the MCMC (blue circles). Each point is shaded based on its average outlier probability as determined by the relative strength of the two mixture components. Most of those flagged as outliers are likely to be non-members or binaries that evaded our selection cuts. KOI-3876 and Kepler-970 are shown as red and orange stars. Both have low ($< 1\%$) outlier probabilities. The green lines are 200 PARSEC isochrones with parameters drawn (randomly) from the MCMC posterior. The purple dashed line indicates a 'field' (2 Gyr) population, highlighting that a lot of the age leverage comes from the pre-main-sequence mid-M dwarfs and the small number of AF stars.

Table 1. Properties of MELANGE-3

Parameter	Mean	σ
X (pc)	103	19
Y (pc)	289	18
Z (pc)	63	14
U (km s^{-1})	-9.2	1.4
V (km s^{-1})	-25.54	0.36
W (km s^{-1})	1.0	1.2

a poorer fit to the coolest stars in the sample. Using (PARSEC) non-Solar metallicity models changed the age at the 5 Myr level, but favoring older ages. All ages agree with each other at the 1-2σ level. These ages are also consistent with our measurements using lithium and stellar rotation (Sections 4.3 and 4.2), both of which indicated an age close to Pleiades ($\simeq$112 Myr; Dahm 2015).

4.5. *Galactic Position and Kinematics*

For each of the 1007 candidate members of MELANGE-3, we show the proper motion in Galactic coordinates (l, b) in Figure 6 and the Galactic XYZ position in Figure 7. While there is a clear overdensity of sources within $\simeq$1 km s^{-1} of KOI-3876, our initial selection of stars within $D < 50$ pc and $\Delta v_{tan} < 5$ km s^{-1} of KOI-3876 included a large number of field interlopers. A tighter cut on velocity and distance would lower contamination, but some sources far in separation have matching velocities and show other signs of youth (such as rotation). This made it challenging to derive the $UVWXYZ$ parameters of the association without further cuts on the full membership list.

We selected a set of high probability members independent of their *Gaia* parameters that were used for initial selection and focus on membership based on rotation periods and radial velocities. We included only sources with a rotation period consistent with the Pleiades sequence (as described in Section 4.6) and radial velocities within $\Delta v_{rad} < 8$ km s^{-1} of the source. We removed three additional targets that had low-precision velocities (from LAMOST). Unlike when fitting the isochrones, the low-mass stars offer no particular advantage.

The cuts left us with 31 high-probability members. From these, we estimate the Galactic position (XYZ) and velocity (UVW) of the association. We also calculated the intrinsic scatter in each parameter (σ_X, σ_Y, σ_Z, σ_U, σ_V, and σ_W) after accounting for measurement errors. The resulting parameters for MELANGE-3 are given in Table 1.

A more formal treatment would account for covariance between parameters and derive the full two-dimensional matrix (e.g., Gagné et al. 2018). However, the group may be part of a much larger stellar string, which would require a different model (Kounkel & Covey 2019; Gagné et al. 2021). We discuss this possibility in more detail in Section 4.7. Since we were primarily interested in characterizing the planets, we defer a more detailed analysis of MELANGE-3 and its relation to other groups for a future analysis focused on the association.

4.6. *Contamination Rate*

As discussed above, we expect many of our 1007 candidate members are field interlopers. We were able to make a more quantitative estimate of the contamination rate using our rotation and radial velocity measurements. These were particularly effective because neither metric was used in our initial sample selection (`FriendFinder` only used the velocity of KOI-3876).

We first estimated the contamination rate from the ratio of the number of stars with rotation periods consistent with the Pleiades sequence compared to the total number of stars *for which we could estimate a reliable rotation period.*

For the numerator, we used the Pleiades-like rotation cuts explained in Section 4.3. This yielded 92 stars we considered consistent with the Pleiades rotation sequence. The denominator is effectively the number of stars that would pass the above cut if every single star was a member. *Kepler* light curves were extracted to search for planets (Jenkins et al. 2010), which is generally a much smaller signal than the rotation signal of $\simeq$100 Myr stars. Thus, we assumed we could extract a rotation period for any member with a *Kepler* light curve. For *TESS*, we used the recovery fraction from the *TESS*-$K2$ overlap described in Bush et al. (in prep). The recovery rate is a strong function of magnitude, with almost no periods recovered past $T_{\rm mag} = 15$ and a 63% recovery rate for $14 < T_{\rm mag} < 15$ that increases down to the brightness limit. Based on this, we expect to measure 82 rotation periods out of the 907 stars with *TESS* data available. Combining with the 74 high-quality targets with *Kepler* data, we expect 156 stars to produce a rotation period.

Based on the rotation periods above, we estimated that 59% (92/156) of candidate members were true members. This estimate did not account for stars where the rotation periods were consistent with $\lesssim$100 Myr by chance. However, assuming field stars are uniformly distributed from 0–10 Gyr, the number of candidates matching by chance should have been $\lesssim$1. A more signif-

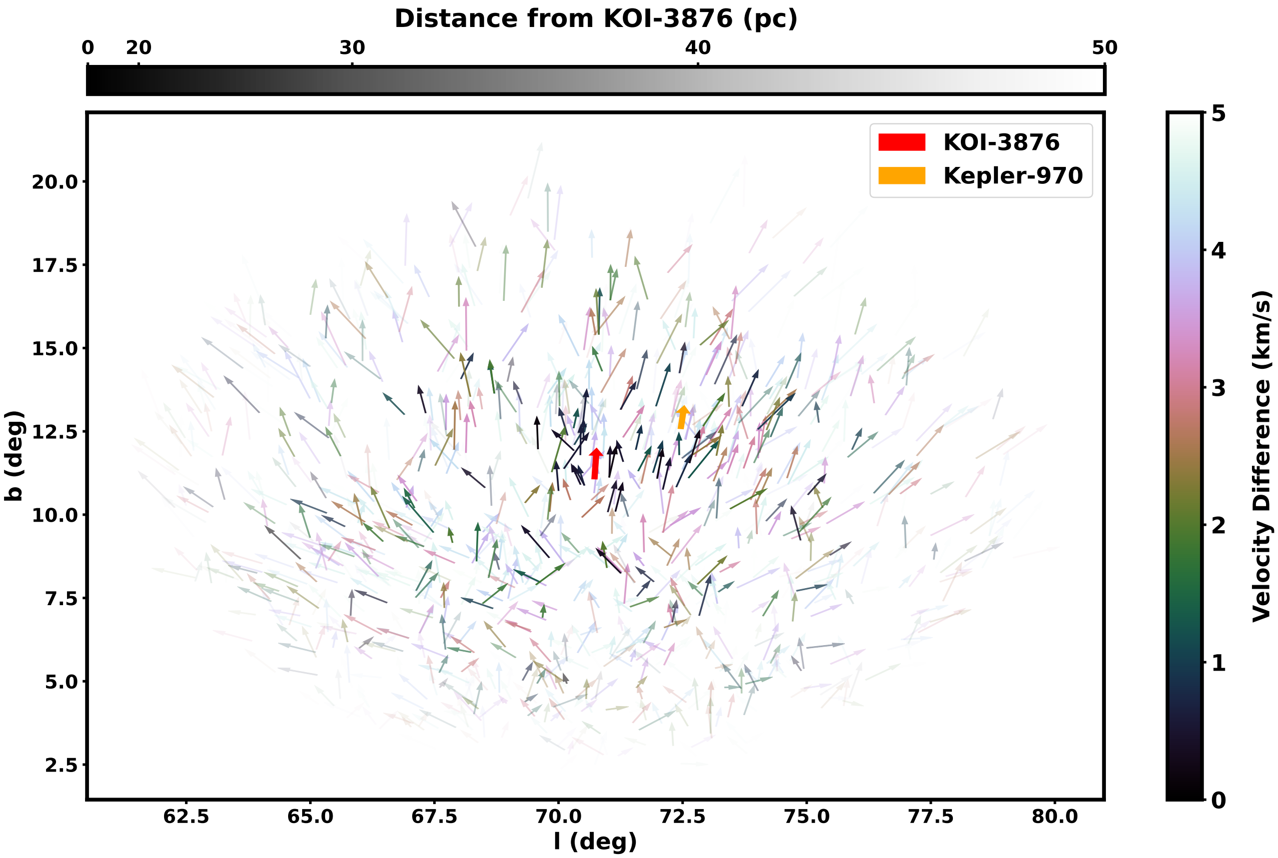

Figure 6. Galactic coordinates and motions for all 1007 candidate members of MELANGE-3. The red arrow shows KOI-3876, Kepler-970 is shown in orange, and other stars are color-coded by their tangential velocity offset from KOI-3876 with transparency set by their physical distance from KOI-3876. Arrows indicate the direction and (relative) magnitude of the proper motion.

icant problem would be tight binaries, where the inferred rotation periods would be fast due to tidal locking or the star spun down at a slower than normal rate due to the influence of the companion. We may also have missed a small number of stars due to low spot modulation, although past rotation period surveys in the Pleiades and Hyades suggest is $< 10\%$ of the sample (e.g., Rebull et al. 2016b; Douglas et al. 2017, 2019).

We performed a similar test using the radial velocities, asking what fraction of the stars are consistent with the association velocity in Table 1. Assuming an internal velocity dispersion of 0.5–1km s^{-1} (Table 1), 52%–57% of the candidate members with velocities are within 3σ of the expected radial velocity for membership. As with rotation periods, some number of these will overlap with the distribution by chance. But the semi-uniform distribution of velocities outside the main locus seen in Figure 2 suggests this number is $< 5\%$. We may miss a similar number of real members due to RV variation from binarity.

The two estimates are broadly consistent with each other given the uncertainties and complicating factors. We conclude 50-60% of the 1007 candidates in our list are real members of MELANGE-3.

4.7. *Connection to Theia 316*

Kounkel & Covey (2019) identified several young stellar associations from *Gaia* DR2 data. One such string, Theia 316, includes KOI-3876. Kounkel & Covey (2019), using a convolutional neural network in combination with traditional isochronal fittings, estimate an age for Theia 316 of 108 Myr. The overlap in members and similar age estimates suggested that MELANGE-3 is a component of the larger Theia 316 string.

As we show in Figure 7, the populations show significant overlap in XYZ space. Many stars in Theia 316 were missing from our list of MELANGE-3 candidates, the great majority of which were more than 50 pc from KOI-3876 (our `FriendFinder` adopted search radius). The density clustering method used in Kounkel & Covey (2019) had no restrictions on the physical size

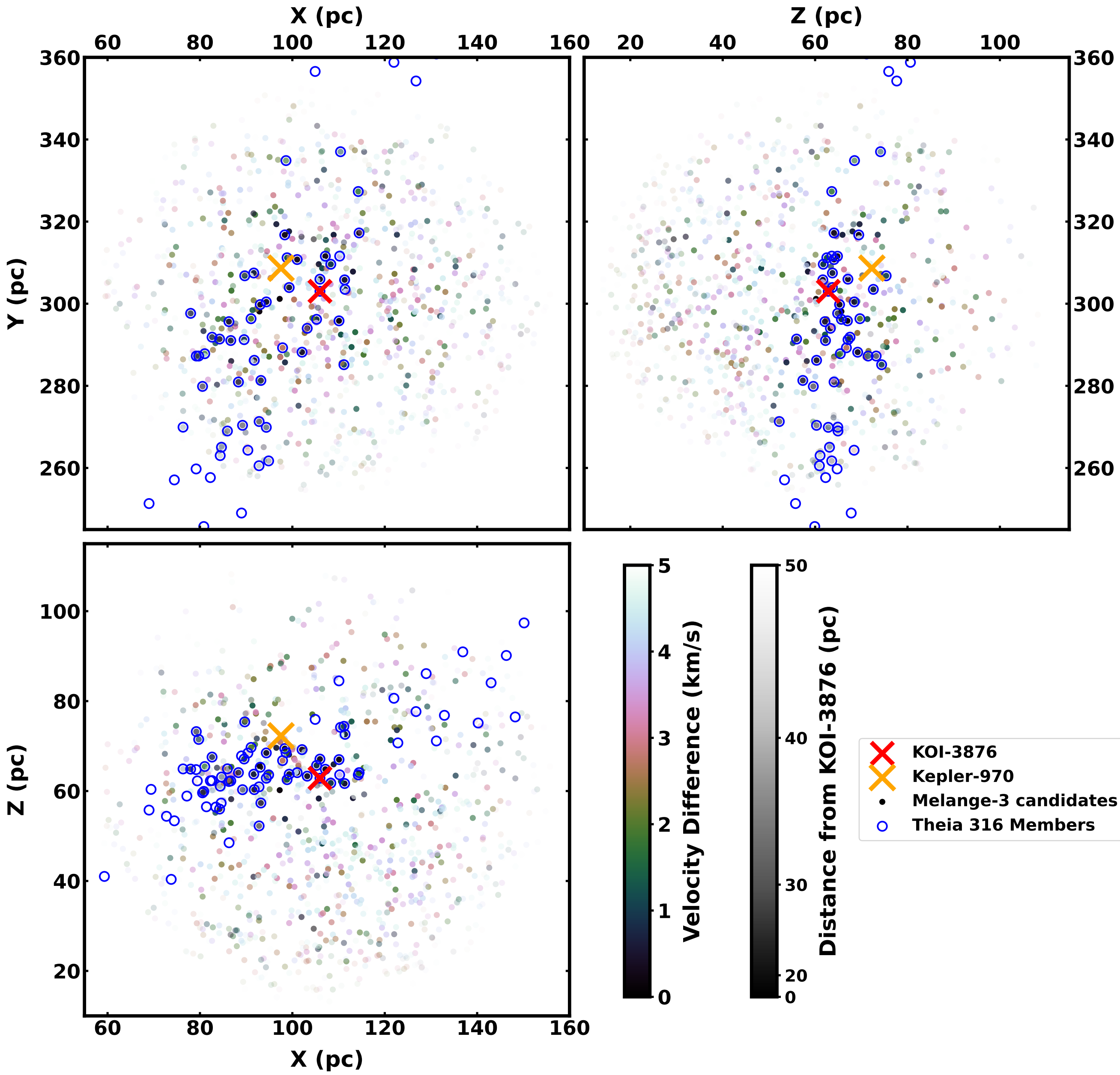

Figure 7. Galactic Heliocentric (XYZ) coordinates of stars within $D < 50\,\mathrm{pc}$ and $\Delta v_{tan} < 5\,\mathrm{km\ s^{-1}}$ of KOI-3876, color-coded by their velocity difference from KOI-3876 and transparency set by their 3D separation from KOI-3876. KOI-3876 is shown as a red X, Kepler-970 as an orange X, and members of Theia 316 from Kounkel & Covey (2019) as blue hollow circles. There is a high overlap between Theia 316 members and the cluster of MELANGE-3 candidates co-moving with and near KOI-3876. A majority of high-probability MELANGE-3 candidates are $\geq$10 pc from the Theia 316 string in low densities that would likely not trigger the clustering method used in Kounkel & Covey (2019).

of the group, as long as the number of sources in a given spatial and proper motion space is sufficiently dense. By contrast, `FriendFinder` was designed to help age-date a specific star, and hence identify targets within a given radius in kinematic and physical space. Increasing the search radius on `FriendFinder` would likely help us recover some of the missing stars, but also increase the contamination rate, likely not improving our ability to assign ages to the two planet hosts.

Similarly, many high-probability members of MELANGE-3 were missing from the Theia 316 list (including Kepler-970). Forty stars match expectations for membership in MELANGE-3 for at least two of the following: rotation period, radial velocity, and lithium levels. These 40 should have had a relatively low field contamination rate. However, only 15 of the 40 were on the Theia 316 list. Adjustments to this high-probability list (e.g., tighter cuts on radial velocity, requiring all three of the criteria to match) yielded almost identical conclusions: slightly more than half the real members were missing from the Theia 316 list. Most of these missing stars landed far from the core of the string in XYZ space and likely failed to pass the minimum density requirements. Even for our analysis, we would not have called most of these clear members without the additional rotation or spectroscopic data.

5. SEARCH FOR PLANETS IN MELANGE-3

To check for other candidate planets or eclipsing binaries in the same association, we searched *Kepler* and *TESS* light curves using the Notch pipeline[3] as described in Rizzuto et al. (2017). To briefly summarize, the Notch filter fits a window of the light curve as a combination of an outlier-robust second-order polynomial (for the stellar variability) and a trapezoidal notch (representing the potential planet). The window moved along the light curve until the variability is detrended (flattened) while preserving the planet signal. At each data point, we calculated the improvement from adding the trapezoidal notch based on the change in the Bayesian Information Criterion (BIC) compared to modeling just a polynomial. Notch then repeated this process over the full curve.

We searched the detrended light curves and the BIC signals that Notch produces for periodic signals. We excluded signals at the stellar rotation period and its harmonics, which arise from imperfect detrending. We also checked for known *Kepler* Objects of Interest (KOIs) orbiting candidate members of MELANGE-3, identified by a simple cross-match against the most recent KOI catalog (Twicken et al. 2016). All but one KOI were flagged by the Notch search.

[3] https://github.com/arizzuto/Notch_and_LOCoR

Table 2. Planetary Candidates in MELANGE-3.

ID	Disposition	Mem?	$P_{\rm orb}$ (days)	T0 (MBJD)	Depth (ppm)
KOI-678.01	Conf	N	6.040	55005.094	241
KOI-678.02	Conf	N	4.139	54964.516	256
KOI-966.01	FP	Y	0.379	55002.748	1973
KOI-966.02	FP	Y	7.769	54965.590	1730
KOI-1838.01	Conf	Y	16.736	54975.632	1147
KOI-3876.01	Conf	Y	19.578	54964.215	450
KOI-5304.01	FP	N	206.310	55064.318	277
KOI-6819.01	Cand	N	3.226	54966.919	36
KOI-7059.01	EB	N	31.973	54966.367	75053
KIC 6366739	Cand	N	22.321	55386.107	2277
TIC 20352534	FP	N	6.377	58687.371	5852
TIC 237181417	FP	N	10.870	58690.062	3178
TIC 272486188	FP	N	9.040	58683.104	779
TIC 28768382	FP	N	11.790	58692.223	1430
TIC 138966713	FP	Y	19.701	58687.157	1858
TIC 158168145	FP	Y	7.107	58689.209	1908
TIC 158415341	FP	N	20.016	58690.003	7571
TIC 164678171	FP	N	12.392	58695.052	1277
TIC 355909811	FP	N	6.065	58686.431	10753

Note—T_* and P for KOIs taken from ExoFOP-*Kepler* (ExoFOP 2019).

In total, we identified 19 targets of interest that pass the SNR and initial quality checks from Notch. Nine of these are known KOIs (KOI-678.01, KOI-678.02, KOI-966.01, KOI-966.02, KOI-1838.01, KOI-3876.01, KOI-5304.01, KOI-6819.01, and KOI-7059.01), while the remaining are newly identified. All 19 targets are listed in Table 2 along with our classification of each.

5.1. *Discussion of Individual Candidate Planet Hosts*

We split the candidate planet hosts into likely (Section 5.1.1) and unlikely (Section 5.1.2) members of MELANGE-3. For each system, we discuss our reasons for accepting or rejecting the candidate planet, based on MELANGE-3 membership and the quality of the planet signal. Other than KOI-3876, we identified only one other system (Kepler-970) that was both likely to host a real planet and be a member of MELANGE-3.

5.1.1. *Candidate planets accepted as MELANGE-3 Members*

KOI-3876 b was the original seed around which we identified MELANGE-3, but it was still useful to confirm it is a member of the group. With a rotation period of 4.67 days, KOI-3876 was an excellent match to the Pleiades sequence for its color. The EW[Li] (134 ± 18Å) was similarly consistent with the Pleiades distribution. Re-running `FriendFinder` on other high-probability members of MELANGE-3 also returned KOI-3876 in the membership list, confirming that kinematic and spatial agreement was robust to the initial seed. Lastly, the star is listed in the Theia 316 membership list, affirming its membership. We confirmed the signal is planetary in origin in Section 7.1.

KOI-1838.01 is a confirmed planet (Kepler-970 b; Morton et al. 2016). The star's rotation (9.23 days) places it right on the Pleiades sequence (see Figure 4), and much faster than the stalling regime seen for > 600 Myr systems (Curtis et al. 2019). The LAMOST (corrected) velocity is -32$\pm$4 km s^{-1}, which is consistent with the value predicted for membership ($\simeq$-27km s^{-1}). A more precise measurement from the CKS-cool project Petigura et al. (2022) yielded an RV of -27.15$\pm$0.10km s^{-1}, an excellent match for the association. The corresponding high-resolution spectrum from Petigura et al. (2022) shows weak lithium ($<$ 40mÅ), but this is consistent with 100 Myr for its spectral type (Baraffe et al. 2015). As we show in Figures 1, 6, and 7, Kepler-970 lands on the expected CMD for a Pleiades-aged star and is nearby other likely members both in Galactic position and proper motion. We classified this planet as real and a member; we included it in our analysis throughout the rest of this paper.

Both planet candidates around KOI-966 are flagged as false positives by the *Kepler* analysis (Coughlin et al. 2016; ExoFOP 2019), with both signals attributed to an eclipsing binary (.02 corresponding to a harmonic of the secondary eclipse). Initially, we came to the same conclusion based on the V-shaped signal and a visible secondary eclipse. However, the depth is unusually small for an eclipsing binary ($\simeq$2 mmag), the depth changes from quarter to quarter, and no matching signal is present in the *TESS* data (it should be marginally detectable at this magnitude). It is possible that this is a more exotic object with an evolving transit depth, but more likely is that this is due to a column anomaly or CCD cross-talk from another eclipsing binary somewhere else on the *Kepler* field (for more details see Coughlin et al. 2014). We recovered the same rotation period in the *TESS* and *Kepler* data (3.9 days), which matches expectations for membership. The star is also only $\Delta v_{tan} \simeq$ 1km s^{-1} and $D \simeq 8$ pc from KOI-3876, near the core of likely members. We classified this system as a member of MELANGE-3but the signal as a false positive.

Using Notch, TICs 138966713 and 158168145 passed the BIC criterion for significance, but upon further visual inspections, we classified these as false positives. The transit signals did not have the expected transit shape and could be more easily explained as systematics or imperfectly removed stellar noise. TIC 138966713 has a radial velocity of -29.9 ± 10.0 km s^{-1}, consistent with the expected radial velocity. TIC 158168145 has a radial velocity -24.4 ± 1.1 and a rotation period of 5.4 ± 0.5, both of which are consistent with the expected values. We classified both targets as members.

5.1.2. *Candidate planets rejected as MELANGE-3 Members*

KOI-678 (.01 and .02) contains two confirmed planets (Kepler-211 bc), and the star's light curve showed a clear rotation signature of $\simeq$13.7 days. However, for a member of the same color, we expected the rotation period to be $\lesssim$8 days. While the detected period could have been a harmonic, the EW[Li] measurement was only 3.8mÅ (Berger et al. 2018), while membership predicted a Li level above 100mÅ. The star's proper motion also put it on the outskirts of the distribution. We classified this star as a non-member.

KOI-5304.01 was flagged as a false positive by the *Kepler* analysis due to a non-transit-like shape. Our visual inspection of the candidate agrees with this. The host star also shows a measurable but slow rotation period of $\simeq$11.4 days, which is slower than expected for membership (see Section 4.3). We classified this system as a non-member and the signal as a false positive.

KOI-6819 (.01) contains a single planet signal that passed visual inspection. However, the star showed no significant rotation, and the *Gaia* DR2 velocity was $\simeq$20km s^{-1} from the expected value for membership in the association. We classified it as a non-member and did not attempt to further validate the transit signal.

KOI-7059.01 was flagged as a false positive by the *Kepler* analysis (Coughlin et al. 2016). Based on the odd-even depth difference we similarly concluded this is an eclipsing binary. The APOGEE velocity was $\simeq$8km s^{-1} from the cluster. The discrepant velocity may have been due to binarity, but the source also lands on the outskirts of the membership list, $>$48 pc from KOI-3876 and near the edge in terms of tangential velocity. We classified this target as non-member eclipsing binary.

The newly identified targets, KIC 6366739 and TICs 20352534, 237181417, 272486188, 28768382, 158415341, 164678171, and 355909811, were all initially flagged by Notch as potentially interesting signals. TIC 272486188, 164678171, and 158415341 have both *TESS* and *Kepler* data, but we could not recover the transit signals we identified from *TESS* data in the higher-quality *Kepler* data. Figure 8 shows TIC 158415341 as an example of this; We was a potentially interesting transit in *TESS*, but we failed to recover TIC 158415341's

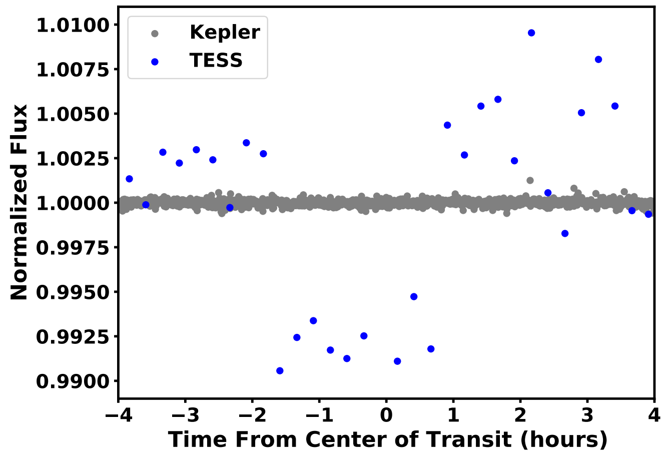

Figure 8. Phase-folded light curve of potential member TIC 158415341 (KIC 9700914) from *TESS* (blue) and *Kepler* (grey) detrended with the Notch filter. We found TIC 158415341 has a best fit period of 20.016 days with an initial transit time of 1690.503 BTJD using *TESS* data, but we fail to detect the transit using *Kepler* data. We reject this signal as noise in the *TESS* data.

(KIC 9700914's) transit signal in the *Kepler* data. We rejected these targets as false positives. KIC 6366739 shows signs of a possible signal in the *Kepler* photometry. However, the target has a long period (22 days) and was observed for only a single quarter, so the SNR was insufficient to reject or confirm this. When using Notch, TICs 20352534, 237181417, 28768382, and 355909811 passed the BIC criterion for significance, but upon further visual inspections, we find the transit signals did not have the expected transit shape and are more easily explained as systematics or imperfectly removed stellar noise. We classified these as FPs.

TICs 272486188, 158415341, and 164678171 are unlikely to be members of MELANGE-3 as the radial velocity measurements are >20km s^{-1} from the predicted values for membership. Additionally, KIC 6366739 is unlikely to be a member since the rotation period is 16.9 ± 1.3 days, which is greater than the expected rotation periods for this association (<10 days).

TICs 20352534, 237181417, and 355909811 did not have available rotation periods, radial velocities, or Lithium measurements, but we concluded all are unlikely to be members. While TIC 20352534 is likely young since it is an A-type, the star landed on the edge of the search region (49.34 pc from KOI-3876) and the edge of the tangential velocity difference allowance (4.45 km s^{-1} from KOI-3876). TICs 237181417 and 355909811 showed little flux variation, and therefore no signs of rotation, indicating they are most likely older stars not a part of the association.

6. PROPERTIES OF KOI-3876 AND Kepler-970

We summarize the properties of both host stars in Table 3, the details of which we provide below.

6.1. *Literature Parameters*

As a reasonably bright ($K_P = 12.6$) star hosting a planet candidate from the *Kepler* mission, KOI-3876 has numerous stellar parameters in the literature. The California *Kepler* Survey (CKS) estimate $T_{\rm eff} = 5720 \pm 60$ K, *log g* $= 4.64 \pm 0.1$, and $v \sin i_* = 9.9 \pm 1.0$km s^{-1}, $R_* = 0.95^{+0.06}_{-0.04} R_\odot$ and $M_* = 1.01 \pm 0.03 M_\odot$ based on comparing their high-resolution spectra and comparison to well-characterized templates (Yee et al. 2017; Petigura et al. 2017) and stellar isochrones (Johnson et al. 2017). Brewer & Fischer (2018), using the same spectra, estimate $T_{\rm eff} = 5642 \pm 27$ K, *log g* $= 4.46 \pm 0.05$, $R_* = 0.93 \pm 0.02 M_\odot$, $M_* = 0.99 \pm 0.02 M_\odot$, and $v \sin i_* = 10.4 \pm 0.5$km s^{-1}, as well as detailed abundances that are generally consistent with the Solar value. Berger et al. (2020) incorporated *Gaia* DR2 data with MIST stellar isochrones to derive an $T_{\rm eff} = 5577 \pm 85$ K, *log g* $= 4.50 \pm 0.02$, and $R_* = 0.908 \pm 0.017 R_\odot$.

For Kepler-970, Berger et al. (2020) estimated $T_{\rm eff} = 4314 \pm 73$ K, *log g* $= 4.63 \pm 0.02$, $R_* = 0.649 \pm 0.012 R_\odot$, and $M_* = 0.657 \pm 0.022 M_\odot$ using the *Gaia* parallax, photometry, and MIST isochrones as with KOI-3876. Based on the CKS spectra, Petigura et al. (2022) found a consistent $T_{\rm eff}$ (4401±70 K), stellar radius ($R_* = 0.70 \pm 0.03 R_\odot$), and mass ($M_* = 0.68 \pm 0.10 M_\odot$). Petigura et al. (2022) also estimated a $v \sin i_*$ of 5.21 ± 1.0km s^{-1} from the CKS spectra. This $v \sin i_*$ may be slightly overestimated due to mild broadening in their templates, but the errors are sufficiently generous for our analysis.

These stellar parameters are generally in agreement with each other. However, literature estimates that relied on model isochrones (e.g., Berger et al. 2020) assigned > 2 Gyr ages for both stars, much older than the true $\simeq$100 Myr age from the association. Although this will not impact purely spectroscopic parameters like $T_{\rm eff}$ and $v \sin i_*$, the assumption can have a strong impact on the estimated stellar mass. Thus, we revisit these parameters with our analysis below.

6.2. *Spectral-Energy Distribution*

We fit the observed spectral-energy-distribution (SED) of both stars following Mann et al. (2016b). To briefly summarize, we fit the observed photometry with a grid of optical and near-infrared flux-calibrated spectra spanning 0.4–2.3μm. We included BT-SETTL

CIFIST atmospheric models (Baraffe et al. 2015) in the fit, both to estimate the $T_{\rm eff}$ and fill in gaps in the template spectra (e.g., beyond 2.3μm). We integrated the resulting absolutely-calibrated spectrum to estimate the bolometric flux ($F_{\rm bol}$), which we combined with the *Gaia* EDR3 parallax to estimate the stellar luminosity (L_*). With $T_{\rm eff}$ and L_*, we calculated R_* using the Stefan-Boltzmann relation. While reddening in this sight-line is low (Schlafly & Finkbeiner 2011), KOI-3876 is well outside the Local Bubble, so we included extinction as part of the fit. To account for variability in the star, we added (in quadrature) 0.02 mags to the errors of all-optical photometry. In total, the fit included six free parameters: the spectral template, A_V, three parameters that describe the model (log g, $T_{\rm eff}$, and [M/H]), and a scale factor between the model and the photometry. We show an example fit in Figure 9.

For KOI-3876, the resulting fit yielded $A_V = 0.16^{+0.10}_{-0.08}$, $T_{\rm eff}$=5672 ± 65 K, $F_{\rm bol}$=$(2.55 \pm 0.10) \times 10^{-10}$ (erg cm^{-2} s^{-1}), $L_* = 0.81 \pm 0.03 L_\odot$, and $R_* = 0.94 \pm 0.03 R_\odot$. For Kepler-970, we found $A_V = 0.28 \pm 0.12$, $T_{\rm eff}$=4290 ± 70 K, $F_{\rm bol}$=$(4.88 \pm 0.23) \times 10^{-11}$ (erg cm^{-2} s^{-1}), $L_* = 0.168 \pm 0.010 L_\odot$, and $R_* = 0.715 \pm 0.03 R_\odot$.

Our SED parameters were in good agreement with the literature spectroscopic values for both stars. Since KOI-3876 is Sun-like, we considered the CKS spectroscopic $T_{\rm eff}$ to be more reliable than the SED-based value, but the SED-based luminosity (and radius) is more reliable than the one derived from the spectroscopic *log g* or isochrone. We combined the two, which yielded a final radius of $0.92 \pm 0.02 R_\odot$. For Kepler-970, we adopted our SED-fit parameters for all values.

6.3. *Stellar mass*

To determine M_* for KOI-3876, we compared the observed photometry to Solar-metallicity magnetic DSEP evolution models and PARSEC models. We used `emcee` to simultaneously fit for age, A_V, M_*, and an additional parameter to capture underestimated uncertainties in the data or models (f, in magnitudes) within an MCMC framework. We used a hybrid interpolation method, first identifying the nearest age in the model grid and then performing a linear interpolation in mass to obtain stellar parameters and model photometry. Since this method could not interpolate between ages, we resampled the input grid using the `isochrones` package (Morton 2015a) to be more dense (0.1 Myr and $0.01 M_\odot$) than expected errors. To redden the model photometry, we used `synphot` (Lim 2020) and the extinction law from Cardelli et al. (1989). We placed a Gaussian prior on the age of 105 ± 10 Myr, while other parameters evolved under uniform priors. The resulting fit from each model grid was very precise, but differences between the two grids suggest larger systematic errors. Considering these, the resulting parameters were generally in agreement with our spectroscopic constraints ($R_* = 0.968 \pm 0.07$, $A_V = 0.27 \pm 0.10$, $T_{\rm eff}$=5710 ± 60) and provided a stellar-mass estimate of $M_* = 1.04 \pm 0.03 M_\odot$. We combined this with our earlier radius estimate to get an estimate of the stellar density ($\rho_* = 1.30 \pm 0.10 \rho_\odot$).

Kepler-970 is expected to be on the main-sequence (see Figure 1) and is low-mass enough to fit within the bounds of the $M_K - M_*$ relation from Mann et al. (2019). We used the *Gaia* EDR3 parallax with uncertainties corrected for underestimated errors following El-Badry et al. (2021) and the 2MASS K_S magnitude. We applied a correction for reddening based on our SED fit (Section 6.2), although this was negligible in the K_S band compared to other uncertainties. We fed the resulting values into the fit posteriors using the provided code[4], which yielded a mass of $0.66 \pm 0.02 M_\odot$. Since the star is near the zero-age main-sequence, we checked our mass estimate using the same methodology as with KOI-3876. The model-based mass was consistent but showed more variation between grids ($0.65 - 0.70 M_\odot$), so we adopted the value from the $\mathrm{M}_K - M_*$ relation. Combining with the radius above, this gives a stellar density of $1.88 \pm 0.24 \rho_\odot$.

6.4. *Stellar inclination*

To test whether the stellar spin and planetary orbit are consistent with alignment, we computed the stellar inclination (i_*) from the $v \sin i_*$, $P_{\rm rot}$, and R_* values estimated above. In its simplest form, this calculation is $V = 2\pi R_*/P_{\rm rot}$, but requires additional statistical corrections (see Morton & Winn 2014; Masuda & Winn 2020). Here we followed the methodology described in Masuda & Winn (2020). For KOI-3876, the resulting stellar inclination was $i_* > 71°$ at 95% confidence and $i_* > 80°$ at 68% confidence. For Kepler-970, the values were $i_* > 52°$ and $i_* > 70°$ at 95% and 68%, respectively. Both are consistent with alignment with the orbital inclinations.

7. TRANSIT PARAMETERS

We fit the *Kepler* photometry using the `misttborn` (MCMC Interface for Synthesis of Transits, Tomography, Binaries, and Others of a Relevant Nature) fitting

[4] https://github.com/awmann/M_-M_K-

Table 3. Properties of KOI-3876 and Kepler-970

Parameter	KOI-3876	Kepler-970	Source
		Name	
Gaia EDR3	2052827207364859264	2101379205604338688	Gaia Collaboration et al. (2021)
KOI	3876	1838	Twicken et al. (2016)
KIC	3440118	5526527	Brown et al. (2011)
TIC	122450696	122069243	Stassun et al. (2018)
2MASS	J19214575+3831248	J19183005+4042314	Skrutskie et al. (2006)
		Astrometry	
α	290.440629	289.625218	*Gaia* EDR3
δ.	38.523572	40.708735	*Gaia* EDR3
μ_α (mas yr^{-1})	-4.154±0.010	-2.739±0.020	*Gaia* EDR3
μ_δ (mas yr^{-1})	2.269±0.011	1.652±.024	*Gaia* EDR3
π (mas)	3.0565±0.0093	3.0153±0.0186	*Gaia* EDR3
		Photometry	
G_{Gaia} (mag)	12.6054±0.0028	14.7876±0.0029	*Gaia* EDR3
BP_{Gaia} (mag)	12.9642±0.0033	15.4884±0.0049	*Gaia* EDR3
RP_{Gaia} (mag)	12.0798±0.0041	13.9759±0.0048	*Gaia* EDR3
B (mag)	13.375 ± 0.094	...	APASS
V (mag)	12.655 ± 0.122	...	APASS
g' (mag)	13.038 ± 0.033	...	APASS
r' (mag)	12.456 ± 0.092	...	APASS
i' (mag)	12.323 ± 0.062	...	APASS
J (mag)	11.456 ± 0.02	12.980±0.023	2MASS
H (mag)	11.152 ± 0.016	12.355±0.023	2MASS
K_S (mag)	11.107 ± 0.019	12.215±0.022	2MASS
$W1$ (mag)	11.06 ± 0.023	12.155±0.022	ALLWISE
$W2$ (mag)	11.09 ± 0.020	12.193±0.022	ALLWISE
$W3$ (mag)	10.91 ± 0.094	12.195±0.282	ALLWISE
		Kinematics & Position	
RV$_{\rm Bary}$ (km s^{-1})	-26.79±0.01	-27.15±0.10	Jönsson et al. (2020); Petigura et al. (2022)
U (km s^{-1})	-9.467 ± 0.016	-8.815 ± 0.047	This work
V (km s^{-1})	-26.034 ± 0.012	-26.146 ± 0.092	This work
W (km s^{-1})	2.048 ± 0.032	-1.034 ± 0.055	This work
X (pc)	105.98 ± 0.42	97.55 ± 0.78	This work
Y (pc)	303.03 ± 1.20	308.66 ± 2.45	This work
Z (pc)	62.86 ± 0.25	72.28 ± 0.58	This work
		Physical Properties	
$P_{\rm rot}$ (days)	4.69 ± 0.04	9.23 ±0.66	Nielsen et al. (2013); Santos et al. (2019)
$v \sin i_*$(km s^{-1})	10.4 ± 0.5	5.2±1.0km s^{-1}	Brewer & Fischer (2018); Petigura et al. (2022)
i_* (°)	> 80	> 52	This work
$F_{\rm bol}$ (erg cm^{-2} s^{-1})	$(2.55 \pm 0.10) \times 10^{-10}$	$(4.88 \pm 0.23) \times 10^{-11}$	This work
$T_{\rm eff}$ (K)	5720 ± 60	4290 ± 70	CKS; This work
[Fe/H]	0.12 ± 0.02	0.04±0.09	Brewer & Fischer (2018); Petigura et al. (2022)
M$_\star$ (M$_\odot$)	1.01 ± 0.03	0.67±0.02	This work
R$_\star$ (R$_\odot$)	0.92 ± 0.02	0.71 ± 0.03	This work
L$_\star$ (L$_\odot$)	0.81 ± 0.03	0.168 ± 0.010	This work
$\rho_\star$ ($\rho_\odot$)	1.30 ± 0.10	1.88±0.24	This work
Age (Myr)	105 ± 10		This work

code[5] first described in Mann et al. (2016a) and expanded upon in Johnson et al. (2018). `misttborn` uses `BATMAN` (Kreidberg 2015) to generate model light curves and `emcee` (Foreman-Mackey et al. 2013) to explore the transit parameter space.

[5] https://github.com/captain-exoplanet/misttborn

The standard implementation of `misttborn` fits for five parameters for each transiting planet: time of periastron (T_0), orbital period of the planet (P), planet-to-star radius ratio ($R_p/R_\star$), impact parameter (b), and stellar density ($\rho_\star$). We fit two linear and quadratic limb-darkening coefficients (q_1, q_2) following the triangular sampling prescription of Kipping (2013).

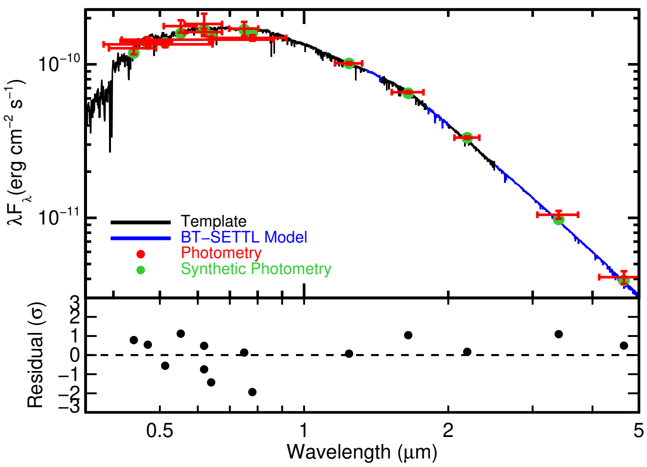

Figure 9. Best-fit template spectrum (G1V; black) and synthetic photometry (green) compared to the observed photometry of KOI-3876 (red). Errors on observed photometry are shown as vertical error bars, while horizontal error bars indicate the approximate width of the filter. BT-SETTL models (blue) were used to fill in regions of high telluric absorption or beyond the template range. The bottom panel shows the photometric residual in units of standard deviations.

We ran two versions of the fit. In the first, the MCMC chain restricted e to 0 and allowed $\rho_\star$ to vary within a uniform distribution, and the second allowed e to vary with a Gaussian prior on $\rho_\star$ from our spectroscopic and SED analysis (Section 6). For both fits, we applied Gaussian priors on the limb-darkening coefficients based on the values derived using our stellar parameters from Section 6 and the `LDTK` toolkit (Parviainen & Aigrain 2015), with errors accounting for the difference between models: $g_1 = 0.42 \pm 0.08$, $g_2 = 0.13 \pm 0.04$ for KOI3876 and $g_1 = 0.51 \pm 0.08$, $g_2 = 0.13 \pm 0.04$ for Kepler-970. Other transit parameters were sampled uniformly with physically motivated boundaries; e.g., T_0 was restricted to the time period sampled by the data, $|b| < 1+R_P/R_*$, $0 < e < 1$, $0 < \rho_*$, and $0 < R_P/R_* < 1$.

To model stellar variations, `misttborn` includes a Gaussian Process (GP) regression module, utilizing the `celerite` code (Foreman-Mackey et al. 2017). We initially used a mixture of two stochastically driven damped simple harmonic oscillators (SHOs) at periods P_{GP} (primary) and $0.5P_{GP}$ (secondary), as is common for fitting stellar variability. However, we found that for both planets, the second SHO was not required (the model was weighting it to zero), and re-ran with a single SHO. There were three GP parameters: the log of the GP period ($\ln(P_{GP})$), the log of the GP amplitude (ln Amp), and a decay timescale for the variability (quality factor, $\ln Q$). We used a weak Gaussian prior (20%) on the GP period to keep walkers from wandering to half and double-period solutions. All other GP parameters evolved under uniform priors.

For each of the four runs (two planets each with and without eccentricity), we ran the MCMC using 50 walkers for 250,000 steps including a burn-in of 20,000 steps. The total run was more than 50 times the autocorrelation time (for all fits), indicating that the steps were sufficient for convergence.

The best-fit parameters with uncertainties for both fits can be found in Table 4. We also show the phase folded light curves in Figure 11 for the preferred fit. As expected, the long baseline of data provided excellent constraints on P and T_0, but the longer (30 m) cadence yielded only weak constraints on impact parameter. This can be seen in the corner plot for the major transit-fit parameters (Figure 10).

For KOI-3876 and Kepler-970, the first fit ($e = 0$) yielded a $\rho_\star$ value larger than the spectroscopic/isochronal value determined in Section 6 ($15.5\rho_\odot$ vs $1.3\rho_\odot$ and $15.2\rho_\odot$ vs $1.9\rho_\odot$). Although the error on the transit-fit density is large ($5.9\rho_\odot$ and $6.7\rho_\odot$), the two values were consistent at $\simeq 2\sigma$. But it is suggestive that the planets are on eccentric orbits. Indeed, in the fits where e is allowed to float, the highest-likelihood models had $e \gtrsim 0.3$ for both planets, with the posteriors shown in Figure 12. For this reason, we prefer the fit where e was allowed to float for both targets.

The SHO GP fits did an excellent job describing the overall variability for both planets, even in the presence of complex changes in the light curve morphology over 4.5 years of observations by *Kepler*. We show two example quarters for each system in Figure 13 that highlight this.

7.1. *False Positive Analysis*

In Morton et al. (2016), the authors run the false-positive probability calculator `VESPA` (Morton 2015b) on all *Kepler* objects of interest available at the time, which included both KOI-3876 b and Kepler-970 b. Kepler-970 b was validated as planetary, and our qualitative inspection of the light curve and archival data re-affirmed this conclusion. The light curve has the expected shape, there are no visible companions in the high-resolution imaging, and the nearest star detected in *Gaia* imaging ($\simeq 4''$ away) is too faint to reproduce the transit depth and shape. We did not revisit this assessment.

However, Morton et al. (2016) assigned a high probability (90%) that the signal associated with KOI-3876 b is an eclipsing binary and a < 1% probability that the

Table 4. Parameters of KOI-3876 and Kepler-970

Parameter	KOI-3876		Kepler-970	
	e=0	e float (preferred)	e=0	e float (preferred)
Measured Parameters				
T_0 (BJD-2454833)	131.71488 ± 0.00088	$131.71484^{+0.00093}_{-0.00092}$	$143.13258^{+0.00099}_{-0.00098}$	143.1326 ± 0.0011
P (days)	$19.577831 \pm 2.1 \times 10^{-5}$	$19.57783 \pm 2.1 \times 10^{-5}$	$16.736525 \pm 2 \times 10^{-5}$	$16.736525 \pm 2 \times 10^{-5}$
$R_P/R_\star$	$0.01945^{+0.00061}_{-0.00044}$	$0.01977^{+0.00116}_{-0.00063}$	$0.03186^{+0.00136}_{-0.00077}$	$0.0337^{+0.0031}_{-0.0022}$
b	$0.31^{+0.28}_{-0.22}$	$0.51^{+0.27}_{-0.33}$	$0.33^{+0.3}_{-0.23}$	$0.7^{+0.18}_{-0.44}$
$\rho_\star$ ($\rho_\odot$)	$15.5^{+2.5}_{-5.9}$	$1.305^{+0.096}_{-0.093}$	$15.2^{+2.9}_{-6.7}$	$1.882^{+0.09}_{-0.088}$
$q_{1,1}$	$0.289^{+0.107}_{-0.1}$	$0.294^{+0.104}_{-0.094}$	0.37 ± 0.12	0.38 ± 0.12
$q_{2,1}$	$0.371^{+0.075}_{-0.086}$	$0.375^{+0.073}_{-0.087}$	$0.374^{+0.07}_{-0.078}$	$0.376^{+0.071}_{-0.076}$
$\sqrt{e}\sin\omega$	–	$0.42^{+0.16}_{-0.31}$	–	$0.25^{+0.25}_{-0.3}$
$\sqrt{e}\cos\omega$	–	$-0.06^{+0.6}_{-0.58}$	–	$-0.0^{+0.55}_{-0.54}$
$\log(P_{GP})$	$1.495^{+0.016}_{-0.014}$	$1.495^{+0.016}_{-0.015}$	$2.839^{+0.056}_{-0.053}$	$2.838^{+0.056}_{-0.051}$
$\log(Amp)$	$-9.338^{+0.057}_{-0.055}$	$-9.338^{+0.058}_{-0.054}$	$-6.797^{+0.079}_{-0.075}$	$-6.799^{+0.078}_{-0.076}$
$\log(Q)$	$1.154^{+0.058}_{-0.055}$	$1.154^{+0.061}_{-0.054}$	$0.664^{+0.029}_{-0.025}$	$0.665^{+0.027}_{-0.025}$
Derived Parameters				
$a/R_\star$	$76.2^{+3.9}_{-10.0}$	$48.0^{+3.3}_{-6.7}$	$68.2^{+4.0}_{-10.0}$	$42.2^{+6.5}_{-7.6}$
i (°)	$89.76^{+0.17}_{-0.29}$	$88.99^{+0.65}_{-0.45}$	$89.72^{+0.2}_{-0.37}$	$88.74^{+0.77}_{-0.26}$
T_{14} (days)	$0.0793^{+0.0016}_{-0.0015}$	$0.106^{+0.071}_{-0.033}$	$0.0763^{+0.0021}_{-0.0018}$	$0.09^{+0.047}_{-0.023}$
T_{23} (days)	$0.0755^{+0.0015}_{-0.0016}$	$0.099^{+0.067}_{-0.032}$	$0.0703^{+0.0019}_{-0.0024}$	$0.075^{+0.046}_{-0.022}$
R_P ($R_\oplus$)	$1.953^{+0.075}_{-0.061}$	$1.985^{+0.124}_{-0.077}$	$2.467^{+0.148}_{-0.149}$	$2.609^{+0.265}_{-0.203}$
a (AU)	$0.313^{+0.046}_{-0.064}$	$0.197^{+0.031}_{-0.039}$	$0.225^{+0.016}_{-0.041}$	$0.139^{+0.022}_{-0.026}$
e	...	$0.42^{+0.18}_{-0.13}$	...	$0.34^{+0.18}_{-0.22}$
ω (°)	...	102.0 ± 62.0	...	$117.0^{+75.0}_{-85.0}$

signal is due to a planet. This conclusion was based primarily on the light curve morphology and available stellar parameters.

As we show in Figure 14, radial velocities from the Apache Point Observatory Galactic Evolution Experiment 16th data release (APOGEE DR16; Jönsson et al. 2020) rule out any stellar companion at the period of the planet. Further, our light curve analysis shows the expected U-shape transit for a planet, and there is no sign of a companion in the extant spectroscopy or adaptive optics imaging and non-redundant aperture masking from Kraus et al. (2016). *Gaia* EDR3 astrometry and imaging similarly show no sign of a companion. There is only one star detected with the *Kepler* PSF, which is too faint to reproduce the transit. KOI-3876 has a low Renormalised Unit Weight Error (RUWE) in EDR3 (0.94). RUWE value is effectively an astrometric reduced χ^2 value, normalized to correct for color and brightness dependent effects[6]. RUWE should be around 1 for well-behaved sources, and higher values (RUWE$\gtrsim$1.3) suggests with the presence of a stellar companion (Ziegler et al. 2020; Wood et al. 2021).

[6] https://gea.esac.esa.int/archive/documentation/GDR2/Gaia_archive/chap_datamodel/sec_dm_main_tables/ssec_dm_ruwe.html

It is possible the high false-positive probability from Morton et al. (2016) was an artifact of poor detrending of the high stellar variability in KOI-3876 and/or the mismatch between the transit duration and that expected for a circular orbit (see Section 7). We reran the `VESPA` analysis using our GP-detrended curve and the updated imaging constraints. We found a 97% probability KOI-3876 b is a planet and a 3% probability KOI-3876 b is an eclipsing binary. Other false-positive scenarios (background EB and hierarchical EB) had negligible (< 0.1%) probabilities. As previously stated and shown in Figure 14, the APOGEE velocities rule out a stellar companion to KOI-3876 at the period of the planet. Including the radial velocities eliminates the EB scenario and reduces the FPP to below 0.1%, validating the signal as planetary in nature.

8. SUMMARY AND CONCLUSIONS

8.1. *MELANGE-3*

MELANGE-3 is a young (105 ± 10 Myr) association that overlaps with the *Kepler* field. We initially identified the association as an overdensity of stars in Galactic positions and tangential velocities around KOI-3876. Through rotation periods and lithium abundances of candidate members, and a comparison to model isochrones, we showed the collection of stars is coeval, with an age similar to that of Pleiades ($\simeq$ 110 Myr).

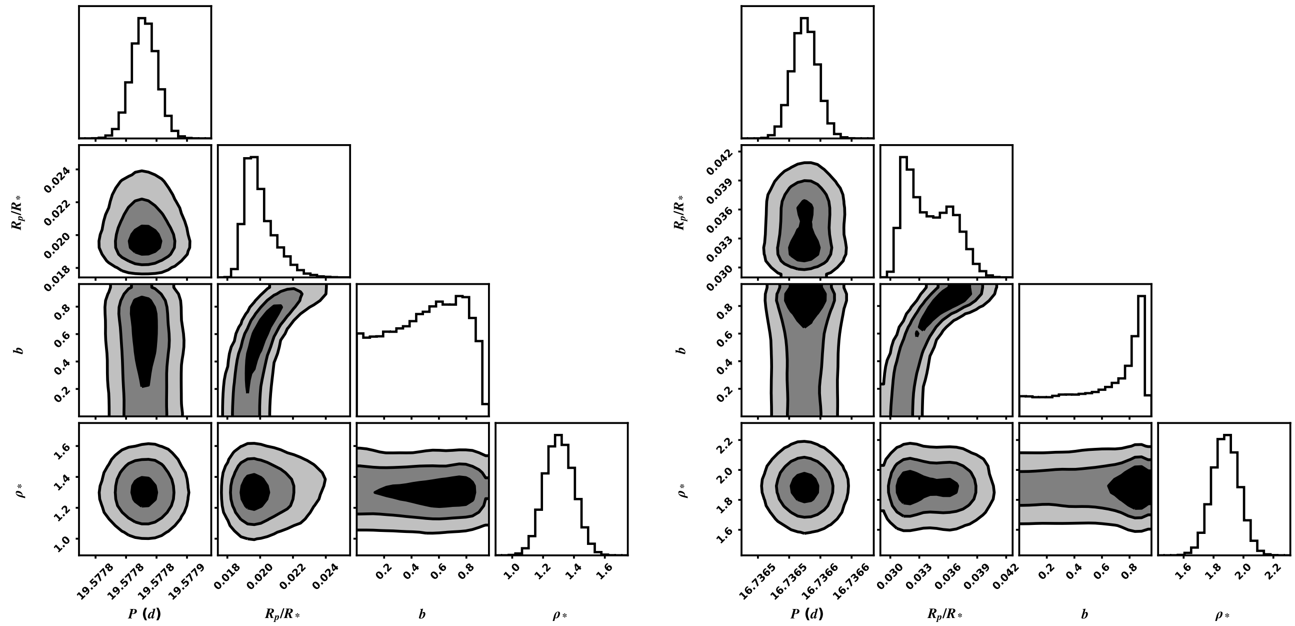

Figure 10. Corner plot of the major transit parameters (P, R_P/R_*, b, and ρ_*) from our `MISTTBORN` fit for KOI-3876 b (left) and Kepler-970 b (right). The contour levels correspond to 1σ, 2σ, and 3σ of the points (from darkest to lightest). The planet-to-star radius ratio and eccentricity are strongly covariant with impact parameter, as a higher impact parameter requires a deeper transit (and lower eccentricity) to reproduce the observed transit depth (and duration). It is difficult to break this degeneracy with *Kepler* long-cadence data alone, as the integration time is longer than the ingress/egress. Plot made using corner.py (Foreman-Mackey 2016).

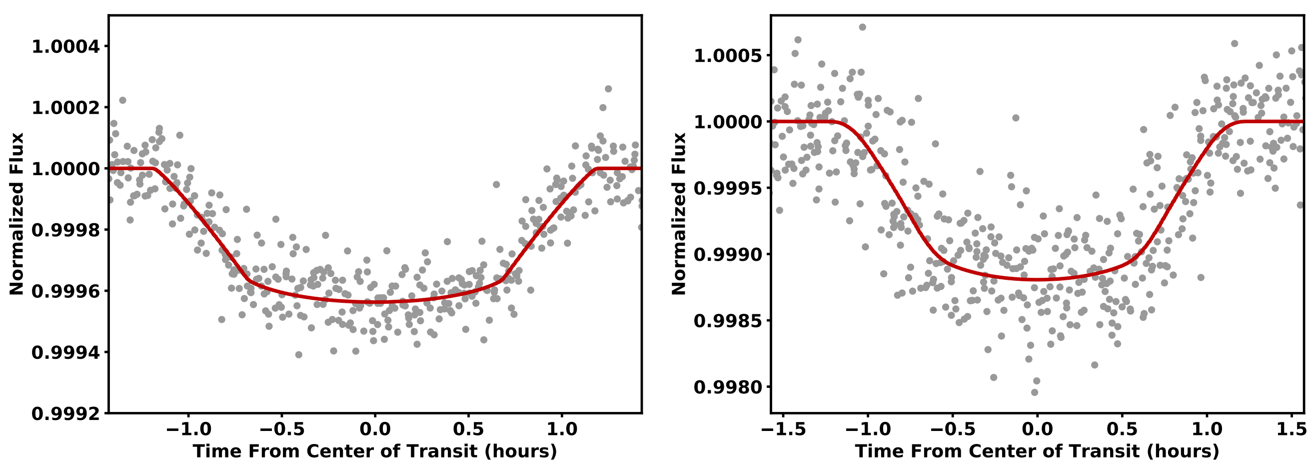

Figure 11. Phase-folded light curve of KOI-3876 (left) and Kepler-970 (right) from *Kepler* (grey points) with the best-fit transit model (red). The best-fit GP model to the stellar variability has been removed from both the data and the model for clarity. Both planets show the expected transit shape.

We refered to this group as MELANGE-3, although it is likely one part of the known Theia 316 string (Kounkel & Covey 2019; Kounkel et al. 2020).

Interestingly, even among our high-probability members of MELANGE-3, more than half were missing from the Theia 316 list. Similarly, our list only contained one branch of Theia 316. The structure likely harbors far more stars than even the combination of the two lists. A more detailed analysis with *TESS* rotations and *Gaia* DR3 velocities would be invaluable here, and similar analysis the thousands of other candidate associations identified by Kounkel et al. (2020).

Stellar angular momentum and rotationally-driven magnetic activity are both age and mass-dependent. Rotation periods in open clusters are useful for studying these phenomena, but there is a lack of low-mass stars

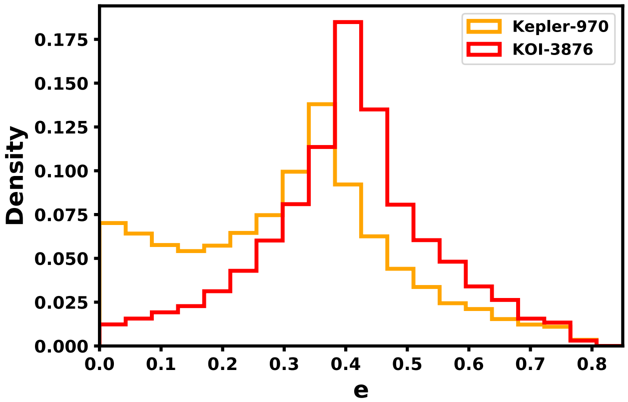

Figure 12. Posteriors of the eccentricity (e) for KOI-3876 b (red) and Kepler-970 b (orange). For both systems, the $e = 0$ fit yields a $\rho_\odot$ greater (shorter duration) than the expected value determined in Section 6. Uncertainties are large due to the long (30 m) cadence, so the final eccentricity is consistent with zero in both cases (marginal consistency for KOI-3876 b).

(<0.5 $M_\odot$) with rotation periods available (Covey et al. 2016). Of the rotation periods in MELANGE-3 utilized here, 49 are K- or M-dwarfs stars, which are more likely to be within this low-mass boundary. Further work on the analysis of the distribution of rotation periods versus color can be done and extend the sample size used in analyses, such as in Rebull et al. (2016a).

The long-baseline of *Kepler* data has enabled studies of spot lifetimes (e.g., Giles et al. 2017). For example, starspots have shorter lifetimes on stars with faster rotation periods (Basri et al. 2022). This is likely due to age, i.e., that younger stars have shorter spot lifetimes. MELANGE-3 and the younger δ-Lyr cluster (Bouma et al. 2021) have enough overlap with the *Kepler* field for a more direct test of how spot lifetimes (among other properties) vary with age.

8.2. *KOI-3876 b and Kepler-970 b*

Taking into account the updated (younger) age and utilizing new methods for analyzing variable light curves, we updated the stellar and transit parameters for KOI-3876 b. We found KOI-3876 b to be about twice the size of the earth, orbiting a young analog to the Sun every 19.577 days. The transit duration also suggests a modest eccentricity, although errors are too large to rule out a circular orbit. Morton et al. (2016) previously found KOI-3876 b likely to be an eclipsing binary, we rule out this disposition based on APOGEE radial velocities and our light curve analysis and validate the signal as planetary in origin.

Kepler-970 b was previously validated as a planet (Morton et al. 2016). As with KOI-3876 b, we update the stellar and planet parameters using the new younger age. We find Kepler-970 b to be about $2.5R_\oplus$, orbiting a young K dwarf every 16.74 days. The planet was previously shown to exhibit transit timing variations (TTVs; e.g., Ford et al. 2012; Holczer et al. 2016). Unfortunately, the period of the variation is $\simeq$2000 days, and our search did not yield any additional planets in the system. Thus, we could not further constrain the system from the TTVs. Our fit assumed a linear ephemeris, which can lead to a distortion in the transit in the presence of a TTV (a shallower depth and longer duration, e.g., Mann et al. 2017a). However, the TTV amplitude was small ($\lesssim$ 10 m; Holczer et al. 2016), and our transit parameters were generally consistent with earlier analyses.

We searched for additional transiting planet candidates in MELANGE-3. Although we identify many candidates and recover some known KOIs (see Table 2), most of these were either not real members, false positives, or did not meet our threshold for significance. Ultimately, only KOI-3876 b and Kepler-970 b passed all tests. Additional *TESS* data of the *Kepler* field, as well as a more complete census of the Theia 316 group, might yield more planets.

These two planets join the growing number of young transiting planets, which we show in Figure 15. KOI-3876 b and Kepler-970 b land in the heavily populated region of mini-Neptunes. Both have similar or smaller radii and similar or longer periods than the similar-aged objects found by $K2$ and *TESS*. They also sit well below the infant (10-50 Myr) planets, which tend to land between Neptune and Jupiter due to a combination of radius evolution (Mann et al. 2017b; Owen 2020) and sensitivity variations with age (Rizzuto et al. 2017).

Recent searches found no transiting planets in the $K2$ data of the similar-aged Pleiades cluster (Gaidos et al. 2017; Rizzuto et al. 2017). Gaidos et al. (2017) argues this deficiency is not surprising given our sensitivity to planets in the Pleiades, although the more effective transit-search methods of Rizzuto et al. (2017) found mild tension with the planet occurrence seen in Pleiades compared to the older Hyades and Praesepe. The discovery of TOI-451 bcd in the $\simeq$120 Myr Psc-Eri cluster (Newton et al. 2021) and the planets in this work suggest the lack of planets in the Pleiades was not related to age. We inspected the sensitivity results from Rizzuto et al. (2017) and concluded that the planets presented in this work would have landed just below the detection limits of the $K2$ data of similar stars in the Pleiades.

We have known there are young planet-hosts in the *Kepler* field from their rotation periods (Walkowicz & Basri 2013; David et al. 2021) and lithium levels (Berger

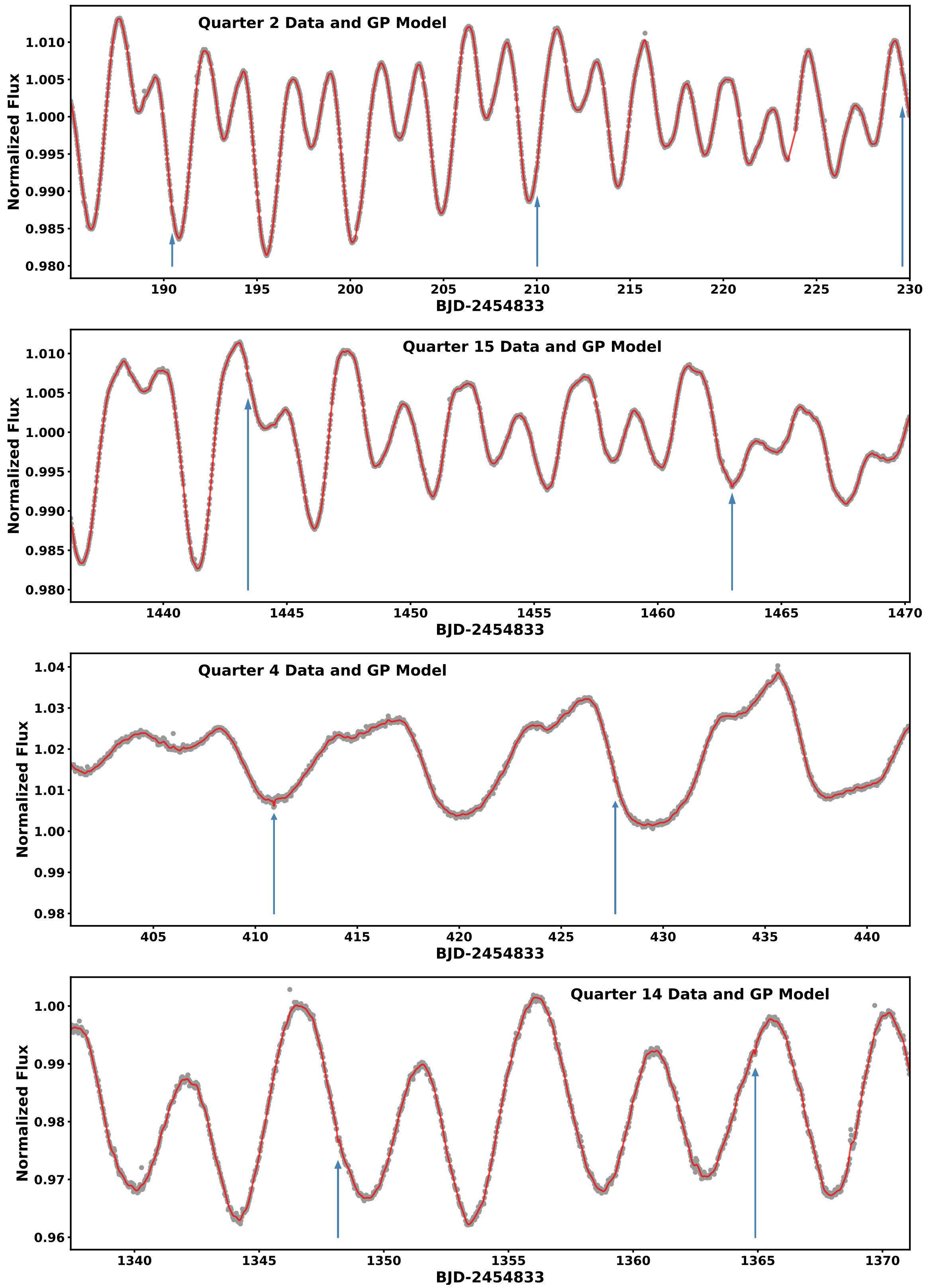

Figure 13. Representative sections of the two planet host light curves. The top two are for KOI-3876, while the bottom two are for Kepler-970. The grey points are the *Kepler* data, the red line shows the best-fit GP model, and the arrows indicate transits.

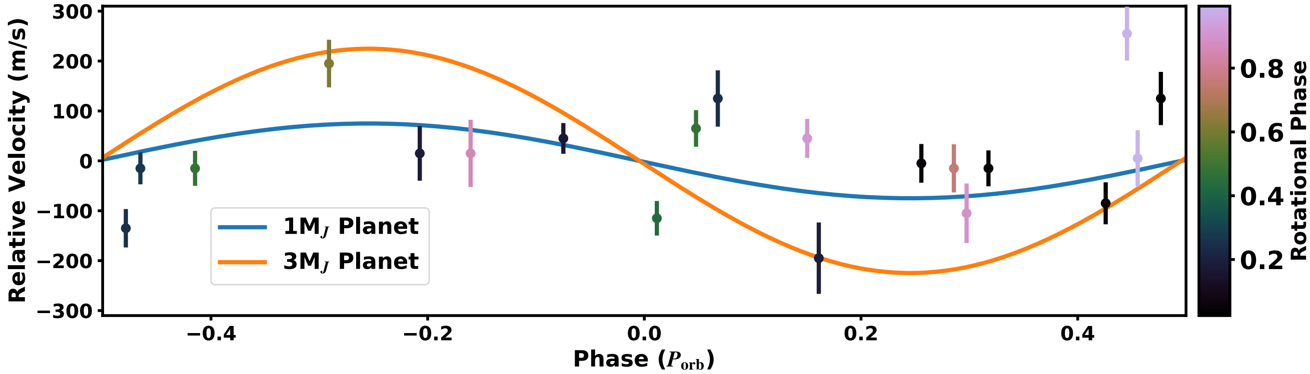

Figure 14. Radial velocities from APOGEE (Jönsson et al. 2020) for KOI-3876 as a function of the planet's orbital phase and colored by the rotational phase. The velocities rule out any companion more massive than $\simeq 2M_J$, ruling out any possibility of an eclipsing binary at the transit period. The scatter is larger than expected for the uncertainties by $\simeq$100m s^{-1}, most likely due to stellar jitter common in young stars (Brems et al. 2019; Tran et al. 2021). The residual jitter is still far below the expected variation for a tight eclipsing binary.

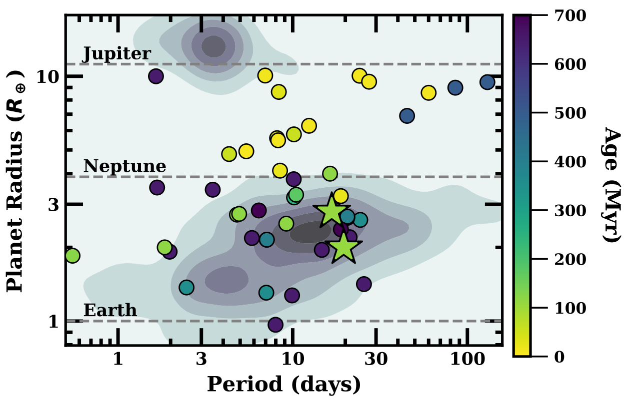

Figure 15. The current census of young (Hyades-age or younger) transiting planets. Points are color-coded by age. The two stars are KOI-3876 b and Kepler-970 b. The contours represent the density of (mostly older) transiting planets from *Kepler*. Planet parameters taken from the NASA exoplanet archive (NASA Exoplanet Science Institute 2020).

et al. 2018), but such ages are generally imprecise when applied to individual stars. The previous challenge for *Kepler* was the lack of young associations. MELANGE-3 and the recently identified δ-Lyr cluster (Bouma et al. 2021) demonstrate that the previous list of just four clusters in the *Kepler* field was incomplete and motivates the work for further searches in the *Kepler*, *K*2, and CoRoT (Auvergne et al. 2009) fields. In addition to surveys like Theia (Kounkel & Covey 2019; Kounkel et al. 2020), the methods applied here may reveal a new population of young associations harboring known transiting systems.

The authors thank Erik Petigura and Luke Bouma for their useful discussions on this manuscript. We also would like to acknowledge Halee, who kept Madyson sane during the lockdown.

MGB was supported by the NC Space Grant Undergraduate Research program and by funding from the Chancellor's Science Scholars Program at the University of North Carolina at Chapel Hill. AWM was supported through a grant from NASA's Exoplanet Research Program (XRP; 80NSSC21K0393). This material is based upon work supported by the National Science Foundation Graduate Research Fellowship Program under Grant No. DGE-1650116 to PCT.

This paper includes data collected by the TESS mission, which are publicly available from the Mikulski Archive for Space Telescopes (MAST). Funding for the TESS mission is provided by NASA's Science Mission directorate. This research has made use of the Exoplanet Follow-up Observation Program website, which is operated by the California Institute of Technology, under contract with the National Aeronautics and Space Administration under the Exoplanet Exploration Program. This work has made use of data from the European Space Agency (ESA) mission *Gaia* [7], processed by the *Gaia* Data Processing and Analysis Consortium (DPAC)[8]. Funding for the DPAC has been provided by national institutions, in particular, the institutions participating in the *Gaia* Multilateral Agreement. This research has made use of the VizieR catalogue access tool, CDS, Strasbourg, France. The original description of the VizieR service was published in A&AS 143, 23. Resources supporting this work were provided by the NASA High-End Computing (HEC) Program through the NASA Advanced Supercomputing (NAS) Division at Ames Research Center for the production of the SPOC data products.

Facilities: TESS, Kepler, Gaia, Sloan (APOGEE), Smith (Coude)

Software: `misttborn.py` (Johnson et al. 2018), `galpy` (Bovy 2015), *emcee* (Foreman-Mackey et al. 2013), *batman* (Kreidberg 2015), matplotlib (Hunter 2007), `corner.py` (Foreman-Mackey 2016), `Celerite` (Foreman-Mackey et al. 2017)

REFERENCES

Aigrain, S., Llama, J., Ceillier, T., et al. 2015, MNRAS, 450, 3211, doi: 10.1093/mnras/stv853

Anguiano, B., Majewski, S. R., Allende Prieto, C., et al. 2018, A&A, 620, A76, doi: 10.1051/0004-6361/201833387

Angus, R., Aigrain, S., Foreman-Mackey, D., & McQuillan, A. 2015, MNRAS, 450, 1787, doi: 10.1093/mnras/stv423

Auvergne, M., Bodin, P., Boisnard, L., et al. 2009, A&A, 506, 411, doi: 10.1051/0004-6361/200810860

Baraffe, I., Homeier, D., Allard, F., & Chabrier, G. 2015, A&A, 577, A42, doi: 10.1051/0004-6361/201425481

Barnes, S. A. 2003, ApJ, 586, 464, doi: 10.1086/367639

—. 2007, ApJ, 669, 1167, doi: 10.1086/519295

Basri, G., Streichenberger, T., McWard, C., et al. 2022, ApJ, 924, 31, doi: 10.3847/1538-4357/ac3420

Batalha, N. M., Borucki, W. J., Koch, D. G., et al. 2010, ApJL, 713, L109, doi: 10.1088/2041-8205/713/2/L109

Berger, T. A., Howard, A. W., & Boesgaard, A. M. 2018, ApJ, 855, 115, doi: 10.3847/1538-4357/aab154

Berger, T. A., Huber, D., van Saders, J. L., et al. 2020, AJ, 159, 280, doi: 10.3847/1538-3881/159/6/280

Bouma, L. G., Hartman, J. D., Bhatti, W., Winn, J. N., & Bakos, G. Á. 2019, ApJS, 245, 13, doi: 10.3847/1538-4365/ab4a7e

Bouma, L. G., Curtis, J. L., Masuda, K., et al. 2021, arXiv e-prints, arXiv:2112.14776. https://arxiv.org/abs/2112.14776

Bouvier, J., Barrado, D., Moraux, E., et al. 2018, A&A, 613, A63, doi: 10.1051/0004-6361/201731881

Bovy, J. 2015, ApJS, 216, 29, doi: 10.1088/0067-0049/216/2/29

Bovy, J., & Hogg, D. W. 2010, ApJ, 717, 617, doi: 10.1088/0004-637X/717/2/617

Brems, S. S., Kürster, M., Trifonov, T., Reffert, S., & Quirrenbach, A. 2019, A&A, 632, A37, doi: 10.1051/0004-6361/201935520

Bressan, A., Marigo, P., Girardi, L., et al. 2012, MNRAS, 427, 127, doi: 10.1111/j.1365-2966.2012.21948.x

Brewer, J. M., & Fischer, D. A. 2018, ApJS, 237, 38, doi: 10.3847/1538-4365/aad501

Brown, T. M., Latham, D. W., Everett, M. E., & Esquerdo, G. A. 2011, AJ, 142, 112, doi: 10.1088/0004-6256/142/4/112

Cardelli, J. A., Clayton, G. C., & Mathis, J. S. 1989, ApJ, 345, 245, doi: 10.1086/167900

Corsaro, E., Stello, D., Huber, D., et al. 2012, ApJ, 757, 190, doi: 10.1088/0004-637X/757/2/190

Coughlin, J. L., Thompson, S. E., Bryson, S. T., et al. 2014, AJ, 147, 119, doi: 10.1088/0004-6256/147/5/119

Coughlin, J. L., Mullally, F., Thompson, S. E., et al. 2016, ApJS, 224, 12, doi: 10.3847/0067-0049/224/1/12

Covey, K. R., Agüeros, M. A., Law, N. M., et al. 2016, ApJ, 822, 81, doi: 10.3847/0004-637X/822/2/81

Cummings, J. D., Deliyannis, C. P., Maderak, R. M., & Steinhauer, A. 2017, AJ, 153, 128, doi: 10.3847/1538-3881/aa5b86

Curtis, J. L., Agüeros, M. A., Douglas, S. T., & Meibom, S. 2019, ApJ, 879, 49, doi: 10.3847/1538-4357/ab2393

Cutri, R. M., & et al. 2014, VizieR Online Data Catalog, II/328

Czekaj, M. A., Robin, A. C., Figueras, F., Luri, X., & Haywood, M. 2014, A&A, 564, A102, doi: 10.1051/0004-6361/201322139

Dahm, S. E. 2015, ApJ, 813, 108, doi: 10.1088/0004-637X/813/2/108

David, T. J., Hillenbrand, L. A., Gillen, E., et al. 2019a, ApJ, 872, 161, doi: 10.3847/1538-4357/aafe09

David, T. J., Petigura, E. A., Luger, R., et al. 2019b, ApJL, 885, L12, doi: 10.3847/2041-8213/ab4c99

David, T. J., Contardo, G., Sandoval, A., et al. 2021, AJ, 161, 265, doi: 10.3847/1538-3881/abf439

Dotter, A., Chaboyer, B., Jevremović, D., et al. 2008, ApJS, 178, 89, doi: 10.1086/589654

Douglas, S. T., Agüeros, M. A., Covey, K. R., & Kraus, A. 2017, ApJ, 842, 83, doi: 10.3847/1538-4357/aa6e52

Douglas, S. T., Curtis, J. L., Agüeros, M. A., et al. 2019, ApJ, 879, 100, doi: 10.3847/1538-4357/ab2468

El-Badry, K., Rix, H.-W., & Heintz, T. M. 2021, MNRAS, 506, 2269, doi: 10.1093/mnras/stab323

ExoFOP. 2019, Exoplanet Follow-up Observing Program - Kepler, IPAC, doi: 10.26134/ExoFOP1

Feiden, G. A., & Chaboyer, B. 2012, ApJ, 761, 30, doi: 10.1088/0004-637X/761/1/30

Ford, E. B., Ragozzine, D., Rowe, J. F., et al. 2012, ApJ, 756, 185, doi: 10.1088/0004-637X/756/2/185

Foreman-Mackey, D. 2016, The Journal of Open Source Software, 1

Foreman-Mackey, D., Agol, E., Ambikasaran, S., & Angus, R. 2017, AJ, 154, 220, doi: 10.3847/1538-3881/aa9332

Foreman-Mackey, D., Hogg, D. W., Lang, D., & Goodman, J. 2013, PASP, 125, 306, doi: 10.1086/670067

Gagné, J., Faherty, J. K., Moranta, L., & Popinchalk, M. 2021, ApJL, 915, L29, doi: 10.3847/2041-8213/ac0e9a

Gagné, J., Mamajek, E. E., Malo, L., et al. 2018, ApJ, 856, 23, doi: 10.3847/1538-4357/aaae09

Gaia Collaboration, Prusti, T., de Bruijne, J. H. J., et al. 2016, A&A, 595, A1, doi: 10.1051/0004-6361/201629272

Gaia Collaboration, Brown, A. G. A., Vallenari, A., et al. 2021, A&A, 649, A1, doi: 10.1051/0004-6361/202039657

Gaidos, E., Mann, A. W., Rizzuto, A., et al. 2017, MNRAS, 464, 850, doi: 10.1093/mnras/stw2345

Giles, H. A. C., Collier Cameron, A., & Haywood, R. D. 2017, MNRAS, 472, 1618, doi: 10.1093/mnras/stx1931

Gray, D. F. 1992, The observation and analysis of stellar photospheres., Vol. 10 (Camb. Astrophys. Ser)

Green, G. M., Schlafly, E., Zucker, C., Speagle, J. S., & Finkbeiner, D. 2019, ApJ, 887, 93, doi: 10.3847/1538-4357/ab5362

Hattori, S., Foreman-Mackey, D., Hogg, D. W., et al. 2021, arXiv e-prints, arXiv:2106.15063. https://arxiv.org/abs/2106.15063

Henden, A. A., Templeton, M., Terrell, D., et al. 2016, VizieR Online Data Catalog, II/336

Hogg, D. W., Bovy, J., & Lang, D. 2010, arXiv e-prints, arXiv:1008.4686. https://arxiv.org/abs/1008.4686

Holczer, T., Mazeh, T., Nachmani, G., et al. 2016, ApJS, 225, 9, doi: 10.3847/0067-0049/225/1/9

Horne, J. H., & Baliunas, S. L. 1986, ApJ, 302, 757, doi: 10.1086/164037

Huang, C. X., Vanderburg, A., Pál, A., et al. 2020, Research Notes of the American Astronomical Society, 4, 204, doi: 10.3847/2515-5172/abca2e

Hunter, J. D. 2007, Computing in science & engineering, 9, 90

Husser, T.-O., Wende-von Berg, S., Dreizler, S., et al. 2013, A&A, 553, A6, doi: 10.1051/0004-6361/201219058

Jeffries, R. D., Jackson, R. J., Franciosini, E., et al. 2017, MNRAS, 464, 1456, doi: 10.1093/mnras/stw2458

Jenkins, J. M., Caldwell, D. A., Chandrasekaran, H., et al. 2010, ApJL, 713, L120, doi: 10.1088/2041-8205/713/2/L120

Johnson, J. A., Petigura, E. A., Fulton, B. J., et al. 2017, AJ, 154, 108, doi: 10.3847/1538-3881/aa80e7

Johnson, M. C., Dai, F., Justesen, A. B., et al. 2018, MNRAS, 481, 596, doi: 10.1093/mnras/sty2238

Jönsson, H., Holtzman, J. A., Allende Prieto, C., et al. 2020, AJ, 160, 120, doi: 10.3847/1538-3881/aba592

Katz, D., Sartoretti, P., Cropper, M., et al. 2019, A&A, 622, A205, doi: 10.1051/0004-6361/201833273

Kerr, R., Rizzuto, A. C., Kraus, A. L., & Offner, S. S. R. 2021, arXiv e-prints, arXiv:2105.09338. https://arxiv.org/abs/2105.09338

Kiman, R., Faherty, J. K., Cruz, K. L., et al. 2021, arXiv e-prints, arXiv:2104.01232. https://arxiv.org/abs/2104.01232

Kipping, D. M. 2013, MNRAS, 435, 2152, doi: 10.1093/mnras/stt1435

Kounkel, M., & Covey, K. 2019, AJ, 158, 122, doi: 10.3847/1538-3881/ab339a

Kounkel, M., Covey, K., & Stassun, K. G. 2020, AJ, 160, 279, doi: 10.3847/1538-3881/abc0e6

Kraus, A. L., Cody, A. M., Covey, K. R., et al. 2015, ApJ, 807, 3, doi: 10.1088/0004-637X/807/1/3

Kraus, A. L., Ireland, M. J., Huber, D., Mann, A. W., & Dupuy, T. J. 2016, AJ, 152, 8, doi: 10.3847/0004-6256/152/1/8

Kreidberg, L. 2015, PASP, 127, 1161, doi: 10.1086/683602

Krumholz, M. R., McKee, C. F., & Bland-Hawthorn, J. 2019, ARA&A, 57, 227, doi: 10.1146/annurev-astro-091918-104430

Lim, P. L. 2020, synphot, 1.0.1, Zenodo, doi: 10.5281/zenodo.3971036

Lodieu, N., Pérez-Garrido, A., Smart, R. L., & Silvotti, R. 2019, A&A, 628, A66, doi: 10.1051/0004-6361/201935533

Luo, A. L., Zhao, Y. H., Zhao, G., & et al. 2019, VizieR Online Data Catalog, V/164

Luo, A. L., Zhao, Y.-H., Zhao, G., et al. 2015, Research in Astronomy and Astrophysics, 15, 1095, doi: 10.1088/1674-4527/15/8/002

Mann, A. W., Gaidos, E., Mace, G. N., et al. 2016a, ApJ, 818, 46, doi: 10.3847/0004-637X/818/1/46

Mann, A. W., Newton, E. R., Rizzuto, A. C., et al. 2016b, AJ, 152, 61, doi: 10.3847/0004-6256/152/3/61

Mann, A. W., Dupuy, T., Muirhead, P. S., et al. 2017a, AJ, 153, 267, doi: 10.3847/1538-3881/aa7140

Mann, A. W., Gaidos, E., Vanderburg, A., et al. 2017b, AJ, 153, 64, doi: 10.1088/1361-6528/aa5276

Mann, A. W., Dupuy, T., Kraus, A. L., et al. 2019, ApJ, 871, 63, doi: 10.3847/1538-4357/aaf3bc

Mann, A. W., Wood, M. L., Schmidt, S. P., et al. 2021, arXiv e-prints, arXiv:2110.09531. https://arxiv.org/abs/2110.09531

Masuda, K., & Winn, J. N. 2020, AJ, 159, 81, doi: 10.3847/1538-3881/ab65be

McQuillan, A., Aigrain, S., & Mazeh, T. 2013, MNRAS, 432, 1203, doi: 10.1093/mnras/stt536

McQuillan, A., Mazeh, T., & Aigrain, S. 2014, ApJS, 211, 24, doi: 10.1088/0067-0049/211/2/24

Meibom, S., Barnes, S. A., Latham, D. W., et al. 2011, ApJL, 733, L9, doi: 10.1088/2041-8205/733/1/L9

Meibom, S., Torres, G., Fressin, F., et al. 2013, Nature, 499, 55, doi: 10.1038/nature12279

Meingast, S., Alves, J., & Fürnkranz, V. 2019, A&A, 622, L13, doi: 10.1051/0004-6361/201834950

Miglio, A., Brogaard, K., Stello, D., et al. 2012, MNRAS, 419, 2077, doi: 10.1111/j.1365-2966.2011.19859.x

Morton, T. D. 2015a, isochrones: Stellar model grid package. http://ascl.net/1503.010

—. 2015b, VESPA: False positive probabilities calculator, Astrophysics Source Code Library. http://ascl.net/1503.011

Morton, T. D., Bryson, S. T., Coughlin, J. L., et al. 2016, ApJ, 822, 86, doi: 10.3847/0004-637X/822/2/86

Morton, T. D., & Winn, J. N. 2014, ApJ, 796, 47, doi: 10.1088/0004-637X/796/1/47

NASA Exoplanet Science Institute. 2020, Planetary Systems Table, IPAC, doi: 10.26133/NEA12

Newton, E. R., Mann, A. W., Tofflemire, B. M., et al. 2019, ApJL, 880, L17, doi: 10.3847/2041-8213/ab2988

Newton, E. R., Mann, A. W., Kraus, A. L., et al. 2021, AJ, 161, 65, doi: 10.3847/1538-3881/abccc6

Nielsen, M. B., Gizon, L., Schunker, H., & Karoff, C. 2013, A&A, 557, L10, doi: 10.1051/0004-6361/201321912

Owen, J. E. 2020, MNRAS, 498, 5030, doi: 10.1093/mnras/staa2784

Parviainen, H., & Aigrain, S. 2015, MNRAS, 453, 3821, doi: 10.1093/mnras/stv1857

Pecaut, M. J., & Mamajek, E. E. 2013, ApJS, 208, 9, doi: 10.1088/0067-0049/208/1/9

Petigura, E. A., Howard, A. W., Marcy, G. W., et al. 2017, AJ, 154, 107, doi: 10.3847/1538-3881/aa80de

Petigura, E. A., Rogers, J. G., Isaacson, H., et al. 2022, arXiv e-prints, arXiv:2201.10020. https://arxiv.org/abs/2201.10020

Rampalli, R., Agüeros, M. A., Curtis, J. L., et al. 2021, ApJ, 921, 167, doi: 10.3847/1538-4357/ac0c1e

Rebull, L. M., Stauffer, J. R., Hillenbrand, L. A., et al. 2017, ApJ, 839, 92, doi: 10.3847/1538-4357/aa6aa4

Rebull, L. M., Stauffer, J. R., Bouvier, J., et al. 2016a, AJ, 152, 114, doi: 10.3847/0004-6256/152/5/114

—. 2016b, AJ, 152, 113, doi: 10.3847/0004-6256/152/5/113

Ricker, G. R., Winn, J. N., Vanderspek, R., et al. 2014, in Society of Photo-Optical Instrumentation Engineers (SPIE) Conference Series, Vol. 9143, 20, doi: 10.1117/12.2063489

Riello, M., De Angeli, F., Evans, D. W., et al. 2021, A&A, 649, A3, doi: 10.1051/0004-6361/202039587

Rizzuto, A. C., Mann, A. W., Vanderburg, A., Kraus, A. L., & Covey, K. R. 2017, AJ, 154, 224, doi: 10.3847/1538-3881/aa9070

Santos, A. R. G., Breton, S. N., Mathur, S., & García, R. A. 2021, ApJS, 255, 17, doi: 10.3847/1538-4365/ac033f

Santos, A. R. G., García, R. A., Mathur, S., et al. 2019, ApJS, 244, 21, doi: 10.3847/1538-4365/ab3b56

Schlafly, E. F., & Finkbeiner, D. P. 2011, ApJ, 737, 103, doi: 10.1088/0004-637X/737/2/103

Skrutskie, M. F., Cutri, R. M., Stiening, R., et al. 2006, AJ, 131, 1163, doi: 10.1086/498708

Smith, J. C., Stumpe, M. C., Van Cleve, J. E., et al. 2012, PASP, 124, 1000, doi: 10.1086/667697

Stanford-Moore, S. A., Nielsen, E. L., De Rosa, R. J., Macintosh, B., & Czekala, I. 2020, ApJ, 898, 27, doi: 10.3847/1538-4357/ab9a35

Stassun, K. G., Oelkers, R. J., Pepper, J., et al. 2018, AJ, 156, 102, doi: 10.3847/1538-3881/aad050

Stassun, K. G., Oelkers, R. J., Paegert, M., et al. 2019, AJ, 158, 138, doi: 10.3847/1538-3881/ab3467

Stumpe, M. C., Smith, J. C., Van Cleve, J. E., et al. 2012, PASP, 124, 985, doi: 10.1086/667698

Tofflemire, B. M., Mathieu, R. D., & Johns-Krull, C. M. 2019, AJ, 158, 245, doi: 10.3847/1538-3881/ab4f7d

Tofflemire, B. M., Rizzuto, A. C., Newton, E. R., et al. 2021, AJ, 161, 171, doi: 10.3847/1538-3881/abdf53

Tran, Q. H., Bowler, B. P., Cochran, W. D., et al. 2021, AJ, 161, 173, doi: 10.3847/1538-3881/abe041

Tull, R. G., MacQueen, P. J., Sneden, C., & Lambert, D. L. 1995, PASP, 107, 251, doi: 10.1086/133548

Twicken, J. D., Jenkins, J. M., Seader, S. E., et al. 2016, AJ, 152, 158, doi: 10.3847/0004-6256/152/6/158

Van Cleve, J. E., Howell, S. B., Smith, J. C., et al. 2016, PASP, 128, 075002, doi: 10.1088/1538-3873/128/965/075002

van Saders, J. L., Ceillier, T., Metcalfe, T. S., et al. 2016, Nature, 529, 181, doi: 10.1038/nature16168

Walkowicz, L. M., & Basri, G. S. 2013, MNRAS, 436, 1883, doi: 10.1093/mnras/stt1700

Wood, M. L., Mann, A. W., & Kraus, A. L. 2021, AJ, 162, 128, doi: 10.3847/1538-3881/ac0ae9

Yee, S. W., Petigura, E. A., & von Braun, K. 2017, ApJ, 836, 77, doi: 10.3847/1538-4357/836/1/77

Ziegler, C., Tokovinin, A., Briceño, C., et al. 2020, AJ, 159, 19, doi: 10.3847/1538-3881/ab55e9

Table 5.

Gaia EDR3	α	δ	Gmag	$V_{\rm off}$	Spectral[a]	TESS[b]	Kepler[b]	π	σ_π	$P_{\rm rot}$	$\sigma_{P_{\rm rot}}$	$P_{\rm rot}$[c]	Li	$\sigma_{\rm li}$	RV	$\sigma_{\rm RV}$	RV[d]
	(J2016)	(J2016)	(mag)	(km/s)	Class			(mas)	(mas)	(days)	(days)	ref	(mÅ)	(mÅ)	(km/s)	(km/s)	ref
2052827207364859264	290.44063	38.52357	12.605	0.000	G7.3	Y	Y	3.057	0.009	4.665	0.035	2, 3	134.0	18.0	-26.09	0.03	5
2101379205604338688	289.62522	40.70874	14.788	3.102	K5.3	N	Y	3.015	0.019	9.23	0.66	3	<40	...	-27.15	0.1	9
2052804323776522624	290.46921	38.20201	18.977	3.554	M3.9	N	N	3.036	0.172	...	...	...	...	...	...	...	...
2100939194794324608	289.80783	38.95042	10.829	0.478	F4.4	Y	N	3.024	0.012	...	...	...	<20	...	-27.03	0.18	5
2052954995531623040	291.28017	39.20070	14.355	4.348	K4.7	N	Y	3.055	0.016	13.849	0.035	1, 2, 3	...	...	...	...	...
2100967537279486336	290.14895	39.26079	18.451	3.806	M4.1	N	N	3.094	0.136	...	...	...	...	...	...	...	...
2051102868195719168	290.43983	37.73210	17.503	0.516	M3.2	N	N	3.019	0.069	...	...	...	...	...	...	...	...
2053037660761796096	290.86832	39.65124	17.902	0.605	M3.7	N	N	3.067	0.084	...	...	...	...	...	...	...	...
2052645379929910144	290.91118	38.33558	13.747	0.988	K2.8	N	Y	2.996	0.033	7.84	0.784	4	...	...	-27.05	3.02	6
2052559995978462208	291.61221	37.79730	11.75	3.744	F9.3	Y	Y	3.082	0.01	10.55	0.552	1, 3	...	...	-16.07	0.95	7
2100996639982248320	289.86923	39.64549	19.678	2.692	M3.7	N	N	3.083	0.322	...	...	...	...	...	...	...	...
2099426507311747200	289.44803	38.58778	17.385	0.897	M3.1	N	N	3.114	0.07	...	...	...	...	...	...	...	...
2052684790548985728	291.78531	38.46727	14.077	0.641	K4.6	N	N	3.009	0.038	...	...	...	...	...	...	...	...
2052858307226740352	290.54042	38.81248	11.42	0.350	F9.4	N	Y	2.978	0.019	4.419	0.347	2	<70	...	-25.11	0.16	5
2053046907832580992	291.12056	39.64699	16.939	0.389	M2.6	N	N	3.003	0.046	...	...	...	...	...	...	...	...
2099289446315734784	288.78892	37.90815	10.835	0.240	F4.3	Y	N	3.099	0.011	...	...	...	<20	...	-27.46	0.13	5
2053001690416510720	291.56724	39.60279	18.441	0.159	M4.5	N	N	3.104	0.122	...	...	...	...	...	...	...	...
2052887478644057472	289.93506	38.64045	14.636	0.506	K5.3	N	Y	3.145	0.018	1.529	0.017	1, 2, 3	...	...	-30.74	5.17	6
2052807794117101312	290.53790	38.25958	14.736	3.776	K5.4	N	Y	2.971	0.031	7.595	0.222	1, 2, 3	...	...	...	...	...
2052517145084325888	291.05028	37.29823	19.789	0.587	M4.1	N	N	3.002	0.33	...	...	...	...	...	...	...	...
2053028319213859072	290.64738	39.41039	20.044	2.510	M2.4	N	N	3.141	0.449	...	...	...	...	...	...	...	...
2053384286102387200	291.63783	39.87497	16.359	1.316	M2.7	N	N	3.008	0.037	...	...	...	...	...	...	...	...
2099371153774293888	288.14566	38.42085	13.864	0.791	K3.3	N	Y	3.018	0.025	7.556	0.049	1, 2, 3	...	...	-33.36	10.0	6
2053444896681432704	291.46297	40.21305	17.606	4.287	M3.8	N	N	3.093	0.076	...	...	...	...	...	...	...	...
2051172511083958400	289.48378	37.33728	20.024	1.298	M2.3	N	N	3.137	0.394	...	...	...	...	...	...	...	...
2053078450072688000	291.08713	40.21787	15.897	4.996	M0.3	Y	Y	3.112	0.03	26.792	0.394	1, 2, 3	...	...	...	...	...
2101290488760369920	288.83978	40.10791	16.391	4.143	M2.5	N	N	3.024	0.135	2.254	0.225	4	...	...	...	...	...
2101187134663932544	290.69156	40.59631	19.858	4.582	M3.3	N	N	3.084	0.312	...	...	...	...	...	...	...	...
2099510688671686656	288.69978	39.12272	18.18	2.451	M4.1	N	N	3.145	0.326	...	...	4	...	...	...	...	...
2051660453728442112	292.99289	37.59955	18.4	4.180	M3.7	N	N	3.031	0.111	...	...	...	...	...	...	...	...
2051357984953957504	289.74650	38.12294	19.944	4.604	M3.5	N	N	2.944	0.315	...	...	...	...	...	...	...	...
2101386764746445440	290.06201	40.66262	13.414	0.530	K1.9	N	Y	3.103	0.011	6.956	0.054	1, 2, 3	...	...	-29.12	4.59	6
2099551817277084800	287.59245	38.47925	11.268	3.720	G1.7	Y	Y	3.019	0.019	17.73	1.773	4	...	...	9.15	0.38	7
2099422624663498752	289.22523	38.52196	18.873	4.687	M3.5	N	N	2.946	0.352	...	...	...	...	...	...	...	...
2101515373247903488	290.78512	40.61023	16.586	0.442	M2.1	N	N	3.119	0.04	...	...	...	...	...	...	...	...
2101379205604335104	289.61835	40.71217	10.781	3.281	F3.7	Y	Y	3.015	0.012	1.041	0.104	4	...	...	-28.64	4.84	6
2099491584657132544	288.89020	38.86011	14.495	4.403	K5.2	N	N	2.948	0.017	...	...	...	...	...	...	...	...

Table 5 *continued*

Table 5 *(continued)*

Gaia EDR3	α	δ	Gmag	$V_{\rm off}$	Spectral[a]	TESS[b]	Kepler[b]	π	σ_π	$P_{\rm rot}$	$\sigma_{P_{\rm rot}}$	$P_{\rm rot}$[c]	Li	$\sigma_{\rm li}$	RV	$\sigma_{\rm RV}$	RV[d]
	(J2016)	(J2016)	(mag)	(km/s)	Class			(mas)	(mas)	(days)	(days)	ref	(mÅ)	(mÅ)	(km/s)	(km/s)	ref
2052858307222586880	290.53999	38.81210	12.551	0.678	...	N	Y	2.929	0.02	...	...	...	...	...	-27.2	0.05	8
2101187924942527232	290.59545	40.61559	18.766	0.187	M4.1	N	N	3.134	0.154	...	...	...	...	...	...	...	...
2053117169195406464	292.90398	39.25458	19.135	4.379	M4.8	N	N	3.139	0.206	...	...	...	...	...	...	...	...
2052807798410325376	290.53830	38.25984	15.184	3.513	...	N	Y	2.926	0.034	...	...	...	...	...	...	...	...
2053500112781924352	291.76006	40.95293	14.855	0.712	K5.4	N	N	3.057	0.019	7.674	0.767	4	...	...	...	...	...
2101130883477144320	290.53660	40.34722	17.688	3.247	M3.5	N	N	2.955	0.072	...	...	...	...	...	...	...	...
2051975983509190016	293.59015	37.53718	18.726	1.161	M3.4	N	N	3.03	0.137	...	...	...	...	...	...	...	...
2100429536793570944	287.23632	39.56530	17.228	2.013	M3.2	N	N	3.09	0.066	...	...	...	...	...	...	...	...
2099625686416174080	287.21171	38.93991	17.714	4.263	M2.4	N	N	3.004	0.308	...	...	...	...	...	...	...	...
2101136449751777152	290.65080	40.41471	17.517	4.625	M3.5	N	N	3.17	0.067	...	...	...	...	...	...	...	...
2051976189671275008	293.59444	37.57975	17.915	4.322	G9.9	N	N	3.014	0.322	...	...	...	...	...	...	...	...
2052065490625516672	293.96062	38.21336	19.339	4.543	M5.1	N	N	3.032	0.232	...	...	...	...	...	...	...	...
2050726216742395264	288.61584	36.22530	17.324	3.622	M3.2	N	N	3.016	0.061	...	...	...	...	...	...	...	...
2051982614938994176	293.91062	37.73004	16.179	4.263	M1.1	N	N	3.074	0.037	...	...	...	...	...	...	...	...
2052596000688765056	290.88294	37.81954	18.914	3.356	M4.3	N	N	3.211	0.171	...	...	...	...	...	...	...	...
2101027602401894784	289.29738	39.57910	14.506	2.717	K5.3	N	Y	3.199	0.016	15.838	0.124	1, 3	...	...	...	...	...
2099516529827404544	289.06408	39.25474	17.771	3.187	M4.0	N	N	2.926	0.078	...	...	4	...	...	...	...	...
2100368479537871872	286.96423	38.78460	12.764	4.039	G8.4	N	Y	3.01	0.01	10.625	0.082	1, 2, 3	...	...	-0.49	1.98	7
2051982340061089536	293.93921	37.70142	11.118	4.398	F6.0	Y	N	3.043	0.015	...	...	...	...	...	14.5	1.22	7
2052608133965272192	290.49563	37.88866	11.489	0.351	F6.7	Y	Y	2.913	0.014	1.399	0.011	1, 2, 3	72.0	16.0	-26.62	0.1	5
2051499340914162944	292.58691	36.65583	18.966	4.501	M3.6	N	N	3.138	0.173	...	...	...	...	...	...	...	...
2099676195231124736	288.37220	39.03775	8.022	0.460	B8.5	Y	N	3.19	0.027	...	...	4	...	...	-23.84	0.21	8
2101498055932035584	290.93940	40.42672	19.409	0.648	M3.9	N	N	2.944	0.237	...	...	...	...	...	...	...	...
2101187473966365312	290.69120	40.63618	18.454	0.248	M4.1	N	N	2.951	0.123	...	...	...	...	...	...	...	...
2053343294931373184	293.04096	40.53396	17.915	4.679	M3.5	N	N	3.005	0.084	...	...	...	...	...	...	...	...
2101459298154930816	289.77613	41.14883	12.288	2.013	G3.1	Y	Y	3.147	0.01	6.502	0.021	1, 2, 3	...	...	-31.44	1.55	7
2050796997800195200	288.15730	36.57569	19.55	1.907	M4.1	N	N	3.158	0.259	...	...	...	...	...	...	...	...
2050008265711307648	290.25154	35.46237	18.884	3.316	M3.7	N	N	3.01	0.169	...	...	...	...	...	...	...	...
2051554316501700992	292.92786	36.84369	19.32	4.618	M3.6	N	N	2.96	0.245	...	...	...	...	...	...	...	...
2051555381654674816	293.04802	36.87642	19.867	3.756	M3.2	N	N	2.96	0.383	...	...	...	...	...	...	...	...
2099477600243489408	288.44081	38.81109	16.85	4.634	M3.1	N	N	3.218	0.054	...	...	...	...	...	...	...	...
2098740205899557248	287.17565	36.50723	14.721	1.246	K5.5	N	N	3.049	0.019	...	...	...	...	...	...	...	...
2050250364427230336	290.97922	36.84736	19.939	3.570	M3.6	N	N	3.22	0.348	...	...	...	...	...	...	...	...
2049971122838191744	291.52801	36.11546	20.255	4.593	M4.2	N	N	3.182	0.475	...	...	...	...	...	...	...	...
2048412908706584704	293.33621	36.05485	19.811	4.683	M3.7	N	N	3.059	0.353	...	...	...	...	...	...	...	...
2101713525854617600	291.54762	41.70727	20.338	1.833	M2.6	N	N	3.105	0.477	...	...	...	...	...	...	...	...
2051859847591509632	293.15138	37.96614	17.899	3.376	M3.4	N	N	2.927	0.089	...	...	...	...	...	...	...	...
2053485368151986560	291.70203	40.54178	19.786	4.379	M4.2	N	N	3.201	0.271	...	...	...	...	...	...	...	...
2049856365599578112	291.88064	35.32776	20.199	3.467	M3.4	N	N	3.055	0.38	...	...	...	...	...	...	...	...

Table 5 *continued*

Table 5 *(continued)*

Gaia EDR3	α	δ	Gmag	$V_{\rm off}$	Spectral[a]	TESS[b]	Kepler[b]	π	σ_π	$P_{\rm rot}$	$\sigma_{P_{\rm rot}}$	$P_{\rm rot}$[c]	Li	$\sigma_{\rm li}$	RV	$\sigma_{\rm RV}$	RV[d]
	(J2016)	(J2016)	(mag)	(km/s)	Class			(mas)	(mas)	(days)	(days)	ref	(mÅ)	(mÅ)	(km/s)	(km/s)	ref
2049898658148818560	292.06502	35.76656	20.066	1.536	M3.7	N	N	3.145	0.421	...	...	...	...	...	...	...	...
2049812385145800576	291.00696	35.15286	17.622	4.287	M3.7	N	N	3.076	0.076	...	...	...	...	...	...	...	...
2101045843121578112	289.94136	39.77116	19.278	1.929	M5.1	N	N	3.235	0.242	...	...	...	...	...	...	...	...
2048415794911879552	293.30144	36.15446	18.307	4.764	M4.0	N	N	3.008	0.122	...	...	...	...	...	...	...	...
2099188291245626112	286.41346	37.82263	12.835	1.336	G9.2	N	Y	3.128	0.01	5.323	0.044	1, 2, 3	206.0	18.0	-25.92	0.03	5
2099794736328175360	288.28803	39.89458	15.28	1.385	M0.1	N	N	3.212	0.129	7.259	0.726	4	...	...	...	...	...
2099794740628450304	288.28630	39.88271	13.386	2.816	K2.3	N	N	3.213	0.021	7.44	0.744	4	...	...	-26.68	6.44	6
2101574781231282048	290.98190	41.00074	19.479	0.657	M3.9	N	N	2.934	0.254	...	...	...	...	...	...	...	...
2098898638653849984	287.37642	37.07199	15.751	2.272	G7.6	N	N	2.951	0.391	...	...	...	...	...	...	...	...
2101600447956566272	291.18180	41.19366	20.003	3.194	M0.6	N	N	3.187	0.387	...	...	...	...	...	...	...	...
2050765077606951936	287.92623	36.40692	15.165	4.438	K7.6	N	N	3.174	0.027	...	...	...	...	...	...	...	...
2099067482406884480	286.28303	37.35236	13.746	2.531	K3.3	N	Y	3.106	0.013	14.899	1.49	4	...	...	...	...	...
2102189236436155648	288.28074	41.59781	18.367	2.335	M3.4	N	N	3.106	0.114	...	...	...	...	...	...	...	...
2052805015271414144	290.33934	38.20789	16.895	3.818	M3.2	N	N	3.26	0.082	...	...	...	...	...	...	...	...
2051432515527787648	292.80905	36.28937	14.604	3.741	K7.2	N	N	3.178	0.102	10.752	1.075	4	...	...	...	...	...
2101841756399109376	290.50906	42.08187	19.23	4.591	M4.0	N	N	3.029	0.201	...	...	...	...	...	...	...	...
2101401294615346048	290.06632	41.03278	18.343	0.954	M4.8	N	N	3.205	0.115	...	...	...	...	...	...	...	...
2050996902763454720	290.48481	36.98170	17.769	4.269	K0.4	N	N	2.892	0.464	...	...	...	...	...	...	...	...
2102066224271232640	288.54303	40.55671	17.727	2.355	M4.1	N	N	3.208	0.125	...	...	...	...	...	...	...	...
2102626051789293184	289.48005	42.09400	16.756	1.067	M1.1	N	N	3.045	0.044	...	...	...	...	...	...	...	...
2052677742500567040	291.71671	38.32551	18.864	0.768	M4.1	N	N	3.258	0.176	...	...	...	...	...	...	...	...
2101641026810864896	291.74997	41.31697	16.814	0.429	M2.8	N	N	3.183	0.043	...	...	...	...	...	...	...	...
2050508749656858752	288.65522	35.96429	19.486	3.062	WD	N	N	2.944	0.224	...	...	...	...	...	...	...	...
2051282943283164928	289.72714	37.85968	19.862	4.159	M5.4	N	N	3.262	0.29	...	...	...	...	...	...	...	...
2049661232351248000	289.25314	35.06804	19.659	1.966	M3.6	N	N	3.117	0.297	...	...	...	...	...	...	...	...
2049851761393686272	291.89812	35.22806	19.954	3.436	M3.6	N	N	3.132	0.304	...	...	...	...	...	...	...	...
2100669883163024384	285.93631	39.77662	20.103	3.728	M2.9	N	N	3.084	0.476	...	...	...	...	...	...	...	...
2050127876250166400	290.99730	35.84448	20.296	4.190	M1.6	N	N	3.204	0.447	...	...	...	...	...	...	...	...
2101581786320148736	290.56567	40.93404	20.178	3.940	M3.3	N	N	2.911	0.368	...	...	...	...	...	...	...	...
2049644228586014720	289.45514	34.93926	17.264	3.197	K1.8	N	N	3.013	0.334	...	...	...	...	...	...	...	...
2049640311574098816	289.46804	34.83151	11.621	1.523	F9.0	Y	N	3.045	0.012	...	...	...	83.0	11.0	-21.37	0.04	5
2049610792258197888	290.24711	34.99724	17.003	4.179	M3.1	N	N	2.985	0.052	...	...	...	...	...	...	...	...
2099415168600260224	289.02984	38.61517	17.833	4.217	...	N	N	3.267	0.115	...	...	...	...	...	...	...	...
2099188355664401280	286.40002	37.82268	16.209	1.010	M1.1	N	N	3.175	0.033	...	...	...	...	...	...	...	...
2077329587775173632	294.40388	40.85595	18.799	1.898	K2.9	N	N	3.092	0.463	...	...	...	...	...	...	...	...
2076165514199980544	295.23985	38.90275	16.175	3.502	M1.0	N	N	3.014	0.034	...	...	...	...	...	...	...	...
2098766383721551232	286.39864	36.35114	19.464	2.185	M3.9	N	N	3.048	0.231	...	...	...	...	...	...	...	...
2053068554467825792	290.96130	39.96478	14.875	0.393	K5.6	N	Y	3.262	0.018	9.749	0.12	1, 2, 3	...	...	...	...	...
2051433099643453824	292.86453	36.35512	16.324	3.473	M1.7	N	N	3.206	0.037	...	...	...	...	...	...	...	...

Table 5 *continued*

Table 5 *(continued)*

Gaia EDR3	α	δ	Gmag	$V_{\rm off}$	Spectral[a]	TESS[b]	Kepler[b]	π	σ_π	$P_{\rm rot}$	$\sigma_{P_{\rm rot}}$	$P_{\rm rot}$[c]	Li	$\sigma_{\rm li}$	RV	$\sigma_{\rm RV}$	RV[d]
	(J2016)	(J2016)	(mag)	(km/s)	Class			(mas)	(mas)	(days)	(days)	ref	(mÅ)	(mÅ)	(km/s)	(km/s)	ref
2049794410699814528	290.46408	34.94806	18.838	4.837	M3.6	N	N	2.982	0.155	...	...	...	...	...	...	...	...
2102386564412516864	287.94048	41.83689	19.375	1.368	M4.4	N	N	3.106	0.247	...	...	...	...	...	...	...	...
2101894498601593344	290.25264	42.29074	14.121	3.373	K4.3	N	N	3.129	0.013	...	...	...	...	...	-10.66	3.41	6
2099459801898399104	288.62787	38.60796	17.016	2.544	M3.0	N	N	3.269	0.216	...	...	...	...	...	...	...	...
2101558146822313600	291.35381	41.11857	12.001	0.696	G0.9	N	N	3.226	0.009	3.015	0.301	4	138.0	12.0	-26.33	0.04	5
2077667275280949760	292.79897	42.02346	14.567	3.621	K7.5	N	N	3.102	0.019	...	...	...	...	...	3.61	0.05	8
2048509356487226240	293.47600	36.20824	17.752	4.669	M3.9	N	N	3.184	0.083	...	...	...	...	...	...	...	...
2049637150478083584	289.35761	34.80607	15.226	3.671	M0.8	N	N	3.131	0.147	...	...	...	...	...	...	...	...
2052270755704597504	293.50351	38.41166	12.65	3.648	G2.8	N	N	2.896	0.01	...	...	...	...	...	-29.68	3.1	7
2102345092202557440	287.59128	41.37192	14.606	3.233	K7.1	N	N	3.177	0.052	0.631	0.063	4	...	...	...	...	...
2077664178604808448	292.85009	41.89001	19.06	4.127	M3.7	N	N	3.15	0.184	...	...	...	...	...	...	...	...
2048116732063862016	293.47266	35.22558	15.191	4.442	K5.8	N	N	3.026	0.021	0.535	0.054	4	...	...	...	...	...
2099807346353626880	285.58136	37.40294	18.807	4.117	M4.0	N	N	2.993	0.164	...	...	...	...	...	...	...	...
2099246153044663552	288.13089	37.34614	17.079	0.805	M2.8	N	N	2.877	0.057	...	...	...	...	...	...	...	...
2099930732173359744	285.37325	38.36397	18.773	4.707	M3.4	N	N	3.144	0.148	...	...	...	...	...	...	...	...
2048235548040376704	294.47474	35.70107	12.166	3.821	G9.0	Y	N	3.073	0.013	...	...	...	...	...	-48.93	2.6	7
2101723971214893312	291.36851	41.80634	20.135	1.788	M1.1	N	N	2.925	0.417	...	...	...	...	...	...	...	...
2073189789067905408	295.90726	39.04507	17.406	3.106	M3.0	N	N	3.034	0.079	...	...	...	...	...	...	...	...
2048101094081242240	293.33299	34.85106	20.023	4.497	M3.6	N	N	3.054	0.419	...	...	...	...	...	...	...	...
2077298114252198272	294.19000	40.65083	16.661	1.773	M3.7	N	N	3.2	0.047	...	...	...	...	...	...	...	...
2099466635187892352	288.70100	38.73065	20.023	4.605	M3.6	N	N	3.295	0.395	...	...	...	...	...	...	...	...
2103373307377627776	285.33978	40.32992	13.848	3.732	K2.6	N	Y	3.039	0.03	35.463	5.026	1	...	...	-24.47	4.05	6
2103748756239087104	285.35967	40.39370	15.689	2.636	K7.8	N	Y	3.042	0.029	25.58	0.255	1, 3	...	...	...	...	...
2048902741138843136	295.23828	37.11420	19.023	1.188	M5.2	N	N	2.978	0.181	...	...	...	...	...	...	...	...
2099705783264969600	288.57042	39.35435	15.371	4.661	K7.2	N	N	2.856	0.023	4.129	0.413	4	...	...	...	...	...
2048921295383318784	294.99056	37.33531	19.543	3.854	M3.5	N	N	3.189	0.247	...	...	...	...	...	...	...	...
2099663688286415488	288.24115	38.74287	18.172	3.321	M3.7	N	N	3.291	0.109	...	...	...	...	...	...	...	...
2101393602330328960	290.01834	40.88420	16.336	4.930	M1.0	N	N	3.274	0.098	...	...	...	...	...	...	...	...
2046668228567081728	292.16704	34.38497	16.821	3.973	M2.7	N	N	3.113	0.047	...	...	...	...	...	...	...	...
2048306359159003008	293.45553	35.36816	19.442	4.558	M3.7	N	N	3.176	0.268	...	...	...	...	...	...	...	...
2050912583964302336	289.53436	36.45761	16.37	3.963	M0.8	N	N	2.863	0.038	...	...	...	...	...	...	...	...
2053549968761310720	292.95777	41.01805	12.649	0.434	G8.5	N	Y	3.242	0.011	5.43	0.026	1, 2, 3	177.0	16.0	-26.59	0.03	5
2073178931389394176	296.12981	38.96220	18.412	2.766	M3.4	N	Y	3.096	0.123	...	...	...	...	...	...	...	...
2100503994346936448	286.71911	40.01675	19.895	3.861	M1.3	N	Y	2.904	0.488	...	...	...	...	...	...	...	...
2052631876552612992	291.23955	38.25029	13.329	1.688	K3.1	N	Y	2.837	0.012	8.049	0.1	1, 2, 3	...	...	...	...	...
2076686029877527808	294.99237	41.32934	15.949	4.227	K2.1	N	N	3.039	0.416	...	...	...	...	...	...	...	...
2052970934148672384	291.11311	39.30349	18.409	0.454	M4.1	N	N	3.313	0.114	...	...	...	...	...	...	...	...
2077635625662537856	293.46960	42.09709	12.006	2.734	F9.7	N	Y	2.981	0.011	10.468	0.598	1, 3	...	...	6.88	0.79	7
2053479943611910656	291.86027	40.61269	19.666	0.524	M3.8	N	N	3.284	0.252	...	...	...	...	...	...	...	...

Table 5 *continued*

Table 5 *(continued)*

Gaia EDR3	α	δ	Gmag	$V_{\rm off}$	Spectral[a]	TESS[b]	Kepler[b]	π	σ_π	$P_{\rm rot}$	$\sigma_{P_{\rm rot}}$	$P_{\rm rot}$[c]	Li	$\sigma_{\rm li}$	RV	$\sigma_{\rm RV}$	RV[d]
	(J2016)	(J2016)	(mag)	(km/s)	Class			(mas)	(mas)	(days)	(days)	ref	(mÅ)	(mÅ)	(km/s)	(km/s)	ref
2072871785381251968	296.20200	37.90509	18.138	2.587	M3.6	N	N	3.039	0.103	...	...	...	...	...	...	...	...
2046575835238489984	293.11918	34.45978	19.18	3.120	G8.8	N	N	3.044	0.361	...	...	...	...	...	...	...	...
2073103408681272320	296.31219	38.47227	18.115	4.777	M4.2	N	N	3.042	0.114	...	...	...	...	...	...	...	...
2101938032388591616	290.62441	42.22492	16.921	0.749	M2.9	N	N	3.218	0.05	...	...	...	...	...	...	...	...
2105445783717260800	286.87475	42.27021	14.923	2.248	K7.0	N	Y	3.07	0.032	4.368	0.039	1, 3	...	...	...	...	...
2049303173820385664	290.21307	33.93032	16.802	2.902	M3.3	N	N	3.033	0.392	...	...	...	...	...	...	...	...
2102705796441216512	289.02294	42.76164	16.838	1.817	M1.8	N	Y	3.153	0.158	...	...	...	...	...	...	...	...
2053111018802015744	292.41151	39.28452	19.103	4.116	M4.1	N	N	3.308	0.183	...	...	...	...	...	...	...	...
2052226397286715648	294.57619	39.13470	19.705	3.671	M2.5	N	N	2.894	0.425	...	...	...	...	...	...	...	...
2094077825620035456	284.64331	37.83481	14.274	4.574	K4.5	N	N	3.107	0.016	...	...	...	...	...	-34.79	3.33	6
2101586978937793792	290.58410	41.07407	20.24	3.283	M3.1	N	N	3.285	0.441	...	...	...	...	...	...	...	...
2052359021571311872	293.05992	39.02231	18.166	4.774	M3.6	N	N	3.3	0.42	...	...	...	...	...	...	...	...
2076520793894027904	294.50512	40.13601	18.132	2.956	M3.7	N	N	2.903	0.113	...	...	...	...	...	...	...	...
2092738551739448448	286.23905	35.94755	19.03	3.858	M3.7	N	N	2.954	0.185	...	...	...	...	...	...	...	...
2053548693152172928	293.15127	41.06617	19.95	1.145	M3.4	N	N	3.256	0.4	...	...	4	...	...	...	...	...
2049505518311453696	288.81921	34.29626	20.156	2.486	M3.3	N	N	2.973	0.474	...	...	...	...	...	...	...	...
2048163353926979840	294.80566	35.28248	18.597	4.213	M4.3	N	N	3.08	0.148	...	...	...	...	...	...	...	...
2049069046572592896	294.90648	37.66794	18.77	3.157	...	N	N	3.239	0.218	...	...	...	...	...	...	...	...
2077663113450387072	292.60935	41.95511	18.774	0.741	M3.9	N	N	3.225	0.158	...	...	...	...	...	...	...	...
2048403842033278464	293.10637	35.84932	14.666	2.661	K7.1	N	N	3.252	0.182	...	...	...	...	...	...	...	...
2049596429885240064	290.00013	34.66415	19.694	4.331	M3.6	N	N	2.921	0.32	...	...	...	...	...	...	...	...
2103950413544342144	286.44627	42.04798	18.503	2.664	M3.6	N	N	3.007	0.121	...	...	...	...	...	...	...	...
2049371652780179968	289.84622	34.22568	14.288	4.484	K4.3	N	N	2.955	0.015	...	...	...	...	...	...	...	...
2048376766558231040	293.08213	35.73130	16.705	2.181	K3.0	N	N	2.895	0.432	...	...	...	...	...	...	...	...
2049266683779523072	289.39208	33.86472	15.636	3.771	K7.6	N	N	3.018	0.027	7.259	0.726	4	...	...	...	...	...
2077635629961702400	293.47052	42.09652	12.305	2.591	G1.7	N	Y	2.948	0.011	11.223	0.26	1, 3	...	...	7.64	2.06	7
2073127219968464512	296.47747	38.83061	18.841	4.855	M4.5	N	N	3.122	0.157	...	...	...	...	...	...	...	...
2048096803406416640	293.60621	34.94786	17.863	4.935	...	N	N	3.179	0.117	...	...	...	...	...	...	...	...
2049262182644653824	289.46816	33.77830	18.775	0.991	M3.9	N	N	3.033	0.166	...	...	...	...	...	...	...	...
2048317736525727488	293.04452	35.35775	12.008	2.441	G8.8	N	N	3.235	0.01	5.967	0.597	4	108.0	17.0	-25.0	3.0	5
2046853599359016832	292.63607	35.10576	16.144	4.455	M1.3	N	N	3.231	0.034	...	...	...	...	...	...	...	...
2051615859085757568	292.92783	37.20435	18.25	4.935	M4.3	N	N	3.305	0.124	...	...	...	...	...	...	...	...
2046614897947238016	291.93056	33.80261	18.734	4.481	M4.0	N	N	3.06	0.164	...	...	...	...	...	...	...	...
2046845215582445824	292.28353	35.14966	14.37	4.743	K5.0	N	N	2.901	0.016	...	...	...	...	...	...	...	...
2048258294180066688	294.60031	35.71329	19.99	4.871	M3.7	N	N	2.951	0.47	...	...	...	...	...	...	...	...
2046553741917468928	292.66337	34.19332	19.924	3.549	M3.6	N	N	2.994	0.356	...	...	...	...	...	...	...	...
2103748756240476672	285.35982	40.39209	19.544	2.852	M4.0	N	Y	2.95	0.346	...	...	...	...	...	...	...	...
2048496304087509376	294.30790	36.49436	18.4	2.095	K2.0	N	N	2.899	0.42	...	...	...	...	...	...	...	...
2049241395011726848	289.34502	33.74147	19.092	4.238	M3.1	N	N	3.033	0.211	...	...	...	...	...	...	...	...

Table 5 *continued*

Table 5 *(continued)*

Gaia EDR3	α	δ	Gmag	V_{off}	Spectral[a]	TESS[b]	Kepler[b]	π	σ_π	P_{rot}	$\sigma_{P_{\mathrm{rot}}}$	P_{rot}[c]	Li	σ_{li}	RV	σ_{RV}	RV[d]
	(J2016)	(J2016)	(mag)	(km/s)	Class			(mas)	(mas)	(days)	(days)	ref	(mÅ)	(mÅ)	(km/s)	(km/s)	ref
2049772596567899008	290.66676	34.67603	13.407	4.450	K2.6	N	N	2.908	0.011	3.397	0.34	4	...	...	...	...	...
2105440006984005120	286.77824	42.08943	18.56	4.706	M4.4	N	N	3.175	0.124	...	...	...	...	...	...	...	...
2102245856985443328	289.35214	41.84996	19.765	2.112	M4.3	N	N	2.883	0.304	...	...	...	...	...	...	...	...
2102345298366272768	287.58664	41.38399	18.987	2.266	M4.0	N	N	3.256	0.166	...	...	...	...	...	...	...	...
2101386730386700800	290.03838	40.65253	16.584	0.373	M2.4	N	N	3.318	0.042	...	...	...	...	...	...	...	...
2049868838198454016	291.82534	35.41762	18.353	3.964	M4.0	N	N	2.874	0.118	...	...	...	...	...	...	...	...
2100920258280235520	286.67814	41.58228	19.04	4.072	M4.3	N	N	3.217	0.173	...	...	...	...	...	...	...	...
2052100125245266048	294.61773	38.16003	15.451	4.509	M0.2	N	N	3.277	0.022	...	...	...	...	...	...	...	...
2125817844397609216	292.06886	42.93310	13.724	0.646	K3.2	N	Y	3.18	0.011	0.72	0.05	3	...	...	-28.61	4.64	6
2050691062426634752	288.26898	35.86766	17.799	4.747	M3.4	N	N	2.866	0.087	...	...	...	...	...	...	...	...
2100719636059739904	285.77146	39.94893	18.893	2.303	...	N	N	2.902	0.205	...	...	...	...	...	...	...	...
2048868965507939840	294.82361	36.82820	17.813	3.342	M4.1	N	N	3.246	0.169	...	...	...	...	...	...	...	...
2048064264742088576	294.43151	35.08663	10.209	4.138	F4.5	Y	N	3.175	0.015	...	...	...	...	...	7.17	0.84	7
2105484812081360512	286.85490	42.71288	19.108	4.851	M4.4	N	N	3.014	0.178	...	...	...	...	...	...	...	...
2052358991509805056	293.05244	39.01205	19.869	3.330	K7.2	N	N	3.33	0.452	...	...	...	...	...	...	...	...
2046865350389884672	292.55629	35.31392	15.8	3.420	M0.8	N	N	3.271	0.03	...	...	...	...	...	...	...	...
2101929025836317184	290.92568	42.20696	17.303	1.701	M3.3	N	N	3.267	0.061	...	...	...	...	...	...	...	...
2126004623933648896	290.92644	43.08124	17.578	1.266	M3.0	N	N	2.943	0.071	...	...	...	...	...	...	...	...
2049747273439777664	291.70061	34.90528	17.782	4.678	M3.8	N	N	3.265	0.079	...	...	...	...	...	...	...	...
2102853444538058368	289.03436	43.42979	13.172	3.167	K1.9	N	N	3.002	0.063	...	...	...	...	...	-24.18	3.86	7
2072789807332417152	296.65993	37.45944	19.999	4.109	M3.2	N	N	3.001	0.42	...	...	...	...	...	...	...	...
2125926111928653696	292.34789	43.48464	19.632	3.899	M4.1	N	N	3.09	0.255	...	...	...	...	...	...	...	...
2046543395336781568	293.02397	34.11078	18.49	1.017	M3.4	N	N	2.977	0.135	...	...	...	...	...	...	...	...
2051446190695378048	292.70012	36.44762	19.786	2.362	...	N	N	2.842	0.491	...	...	...	...	...	...	...	...
2047949434505140864	296.36220	36.33189	18.779	4.514	K4.4	N	N	3.076	0.483	...	...	...	...	...	...	...	...
2046633383486064000	291.91075	34.00953	10.146	4.969	WD	Y	N	2.95	0.031	...	...	...	...	...	...	...	...
2049490262585555712	288.69613	33.93594	17.752	4.774	...	N	N	3.178	0.097	...	...	...	...	...	...	...	...
2046235325916931456	291.28254	33.37423	18.3	4.397	M3.3	N	N	3.058	0.127	...	...	...	...	...	...	...	...
2049472773490612096	289.22840	34.12118	16.717	3.577	K1.4	N	N	2.932	0.393	...	...	...	...	...	...	...	...
2073210267465182848	296.60195	38.90562	13.081	4.480	G9.6	N	N	2.962	0.009	...	...	...	...	...	...	...	...
2076730624508859520	296.72133	40.53190	18.212	4.843	M3.8	N	N	3.054	0.112	...	...	...	...	...	...	...	...
2049523763336273792	288.59489	34.46903	19.496	0.984	M1.9	N	N	2.913	0.411	...	...	...	...	...	...	...	...
2049859831635953792	291.69088	35.23091	12.129	4.884	G4.4	N	N	3.29	0.01	3.397	0.34	4	...	...	...	...	...
2047957337248140416	296.51880	36.47964	19.179	4.286	M0.6	N	N	3.099	0.439	...	...	...	...	...	...	...	...
2077531481295134208	294.10723	42.17228	17.62	4.431	M3.2	N	N	2.934	0.066	...	...	...	...	...	...	...	...
2076371603912351488	295.70433	39.97570	15.593	2.290	K7.7	N	Y	3.236	0.025	18.485	0.076	1, 2	...	...	...	...	...
2049003105921386240	295.18284	37.39491	18.265	4.755	M3.8	N	N	2.885	0.107	...	...	...	...	...	...	...	...
2046475573523834752	293.52058	33.87028	18.605	1.870	...	N	N	3.083	0.419	...	...	...	...	...	...	...	...
2046428535039574528	292.16087	33.85574	19.334	3.870	K3.2	N	N	3.182	0.447	...	...	...	...	...	...	...	...

Table 5 *continued*

Table 5 *(continued)*

Gaia EDR3	α	δ	Gmag	$V_{\rm off}$	Spectral[a]	TESS[b]	Kepler[b]	π	σ_π	$P_{\rm rot}$	$\sigma_{P_{\rm rot}}$	$P_{\rm rot}$[c]	Li	$\sigma_{\rm li}$	RV	$\sigma_{\rm RV}$	RV[d]
	(J2016)	(J2016)	(mag)	(km/s)	Class			(mas)	(mas)	(days)	(days)	ref	(mÅ)	(mÅ)	(km/s)	(km/s)	ref
2098758485280057216	286.71481	36.38912	17.276	1.319	M3.3	N	N	3.282	0.064	...	...	...	...	...	...	...	...
2076243785686210176	295.10809	39.46659	13.002	4.264	K1.3	N	Y	2.876	0.024	5.474	0.025	1, 2, 3	...	...	-17.64	6.87	6
2046455056449426816	292.51811	33.88864	19.117	3.099	M3.2	N	N	3.174	0.286	...	...	...	...	...	...	...	...
2072856705763693568	296.28591	37.68820	15.291	4.171	M0.0	N	N	2.94	0.023	...	...	...	...	...	...	...	...
2077320787375508992	294.23449	40.65316	18.61	2.462	K4.4	N	N	3.284	0.337	...	...	...	...	...	...	...	...
2077786263053725696	293.24521	42.53818	17.525	2.810	M2.5	N	Y	2.922	0.442	...	...	...	...	...	...	...	...
2094081712569602304	284.52365	37.89468	8.292	3.460	K3.9	N	N	2.934	0.016	3.778	0.378	4	...	...	-8.94	0.29	7
2049216514256835840	289.32911	33.44857	17.538	4.707	M3.0	N	N	2.992	0.069	...	...	...	...	...	...	...	...
2100615521758893312	287.71928	40.42630	19.417	0.806	M4.3	N	N	3.325	0.226	...	...	...	...	...	...	...	...
2051762643892077952	291.29575	37.15587	15.298	0.787	K7.8	Y	Y	3.36	0.023	0.371	0.003	1, 3	...	...	...	...	...
2046228660126600320	291.73331	33.45488	19.979	1.918	M4.4	N	N	2.992	0.335	...	...	...	...	...	...	...	...
2048280971615762688	294.40162	36.04810	17.348	4.859	M3.0	N	N	2.883	0.065	...	...	...	...	...	...	...	...
2047837799716572672	296.03591	35.80611	16.87	3.484	M1.8	N	N	3.143	0.052	...	...	...	...	...	...	...	...
2077440913315898496	294.69233	41.42808	16.38	4.067	M1.1	N	N	2.905	0.079	...	...	...	...	...	...	...	...
2047954794624184320	296.47496	36.35269	11.967	1.815	G0.7	Y	N	3.006	0.009	...	...	...	<20	...	16.17	0.02	5
2102675117496880128	289.51617	42.67499	16.169	4.523	M1.3	N	N	3.258	0.032	...	...	...	...	...	...	...	...
2049502868317059584	288.71793	34.15075	18.42	4.471	M4.3	N	N	3.229	0.138	...	...	...	...	...	...	...	...
2044463467230575232	286.14399	34.40994	12.798	4.979	G5.7	N	N	3.03	0.012	...	...	...	...	...	-35.82	2.25	7
2052377339601861760	293.95712	38.82834	19.737	4.931	M0.7	N	N	2.829	0.348	...	...	...	...	...	...	...	...
2073718443688404224	296.97364	40.30653	19.098	2.479	M3.6	N	N	3.015	0.195	...	...	...	...	...	...	...	...
2049676625514314496	289.96239	35.25870	19.722	4.630	M4.1	N	N	2.844	0.306	...	...	...	...	...	...	...	...
2073194393271316352	295.76270	39.15705	17.922	4.223	M3.6	N	N	2.886	0.083	...	...	...	...	...	...	...	...
2049238916808552960	289.41310	33.76650	18.605	1.221	M3.3	N	N	3.215	0.126	...	...	...	...	...	...	...	...
2053249969586660224	293.29114	40.11332	18.933	4.772	...	N	N	2.824	0.179	...	...	...	...	...	...	...	...
2043405354789153664	288.70471	33.30000	18.56	4.891	M4.4	N	N	3.016	0.135	...	...	...	...	...	...	...	...
2052172207674248704	294.23524	38.63339	19.119	0.902	K1.9	N	N	2.831	0.445	...	...	4	...	...	...	...	...
2099415718354203392	288.94581	38.61849	13.128	2.547	G9.7	N	N	2.795	0.009	...	...	...	...	...	-37.92	17.34	6
2046175402538070144	290.39919	33.29344	18.425	4.969	K4.0	N	N	2.978	0.434	...	...	...	...	...	...	...	...
2052628333198584192	291.12990	38.19646	19.551	4.382	M4.1	N	N	2.79	0.258	...	...	...	...	...	...	...	...
2126901133926391808	289.47788	44.01060	18.63	2.770	M3.8	N	N	3.072	0.157	...	...	...	...	...	...	...	...
2073088496558358400	295.79422	38.35530	19.843	3.628	G9.2	N	N	2.883	0.469	...	...	...	...	...	...	...	...
2046432623842804096	292.61325	33.72433	19.455	2.940	M3.6	N	N	2.957	0.422	...	...	...	...	...	...	...	...
2126059771307820928	290.94696	43.24457	18.256	4.925	M3.7	N	N	2.918	0.116	...	...	...	...	...	...	...	...
2102777543875489920	289.64852	42.87716	15.599	0.956	M0.4	N	N	3.262	0.026	6.55	0.655	4	...	...	...	...	...
2049723290332877312	290.82364	34.58311	19.547	4.920	K4.5	N	N	2.866	0.323	...	...	...	...	...	...	...	...
2103661104545810432	284.21346	40.99417	15.005	1.679	K7.6	N	Y	3.153	0.066	0.513	0.051	4	...	...	...	...	...
2093739798814089600	283.73975	36.78434	17.274	1.793	M3.7	N	N	3.046	0.062	...	...	...	...	...	...	...	...
2102291589798165376	288.37011	41.87812	17.795	3.815	M4.1	N	N	3.305	0.155	...	...	...	...	...	...	...	...
2101799249104302848	290.15740	41.50479	19.317	0.677	M4.6	N	N	3.337	0.212	...	...	...	...	...	...	...	...

Table 5 *continued*

Table 5 *(continued)*

Gaia EDR3	α	δ	Gmag	V_{off}	Spectral[a]	TESS[b]	Kepler[b]	π	σ_π	P_{rot}	$\sigma_{P_{\mathrm{rot}}}$	P_{rot}[c]	Li	σ_{li}	RV	σ_{RV}	RV[d]
	(J2016)	(J2016)	(mag)	(km/s)	Class			(mas)	(mas)	(days)	(days)	ref	(mÅ)	(mÅ)	(km/s)	(km/s)	ref
2077493552446357248	294.73757	42.02756	18.46	3.854	K5.1	N	N	2.918	0.358	...	...	...	...	...	...	...	...
2047190732806508672	294.31733	33.85950	18.825	3.452	M3.7	N	N	3.084	0.174	...	...	...	...	...	...	...	...
2076756982735231360	296.67164	40.95586	14.907	4.137	K5.8	N	N	3.166	0.018	...	...	...	...	...	...	...	...
2050177384342536192	291.22837	36.37111	19.194	4.672	M3.9	N	N	3.364	0.213	...	...	...	...	...	...	...	...
2077655627328621440	292.70163	41.71265	16.314	4.288	M0.9	Y	Y	2.846	0.035	16.88	1.34	3	...	...	...	...	...
2046346346541725312	292.22507	33.15790	18.629	4.069	M4.9	N	N	3.134	0.174	...	...	...	...	...	...	...	...
2073267991816125952	297.13574	39.57766	19.302	0.551	K3.9	N	N	2.965	0.461	...	...	...	...	...	...	...	...
2092509651456260608	285.28355	34.65127	8.637	1.733	A3.4	Y	N	3.055	0.027	...	...	...	...	...	...	...	...
2049229880197260928	289.27784	33.56525	19.282	4.635	M3.9	N	N	2.935	0.225	...	...	...	...	...	...	...	...
2046623457827053952	291.59165	33.77240	18.144	4.966	M3.2	N	N	2.916	0.105	...	...	...	...	...	...	...	...
2093794735734075904	285.09585	37.07653	19.876	4.893	M3.7	N	N	2.888	0.348	...	...	...	...	...	...	...	...
2101817459768323072	290.72718	41.77075	18.943	3.425	M3.5	N	N	3.333	0.196	...	...	...	...	...	...	...	...
2047430117103168384	295.50835	35.42486	16.559	2.933	M2.2	N	N	3.214	0.046	...	...	4	...	...	...	...	...
2077977646799305344	294.57788	43.06493	15.541	4.420	M0.4	N	N	2.992	0.042	...	...	...	...	...	...	...	...
2049282145660063488	290.41415	33.67146	14.564	4.670	K5.2	N	N	3.239	0.016	...	...	...	...	...	...	...	...
2046099815414280064	290.51308	32.82502	13.976	2.984	K2.9	N	N	3.1	0.015	...	...	...	...	...	...	...	...
2100525327447178880	287.47804	39.74656	19.199	3.838	M4.0	N	N	3.358	0.209	...	...	...	...	...	...	...	...
2073735348681875712	297.43202	40.42171	18.281	2.671	M3.7	N	N	3.092	0.109	...	...	...	...	...	...	...	...
2077986442892481536	294.68751	43.26125	17.274	4.070	M3.1	N	N	3.093	0.055	...	...	...	...	...	...	...	...
2099214434707252736	287.05931	38.18382	20.138	4.286	M3.9	N	N	3.358	0.465	...	...	...	...	...	...	...	...
2102736788929491200	289.30240	43.09566	18.35	0.579	M4.1	N	N	3.259	0.122	...	...	...	...	...	...	...	...
2098799854405484160	286.98424	36.88983	13.316	1.203	K1.1	N	N	2.824	0.014	11.634	1.163	4	...	...	-23.08	3.02	7
2052206331199215744	294.64585	38.96317	12.349	2.709	K0.3	N	Y	3.337	0.072	12.416	0.078	1, 2, 3	...	...	-15.22	0.9	7
2100502516878291328	286.97658	40.09780	17.245	2.504	M3.3	N	N	3.345	0.057	...	...	...	...	...	...	...	...
2045691930973687168	293.55338	33.31776	16.472	3.680	...	N	N	3.063	0.076	...	...	...	...	...	...	...	...
2048367111471781248	292.89827	35.47805	15.085	3.415	K7.2	N	N	3.324	0.02	...	...	...	...	...	...	...	...
2047184032661236224	294.75054	33.93309	19.998	4.500	M3.9	N	N	3.107	0.397	...	...	...	...	...	...	...	...
2102510289530615296	287.83593	42.49782	17.404	1.547	M3.4	N	N	2.879	0.066	...	...	...	...	...	...	...	...
2047184586726306816	294.79615	33.98625	19.41	2.815	K2.2	N	N	3.028	0.438	...	...	...	...	...	...	...	...
2047737434923255680	295.99340	35.19052	18.513	2.845	K4.0	N	N	3.163	0.437	...	...	...	...	...	...	...	...
2103658149608310400	284.21776	40.98972	14.693	3.007	M0.2	N	Y	3.191	0.1	0.505	0.013	1, 3	...	...	...	...	...
2053592845414583552	292.02280	41.05892	18.345	1.784	M3.6	N	N	2.811	0.114	...	...	...	...	...	...	...	...
2046090916241821184	290.85419	32.80047	17.066	4.636	M3.1	N	N	3.022	0.055	...	...	...	...	...	...	...	...
2046446814419494400	292.37751	33.75325	18.673	4.595	K4.2	N	N	3.234	0.437	...	...	...	...	...	...	...	...
2102456619619160320	287.44235	42.21178	18.878	1.483	M3.9	N	N	2.871	0.161	...	...	...	...	...	...	...	...
2047817355657805696	295.80402	35.75045	18.069	4.285	K1.2	N	N	2.925	0.307	...	...	...	...	...	...	...	...
2072036229578432384	297.07039	37.34696	16.315	4.858	M2.5	N	N	2.952	0.055	0.401	0.04	4	...	...	...	...	...
2126829773049993984	290.14802	43.58705	18.897	3.732	M4.0	N	N	2.921	0.151	...	...	...	...	...	...	...	...
2093871461032734208	284.80373	37.51411	18.81	4.283	M4.4	N	N	3.275	0.158	...	...	...	...	...	...	...	...

Table 5 *continued*

Table 5 *(continued)*

Gaia EDR3	α	δ	Gmag	$V_{\rm off}$	Spectral[a]	TESS[b]	Kepler[b]	π	σ_π	$P_{\rm rot}$	$\sigma_{P_{\rm rot}}$	$P_{\rm rot}$[c]	Li	$\sigma_{\rm li}$	RV	$\sigma_{\rm RV}$	RV[d]
	(J2016)	(J2016)	(mag)	(km/s)	Class			(mas)	(mas)	(days)	(days)	ref	(mÅ)	(mÅ)	(km/s)	(km/s)	ref
2078182018516031488	294.46156	43.52444	15.601	2.106	...	N	Y	3.066	0.04	...	...	...	...	...	...	...	...
2078182018520784768	294.46207	43.52460	14.903	2.657	M0.1	N	Y	3.091	0.054	3.309	0.013	1, 2	...	...	...	...	...
2046231237109317120	291.52433	33.50021	19.148	4.593	M4.4	N	N	2.919	0.198	...	...	...	...	...	...	...	...
2048166416226311680	294.74051	35.29513	19.751	4.651	M4.4	N	N	2.889	0.297	...	...	...	...	...	...	...	...
2045995396176459904	291.18249	32.87689	17.418	2.846	M0.9	N	N	3.159	0.265	...	...	...	...	...	...	...	...
2051932862036919296	292.65995	38.32227	16.504	4.904	M1.7	N	N	2.785	0.041	...	...	...	...	...	...	...	...
2052191178553902336	294.21899	38.74296	14.32	4.405	K5.4	N	N	3.36	0.014	...	...	4	...	...	...	...	...
2047937679164603648	296.97778	36.60412	18.303	3.350	K4.4	N	N	3.186	0.462	...	...	...	...	...	...	...	...
2077036189958524160	295.89958	41.63696	20.131	3.800	M3.8	N	N	2.927	0.455	...	...	...	...	...	...	...	...
2071994787414647296	297.50462	37.12693	10.942	0.456	F5.0	Y	N	2.995	0.01	...	...	...	<20	...	-26.97	0.27	5
2103752394073506432	285.49440	40.56695	18.574	3.281	M3.9	N	N	2.862	0.148	...	...	...	...	...	...	...	...
2045691930959960576	293.55352	33.31800	15.283	3.503	M2.1	N	N	3.148	0.073	...	...	...	...	...	...	...	...
2049000670690771456	295.34225	37.34158	14.576	4.335	K5.4	N	N	3.317	0.016	...	...	...	...	...	...	...	...
2103372998139977984	285.34117	40.31270	14.658	4.457	K5.4	N	N	3.302	0.084	...	...	...	...	...	...	...	...
2047378753596241920	294.98169	34.61665	18.596	2.552	...	N	N	3.221	0.411	...	...	...	...	...	...	...	...
2092180618305880192	284.99203	34.59198	19.066	2.382	M4.1	N	N	3.132	0.203	...	...	...	...	...	...	...	...
2101133155519023744	290.69411	40.35960	12.597	4.198	G9.9	Y	Y	3.395	0.009	12.482	1.248	4	...	...	-9.1	1.67	7
2044306271428703488	286.98351	34.28936	17.304	0.772	M3.7	N	N	2.905	0.061	...	...	...	...	...	...	...	...
2078183152393817472	294.22579	43.28020	20.12	1.831	WD	N	N	3.2	0.388	...	...	...	...	...	...	...	...
2093306075837376896	283.65093	36.04941	20.15	1.091	M3.2	N	N	3.127	0.478	...	...	...	...	...	...	...	...
2052134966021046784	294.87395	38.56141	16.285	4.688	K5.6	N	N	2.82	0.298	...	...	...	...	...	...	...	...
2099051363391935616	285.55493	37.10451	16.112	4.661	M0.8	N	N	3.321	0.03	...	...	...	...	...	...	...	...
2047981217266527488	296.61498	36.54197	19.332	4.952	K4.2	N	N	2.92	0.405	...	...	...	...	...	...	...	...
2045547448271268992	293.59074	33.04173	15.523	4.202	M0.2	N	N	3.068	0.027	4.006	0.401	4	...	...	...	...	...
2097057643869569280	283.02510	38.20678	18.108	2.974	M3.5	N	N	2.985	0.09	...	...	...	...	...	...	...	...
2077320443778087680	293.89652	40.99958	19.835	2.057	M3.9	N	N	2.824	0.332	...	...	...	...	...	...	...	...
2072871789688198400	296.20079	37.90599	14.462	0.768	K4.4	N	N	2.867	0.017	...	...	...	...	...	...	...	...
2101664082195389696	291.67642	41.57321	12.272	0.457	G5.8	Y	N	3.364	0.009	4.709	0.471	4	155.0	15.0	-26.48	0.03	5
2043129141152400640	289.31421	32.68800	14.591	1.623	K7.0	N	N	3.0	0.02	...	...	...	...	...	...	...	...
2100730699900196096	286.02234	40.24899	10.827	1.619	F5.9	Y	N	3.338	0.011	...	...	...	<20	...	-53.74	0.04	5
2076210830391573376	295.85732	39.54145	20.089	4.779	WD	N	N	3.313	0.404	...	...	...	...	...	...	...	...
2049179199583005440	289.97057	33.36831	20.059	3.833	M3.2	N	N	3.252	0.455	...	...	...	...	...	...	...	...
2045547448254684800	293.59006	33.04203	17.962	4.183	M3.9	N	N	3.032	0.107	...	...	...	...	...	...	...	...
2053253920957307264	293.19812	40.15896	18.606	4.292	M3.1	N	Y	2.793	0.134	...	...	...	...	...	...	...	...
2049951885684491520	291.70386	35.83343	14.427	1.021	K4.0	N	N	2.798	0.015	...	...	...	...	...	...	...	...
2051508210033690496	292.74620	36.85441	17.904	3.626	M3.4	N	N	3.389	0.088	...	...	...	...	...	...	...	...
2103254521466603392	283.81743	39.26535	20.01	4.106	M1.9	N	N	3.251	0.358	...	...	...	...	...	...	...	...
2049887770402931584	292.40258	35.61279	15.769	2.954	K2.1	N	N	2.809	0.477	...	...	...	...	...	...	...	...
2099631978547340288	287.51964	38.83304	14.265	0.714	K4.4	N	Y	2.784	0.071	8.967	0.125	1, 2, 3	...	...	...	...	...

Table 5 *continued*

Table 5 *(continued)*

Gaia EDR3	α	δ	Gmag	$V_{\rm off}$	Spectral[a]	TESS[b]	Kepler[b]	π	σ_π	$P_{\rm rot}$	$\sigma_{P_{\rm rot}}$	$P_{\rm rot}$[c]	Li	$\sigma_{\rm li}$	RV	$\sigma_{\rm RV}$	RV[d]
	(J2016)	(J2016)	(mag)	(km/s)	Class			(mas)	(mas)	(days)	(days)	ref	(mÅ)	(mÅ)	(km/s)	(km/s)	ref
2097202641964743936	283.14565	38.49106	12.916	1.718	K1.1	N	N	2.957	0.011	1.0	0.1	4	<20	...	-71.62	0.02	5
2072187579909260800	298.23102	38.14620	18.632	4.628	M3.7	N	N	3.078	0.13	...	...	...	...	...	...	...	...
2073861315789860352	297.50566	41.07821	19.973	4.356	K1.7	N	N	3.007	0.482	...	...	...	...	...	...	...	...
2073161648430437248	295.67351	38.81141	19.046	4.572	M4.8	N	N	3.329	0.194	...	...	...	...	...	...	...	...
2126236616586213888	291.44906	44.52831	11.57	1.627	F7.7	Y	Y	3.02	0.01	2.021	0.011	1, 2, 3	137.0	15.0	-26.62	0.06	5
2048550970429085568	294.15197	36.73524	17.686	3.613	M3.5	N	N	2.812	0.082	...	...	...	...	...	...	...	...
2047558111446645760	296.74260	35.11772	19.709	4.341	K7.9	N	N	3.121	0.37	...	...	...	...	...	...	...	...
2052699668318131072	292.10221	38.62048	17.433	2.328	K1.8	N	N	2.767	0.413	...	...	...	...	...	...	...	...
2099508249130329984	288.91477	39.09686	17.3	0.848	M3.4	N	N	3.416	0.061	...	...	...	...	...	...	...	...
2078278152769573888	294.58435	43.73550	20.087	4.225	M3.9	N	N	3.01	0.462	...	...	...	...	...	...	...	...
2103486385275947776	283.11238	39.90269	18.125	2.931	M3.7	N	N	2.966	0.098	...	...	...	...	...	...	...	...
2126868565194967168	290.31644	44.15147	17.984	2.078	...	N	N	2.939	0.095	...	...	...	...	...	...	...	...
2104099839747778304	284.53967	41.66522	18.158	3.429	M3.8	N	N	2.925	0.112	...	...	...	...	...	...	...	...
2047094662984157440	296.25360	34.43751	19.243	1.983	M4.3	N	N	3.075	0.221	...	...	...	...	...	...	...	...
2051919564817984896	292.49955	38.10192	12.349	0.709	G1.7	N	Y	2.769	0.011	6.298	0.048	1, 2, 3	152.0	13.0	5.87	0.04	5
2100477125029037184	286.79695	39.63686	18.453	2.562	M2.8	N	N	2.796	0.255	...	...	...	...	...	...	...	...
2076683929629705088	294.83936	41.19699	17.228	4.408	M1.2	N	N	2.842	0.212	...	...	...	...	...	...	...	...
2046014912505917184	291.82076	33.11940	14.879	3.207	K5.4	N	N	2.922	0.02	...	...	...	...	...	...	...	...
2126225728851650048	290.85675	44.47642	16.937	4.385	K1.9	N	N	3.176	0.382	...	...	...	...	...	...	...	...
2046644967023918848	292.07952	34.03731	16.97	3.246	M2.5	N	N	2.86	0.072	...	...	...	...	...	...	...	...
2103254525762185088	283.81777	39.26622	18.69	4.989	M4.0	N	N	3.266	0.139	...	...	...	...	...	...	...	...
2099294978235126272	288.48173	37.87229	10.872	4.713	F8.5	Y	N	2.768	0.109	4.4	0.44	4	...	...	-48.31	6.68	6
2053324053476989568	292.78007	40.53985	20.08	4.846	M3.4	N	N	3.394	0.405	...	...	...	...	...	...	...	...
2046291920713165440	291.21655	33.74036	18.183	3.886	M3.9	N	N	3.298	0.111	...	...	...	...	...	...	...	...
2073689890747943552	297.77822	40.40569	18.399	3.424	M3.8	N	N	3.181	0.117	...	...	...	...	...	...	...	...
2047563398537169664	296.88561	35.15438	19.406	3.696	M3.2	N	N	3.01	0.303	...	...	...	...	...	...	...	...
2071748088821424256	297.69852	36.50028	16.827	0.083	M2.1	N	N	2.995	0.046	...	...	...	...	...	...	...	...
2099319884743667840	288.07418	37.77893	19.824	3.595	M3.4	N	N	2.77	0.292	...	...	...	...	...	...	...	...
2092175125046680576	284.76938	34.45483	19.286	3.941	M4.3	N	N	3.162	0.216	...	...	...	...	...	...	...	...
2040051088407230720	289.89638	32.22443	17.079	3.944	M3.1	N	N	3.06	0.059	...	...	...	...	...	...	...	...
2052730793937406592	291.51964	38.53599	18.612	0.062	M4.1	N	N	3.431	0.133	...	...	...	...	...	...	...	...
2045669459703426432	294.36113	33.53556	15.409	3.647	K7.3	N	N	2.956	0.025	...	...	...	...	...	...	...	...
2101094157215298048	290.21328	39.84365	15.38	1.193	K5.9	N	N	2.76	0.022	7.674	0.767	4	...	...	...	...	...
2047848485595811712	296.21319	36.05676	15.95	4.013	M0.1	N	N	2.888	0.044	...	...	...	...	...	...	...	...
2046978668811069568	294.67386	33.45927	18.912	4.634	K3.1	N	N	3.167	0.428	...	...	...	...	...	...	...	...
2047237913043205504	294.26757	33.89340	13.354	3.782	K1.8	N	N	2.915	0.011	8.544	0.854	4	...	...	-11.07	2.29	7
2046049753274265216	290.35680	32.38352	12.872	3.798	G9.4	N	N	3.169	0.012	...	...	...	...	...	9.47	2.84	7
2046968047346848000	295.25952	33.49848	18.364	3.718	M3.8	N	N	3.117	0.111	...	...	...	...	...	...	...	...
2048404082551398016	293.19893	35.86777	16.756	2.876	M2.4	N	N	3.381	0.047	...	...	...	...	...	...	...	...

Table 5 *continued*

Table 5 *(continued)*

Gaia EDR3	α	δ	Gmag	$V_{\rm off}$	Spectral[a]	TESS[b]	Kepler[b]	π	σ_π	$P_{\rm rot}$	$\sigma_{P_{\rm rot}}$	$P_{\rm rot}$[c]	Li	$\sigma_{\rm li}$	RV	$\sigma_{\rm RV}$	RV[d]
	(J2016)	(J2016)	(mag)	(km/s)	Class			(mas)	(mas)	(days)	(days)	ref	(mÅ)	(mÅ)	(km/s)	(km/s)	ref
2051997797636616704	294.41348	37.82159	19.426	4.338	M4.2	N	N	3.39	0.267	...	...	...	...	...	...	...	...
2125873610246145536	292.58582	43.30910	19.984	2.688	M3.9	N	N	3.297	0.415	...	...	...	...	...	...	...	...
2104521163155771264	283.11699	41.63372	17.7	1.373	M3.1	N	N	3.051	0.091	...	...	...	...	...	...	...	...
2047515264836350464	296.97688	35.08727	19.675	2.580	K3.5	N	N	3.155	0.473	...	...	...	...	...	...	...	...
2076916068323795712	297.63372	41.66240	13.597	4.819	K3.8	N	Y	3.135	0.027	2.94	0.006	2	...	...	...	...	...
2048329002227281920	293.54632	35.37401	19.272	4.904	M4.0	N	N	3.359	0.279	...	...	...	...	...	...	...	...
2073078669668987648	296.17783	38.32620	15.14	4.370	K7.2	N	N	3.334	0.024	...	...	...	...	...	...	...	...
2072061552708807168	297.20278	37.41189	16.963	2.283	K1.2	N	N	3.268	0.352	...	...	...	...	...	...	...	...
2049994663554289664	290.59864	35.31034	15.226	4.883	K7.8	N	N	3.393	0.02	9.266	0.927	4	...	...	...	...	...
2100849069200258176	287.00138	41.09824	13.822	4.001	K4.1	N	N	3.375	0.059	0.531	0.053	4	...	...	-30.74	5.54	6
2045160523261880448	292.22579	32.34442	18.318	2.234	K1.8	N	N	3.142	0.397	...	...	...	...	...	...	...	...
2101046014920381312	289.97434	39.80199	17.713	0.498	M4.3	N	N	3.436	0.083	...	...	...	...	...	...	...	...
2050397836421213824	288.28588	35.49266	18.6	3.605	G9.4	N	N	2.796	0.42	...	...	...	...	...	...	...	...
2044150037698600448	286.53831	33.45730	12.872	1.081	G8.4	N	N	2.944	0.012	5.712	0.571	4	48.0	21.0	-25.53	0.03	5
2045857888499785344	290.78961	32.20265	13.055	2.110	K1.6	N	N	3.151	0.011	...	...	...	...	...	...	...	...
2097062999689757952	282.40791	37.77595	17.727	2.590	M3.7	N	N	3.009	0.083	...	...	...	...	...	...	...	...
2045510202313548160	293.16088	32.61947	16.185	3.973	M0.9	N	N	3.159	0.035	...	...	...	...	...	...	...	...
2076791170675704192	297.10120	41.28092	10.152	2.966	WD	N	Y	2.924	0.374	...	...	...	...	...	15.59	7.26	6
2043266408307478656	288.02188	32.69115	19.511	4.339	...	N	N	3.189	0.29	...	...	...	...	...	...	...	...
2046917199252241280	295.20940	33.29376	17.743	4.587	M3.6	N	N	3.066	0.137	...	...	...	...	...	...	...	...
2047845530658609408	296.27545	35.96412	13.726	4.354	K2.4	N	N	2.88	0.014	5.967	0.597	4	...	...	...	...	...
2046121629545429376	290.25569	32.70606	17.183	4.609	M3.5	N	N	3.237	0.06	...	...	...	...	...	...	...	...
2125934525767218304	291.94845	43.44846	18.509	3.073	M3.9	N	N	3.305	0.13	...	...	...	...	...	...	...	...
2105483300251395584	286.84530	42.67696	11.341	4.686	F6.9	Y	Y	3.311	0.012	...	...	...	...	...	3.27	1.17	7
2047473547816550784	296.52449	34.64568	12.616	2.596	G8.8	N	N	3.18	0.061	...	...	...	...	...	-28.81	2.36	7
2092882111026898176	284.90755	35.95876	15.399	1.344	K7.1	N	N	2.865	0.026	...	...	...	...	...	...	...	...
2099107335408623232	286.83280	37.40995	20.27	3.780	M3.9	N	N	2.782	0.467	...	...	...	...	...	...	...	...
2102489574907671424	288.31867	42.19989	17.573	2.897	M3.5	N	N	3.366	0.071	...	...	...	...	...	...	...	...
2046049753274268032	290.35375	32.38311	15.207	3.766	K7.2	N	N	3.196	0.022	...	...	...	...	...	...	...	...
2048590724650826240	295.50206	36.11956	19.01	4.467	M4.0	N	N	3.331	0.179	...	...	...	...	...	...	...	...
2050598531653315584	287.79545	35.55407	18.804	4.165	M4.2	N	N	2.798	0.156	...	...	...	...	...	...	...	...
2076418882914174464	296.27631	40.70380	14.617	3.402	K5.5	N	N	3.312	0.017	...	...	...	...	...	...	...	...
2093967672598363008	282.96152	36.95184	17.321	2.377	M3.1	N	N	2.954	0.062	...	...	...	...	...	...	...	...
2077452007217272448	294.43467	41.55354	17.986	4.407	M4.3	N	N	3.355	0.09	...	...	...	...	...	...	...	...
2052697641091575936	292.08123	38.52384	10.424	2.916	F6.1	Y	Y	2.749	0.011	1.619	0.162	4	...	...	3.65	1.06	7
2072623746745941888	298.61814	38.92210	17.589	4.435	M3.0	N	N	2.998	0.073	...	...	...	...	...	...	...	...
2048053368403171584	294.17305	34.81844	18.994	3.708	M4.2	N	N	2.843	0.191	...	...	...	...	...	...	...	...
2051622696681241088	292.75986	37.24984	16.45	3.375	K1.9	N	N	2.762	0.468	...	...	...	...	...	...	...	...
2043993868387134080	285.82075	33.64317	20.051	1.677	M3.2	N	N	2.953	0.394	...	...	...	...	...	...	...	...

Table 5 *continued*

Table 5 *(continued)*

Gaia EDR3	α	δ	Gmag	V_{off}	Spectral[a]	TESS[b]	Kepler[b]	π	σ_π	P_{rot}	$\sigma_{P_{\mathrm{rot}}}$	P_{rot}[c]	Li	σ_{li}	RV	σ_{RV}	RV[d]
	(J2016)	(J2016)	(mag)	(km/s)	Class			(mas)	(mas)	(days)	(days)	ref	(mÅ)	(mÅ)	(km/s)	(km/s)	ref
2073666186833150080	297.69497	40.01224	17.232	2.008	M4.1	N	N	3.248	0.061	...	...	...	...	...	...	...	...
2101877967268283392	289.93782	42.11501	18.893	2.076	M2.3	N	N	2.794	0.243	...	...	...	...	...	...	...	...
2100438161087360256	286.47598	39.16799	15.949	3.538	M1.8	N	N	2.781	0.029	...	...	...	...	...	...	...	...
2049605397777137792	290.14053	34.85038	19.223	4.486	M4.8	N	N	3.386	0.229	...	...	...	...	...	...	...	...
2049524068273170048	288.56915	34.49988	18.584	4.425	M4.3	N	N	3.359	0.132	...	...	...	...	...	...	...	...
2099150014497672576	287.28333	37.97763	16.126	3.002	M1.1	N	N	3.423	0.032	...	...	...	...	...	...	...	...
2098949108810346112	287.35701	37.62122	18.314	1.695	M3.9	N	N	2.766	0.115	...	...	...	...	...	...	...	...
2126422713231701376	293.37170	44.54717	19.421	0.925	M0.5	N	N	2.99	0.41	...	...	...	...	...	...	...	...
2049080041688578176	295.16918	37.95543	13.128	2.633	K1.9	N	N	3.385	0.01	...	...	...	...	...	-23.56	1.08	7
2046928847204044544	295.68829	33.44455	16.858	3.841	M2.2	N	N	3.077	0.046	...	...	...	...	...	...	...	...
2048328319313617664	293.17507	35.62762	18.466	4.552	M4.2	N	N	3.39	0.128	...	...	...	...	...	...	...	...
2071736161663103360	297.89138	36.30383	18.344	2.926	M4.1	N	N	2.97	0.108	...	...	...	...	...	...	...	...
2092470442701217664	284.00674	35.31025	19.236	2.313	M4.2	N	N	3.227	0.204	...	...	...	...	...	...	...	...
2104897913389395712	283.74023	42.32815	19.102	4.716	M3.9	N	N	3.183	0.217	...	...	...	...	...	...	...	...
2043247029414194816	287.46776	32.40548	17.206	3.016	M2.6	N	N	3.026	0.064	...	...	...	...	...	...	...	...
2092350802089575424	283.97774	34.49539	19.484	4.826	M3.7	N	N	3.133	0.264	...	...	...	...	...	...	...	...
2044456664002834176	285.86589	34.46286	17.929	4.034	M3.8	N	N	3.288	0.104	...	...	...	...	...	...	...	...
2046058515007828096	290.52888	32.54222	15.099	3.573	K7.1	N	N	2.924	0.022	...	...	...	...	...	...	...	...
2048387624236066176	292.60265	35.72764	17.795	3.495	M4.5	N	N	3.406	0.093	...	...	...	...	...	...	...	...
2050322932190356480	288.34806	35.00158	16.151	4.579	M0.8	N	N	2.8	0.034	...	...	...	...	...	...	...	...
2046908300079553408	295.01958	33.09667	17.619	2.677	M2.7	N	N	3.018	0.089	...	...	...	...	...	...	...	...
2077052162943896192	296.58475	41.88910	18.67	1.304	M3.6	N	N	3.264	0.229	...	...	...	...	...	...	...	...
2104394410082061056	282.46681	41.13004	17.209	4.434	M3.1	N	N	3.112	0.059	...	...	...	...	...	...	...	...
2105743987587112064	285.43912	43.16851	13.262	4.216	K1.9	Y	Y	3.242	0.011	13.599	1.36	4	...	...	-25.77	1.81	6
2044412030702242944	286.26474	34.30114	17.003	3.815	M2.9	N	N	2.871	0.056	...	...	...	...	...	...	...	...
2047600300891409408	297.61218	35.26227	18.544	0.741	M3.5	N	N	3.144	0.13	...	...	...	...	...	...	...	...
2049347326084851200	290.79916	34.47631	10.335	2.272	WD	Y	N	3.379	0.012	0.652	0.065	4	...	...	-24.38	3.18	7
2072613503227155712	298.77966	38.93114	18.234	1.550	M3.2	N	N	2.99	0.418	...	...	...	...	...	...	...	...
2093325003752502400	283.27562	36.15754	19.151	4.369	M4.0	N	N	2.937	0.183	...	...	...	...	...	...	...	...
2035028832851565440	296.35381	33.84771	18.457	2.595	K3.8	N	N	3.031	0.359	...	...	...	...	...	...	...	...
2076711937114787712	295.18270	41.46979	11.313	4.181	G1.7	Y	N	3.35	0.037	...	...	...	...	...	-29.89	9.99	7
2077021449639700608	295.84038	41.21400	17.868	2.410	M3.7	N	N	3.335	0.083	...	...	...	...	...	...	...	...
2102345057842818944	287.59104	41.37157	15.408	2.186	...	N	N	3.401	0.039	...	...	...	...	...	...	...	...
2076159638688278144	295.32494	38.73004	15.184	4.150	K2.1	N	Y	2.792	0.435	20.517	0.285	1, 2, 3	...	...	...	...	...
2049394772583984128	290.57425	34.53951	19.992	4.692	M3.6	N	N	2.798	0.455	...	...	...	...	...	...	...	...
2049366150920150016	290.25011	34.36795	18.369	4.507	M4.3	N	N	3.378	0.114	...	...	...	...	...	...	...	...
2093263778998771584	282.89368	35.45736	15.811	3.046	M0.7	N	N	3.092	0.027	...	...	...	...	...	...	...	...
2126868565194967040	290.31722	44.15139	16.385	1.096	M0.9	N	N	2.882	0.037	...	...	...	...	...	...	...	...
2049386526244981760	290.48853	34.36003	18.901	4.428	M4.5	N	N	3.381	0.2	...	...	...	...	...	...	...	...

Table 5 *continued*

Table 5 *(continued)*

Gaia EDR3	α	δ	Gmag	$V_{\rm off}$	Spectral[a]	TESS[b]	Kepler[b]	π	σ_π	$P_{\rm rot}$	$\sigma_{P_{\rm rot}}$	$P_{\rm rot}$[c]	Li	$\sigma_{\rm li}$	RV	$\sigma_{\rm RV}$	RV[d]
	(J2016)	(J2016)	(mag)	(km/s)	Class			(mas)	(mas)	(days)	(days)	ref	(mÅ)	(mÅ)	(km/s)	(km/s)	ref
2096596738040150528	282.06298	37.02287	20.1	2.292	M1.4	N	N	3.09	0.48	...	...	4	...	...	...	...	...
2045047273553574528	291.64421	31.87119	19.935	2.423	K5.0	N	N	3.131	0.47	...	...	...	...	...	...	...	...
2043001563444619136	288.50497	32.07896	15.481	2.264	K2.1	N	N	2.999	0.322	...	...	...	...	...	...	...	...
2051691897192988032	291.76281	36.81307	18.215	3.392	K2.0	N	N	3.449	0.445	...	...	...	...	...	...	...	...
2047600369605430272	297.60809	35.26608	12.159	0.740	G5.4	N	N	2.985	0.009	...	...	...	<20	...	-15.12	0.02	5
2099306656246576768	288.53365	38.06402	16.71	4.767	M1.9	N	N	2.74	0.05	...	...	...	...	...	...	...	...
2052110192648801920	294.71119	38.40776	14.67	4.593	K5.7	N	Y	3.417	0.021	12.204	0.034	1, 3	...	...	...	...	...
2092561981343162752	285.13017	34.79135	17.957	4.648	M4.9	N	N	3.292	0.093	...	...	...	...	...	...	...	...
2047502792280390272	296.93248	34.88786	18.448	1.649	K2.0	N	N	2.944	0.407	...	...	...	...	...	...	...	...
2102516920959555328	288.28318	42.32358	18.953	3.339	M3.6	N	N	2.799	0.163	...	...	...	...	...	...	...	...
2092479758487340672	284.08452	35.49485	20.164	2.921	M3.0	N	N	2.898	0.396	...	...	...	...	...	...	...	...
2047933555987119872	297.13897	36.53422	19.291	4.172	M4.0	N	N	2.878	0.234	...	...	...	...	...	...	...	...
2046102632904887680	290.56902	32.88891	20.048	4.101	M3.6	N	N	3.296	0.412	...	...	...	...	...	...	...	...
2072323884993390592	299.18057	38.24659	18.078	3.506	M3.7	N	N	3.06	0.109	...	...	...	...	...	...	...	...
2047498634751988352	297.15175	34.94840	18.398	1.464	K4.3	N	N	3.207	0.437	...	...	...	...	...	...	...	...
2045939905198326912	292.23920	32.63244	19.073	2.479	K7.4	N	N	2.91	0.348	...	...	...	...	...	...	...	...
2101725856707136000	291.23549	41.77524	17.728	4.855	M3.4	N	Y	3.421	0.073	...	...	...	...	...	...	...	...
2097256174437856384	283.23251	39.07501	16.237	3.905	M0.8	N	N	3.298	0.035	...	...	...	...	...	...	...	...
2050195732454711168	290.87049	36.19128	20.272	1.826	M4.0	N	N	3.448	0.481	...	...	...	...	...	...	...	...
2097357810543012096	281.74257	38.82639	19.321	2.795	M4.6	N	N	3.14	0.244	...	...	...	...	...	...	...	...
2040130425040417024	289.65964	32.75244	12.269	4.813	G7.2	N	N	3.285	0.009	4.006	0.401	4	...	...	-24.15	2.1	7
2035434312143013888	296.96049	34.16051	19.927	3.687	K5.5	N	N	3.132	0.452	...	...	...	...	...	...	...	...
2072147486412951296	298.47570	38.20590	17.969	0.844	M3.1	N	N	3.233	0.086	...	...	...	...	...	...	...	...
2101858691452557568	290.05865	41.82500	19.555	4.952	M4.2	N	N	2.77	0.27	...	...	...	...	...	...	...	...
2072550697944039552	299.26839	38.74165	18.742	1.326	K3.8	N	N	3.075	0.259	...	...	...	...	...	...	...	...
2072538912553419520	299.25306	38.48448	19.655	4.151	K4.7	N	N	3.095	0.43	...	...	...	...	...	...	...	...
2073123784006705280	296.14796	38.77094	16.709	4.319	M2.8	N	N	3.377	0.045	...	...	...	...	...	...	...	...
2046173959423172864	290.39664	33.20921	18.039	4.599	M4.1	N	N	3.327	0.101	...	...	...	...	...	...	...	...
2044081966753894144	287.06714	33.12365	20.086	1.678	M4.1	N	N	3.265	0.395	...	...	...	...	...	...	...	...
2077426890247666816	294.63319	41.09637	18.731	4.225	M4.1	N	N	2.794	0.193	...	...	...	...	...	...	...	...
2102101855319612544	288.94077	40.96879	19.997	1.472	M2.1	N	N	2.754	0.401	...	...	...	...	...	...	...	...
2127085817521473792	290.06926	45.38874	18.867	4.787	M4.0	N	N	3.031	0.156	...	...	...	...	...	...	...	...
2047940844554138752	297.00429	36.71973	19.374	2.868	M3.2	N	N	2.86	0.245	...	...	...	...	...	...	...	...
2099951970789768960	286.13363	38.20211	18.516	3.387	M4.1	N	N	2.769	0.137	...	...	...	...	...	...	...	...
2101333021814076800	289.09094	40.70343	10.722	0.412	F8.2	Y	Y	3.451	0.012	11.921	0.036	1, 2	74.0	10.0	-25.0	3.0	5
2043928451744462208	284.76208	33.37225	17.351	3.296	M3.4	N	N	3.038	0.065	...	...	...	...	...	...	...	...
2047037630134920704	296.18589	33.83057	11.458	0.634	F7.5	N	N	2.963	0.055	...	...	4	72.0	9.0	-24.9	0.05	5
2072318219958215808	299.25408	38.09202	15.686	4.652	M0.4	N	N	3.046	0.026	...	...	...	...	...	...	...	...
2035056522488856320	296.69481	33.94659	18.995	1.042	M4.2	N	N	3.003	0.203	...	...	...	...	...	...	...	...

Table 5 *continued*

Table 5 *(continued)*

Gaia EDR3	α	δ	Gmag	$V_{\rm off}$	Spectral[a]	TESS[b]	Kepler[b]	π	σ_π	$P_{\rm rot}$	$\sigma_{P_{\rm rot}}$	$P_{\rm rot}$[c]	Li	$\sigma_{\rm li}$	RV	$\sigma_{\rm RV}$	RV[d]
	(J2016)	(J2016)	(mag)	(km/s)	Class			(mas)	(mas)	(days)	(days)	ref	(mÅ)	(mÅ)	(km/s)	(km/s)	ref
2093801199665763200	285.16015	37.15539	16.935	4.784	M3.2	N	N	3.385	0.047	...	...	...	...	...	...	...	...
2046287144709183744	290.65878	33.77984	16.687	4.526	M2.6	N	N	3.367	0.046	...	...	...	...	...	...	...	...
2076813985542421376	296.19392	41.01601	12.128	4.215	G1.0	N	Y	2.832	0.009	14.902	0.003	1, 3	...	...	-20.76	1.7	7
2101483448751246976	289.67659	41.43275	19.418	4.086	M4.0	N	N	3.439	0.234	...	...	...	...	...	...	...	...
2071668374223679232	298.35760	36.07075	18.944	4.934	...	N	N	2.986	0.465	...	...	...	...	...	...	...	...
2103092382157713408	288.89602	44.31228	16.735	4.858	M1.9	N	N	2.885	0.042	...	...	4	...	...	...	...	...
2047872296888691840	296.67271	35.73608	18.432	4.471	M2.9	N	N	2.869	0.13	...	...	...	...	...	...	...	...
2092481407757619584	283.99684	35.49197	14.376	4.657	K5.3	N	N	3.281	0.013	...	...	...	...	...	...	...	...
2047601748323083008	297.71111	35.33991	19.045	3.367	K5.2	N	N	3.202	0.388	...	...	...	...	...	...	...	...
2093919152346692352	283.35716	36.85052	12.406	3.813	G6.4	Y	N	3.293	0.01	...	...	...	...	...	...	...	...
2045279815955846144	293.80599	32.09748	18.6	2.950	K2.1	N	N	3.056	0.33	...	...	...	...	...	...	...	...
2047324740098522496	295.44447	34.64008	15.392	3.518	K5.8	N	N	2.86	0.023	...	...	...	...	...	...	...	...
2072538912548248832	299.25298	38.49610	17.943	1.689	K3.8	N	N	3.147	0.417	...	...	...	...	...	...	...	...
2049611616887061760	290.26461	35.06325	19.013	4.411	M4.3	N	N	3.426	0.182	...	...	...	...	...	...	...	...
2106316042870808832	286.27180	44.79768	18.458	4.860	M3.0	N	N	3.063	0.114	...	...	...	...	...	...	...	...
2073506001739529728	298.79720	39.85038	17.507	4.925	M3.7	N	N	3.212	0.08	...	...	...	...	...	...	...	...
2101851578986373504	290.08407	41.71353	18.247	0.790	M4.3	N	N	3.436	0.113	...	...	...	...	...	...	...	...
2076834871960671232	296.68683	41.25121	18.548	2.853	M4.3	N	N	2.853	0.136	...	...	...	...	...	...	...	...
2078439471742656768	297.95685	42.36105	19.922	4.560	M3.7	N	N	3.16	0.368	...	...	...	...	...	...	...	...
2045153616952289152	292.15203	32.14387	19.919	4.336	M4.0	N	N	2.94	0.388	...	...	...	...	...	...	...	...
2048900301596606336	294.96151	37.15246	18.195	4.733	M2.9	N	N	2.777	0.1	...	...	4	...	...	...	...	...
2073728446681835904	296.94598	40.39643	17.92	4.486	K4.0	N	N	3.337	0.462	...	...	...	...	...	...	...	...
2102821554402541312	289.87036	43.47243	18.006	3.498	M3.5	N	N	2.822	0.095	...	...	...	...	...	...	...	...
2126695254669367168	292.61869	45.31928	19.785	3.164	M3.9	N	N	3.135	0.362	...	...	...	...	...	...	...	...
2046117167082959104	290.01542	32.62605	15.17	4.491	K7.4	N	N	3.296	0.027	...	...	...	...	...	...	...	...
2051087234514702080	290.52757	37.57737	17.514	4.524	M3.5	N	N	3.482	0.071	...	...	...	...	...	...	...	...
2072722530995781376	299.46781	39.40105	17.221	4.104	...	N	N	3.084	0.078	...	...	...	...	...	...	...	...
2053233270752968704	293.32059	39.83965	18.885	0.507	M3.8	N	N	2.745	0.178	...	...	...	...	...	...	...	...
2048761320755537536	296.52821	37.09804	17.268	1.182	M3.6	N	N	3.361	0.063	...	...	...	...	...	...	...	...
2045094552559824512	293.01541	31.91806	14.803	1.466	K5.6	N	N	3.002	0.02	...	...	...	...	...	...	...	...
2102039909015221888	290.48246	42.97096	13.288	2.233	K1.5	N	Y	2.797	0.209	12.837	1.284	4	...	...	-26.85	1.0	6
2051743952194400640	291.50746	36.92276	17.409	1.049	M3.5	N	N	3.473	0.07	...	...	...	...	...	...	...	...
2047522583485686656	296.48151	34.79177	16.399	4.366	M1.2	N	N	2.892	0.045	...	...	...	...	...	...	...	...
2099025769684598528	286.45055	37.34895	16.767	4.051	M3.3	N	N	2.761	0.055	...	...	...	...	...	...	...	...
2072307671501281280	299.02385	37.82968	15.57	4.417	M0.5	N	N	3.198	0.025	...	...	...	...	...	...	...	...
2077421878026895616	293.83675	41.55741	19.3	1.323	M4.4	N	N	3.414	0.277	...	...	...	...	...	...	...	...
2126695254674628352	292.61986	45.31982	18.987	3.686	M4.0	N	N	3.158	0.184	...	...	...	...	...	...	...	...
2049869319230388992	291.73865	35.41058	17.044	4.317	M1.6	N	N	2.757	0.255	...	...	...	...	...	...	...	...
2127081320695095936	290.25378	45.28755	13.898	4.112	K4.7	N	N	3.205	0.035	9.954	0.995	4	...	...	-21.94	3.42	6

Table 5 *continued*

Table 5 *(continued)*

Gaia EDR3	α	δ	Gmag	$V_{\rm off}$	Spectral[a]	TESS[b]	Kepler[b]	π	σ_π	$P_{\rm rot}$	$\sigma_{P_{\rm rot}}$	$P_{\rm rot}$[c]	Li	$\sigma_{\rm li}$	RV	$\sigma_{\rm RV}$	RV[d]
	(J2016)	(J2016)	(mag)	(km/s)	Class			(mas)	(mas)	(days)	(days)	ref	(mÅ)	(mÅ)	(km/s)	(km/s)	ref
2072350926100080000	299.55179	38.34902	18.015	4.172	K5.6	N	N	3.085	0.386	...	...	...	...	...	...	...	...
2103792461826460288	285.90783	40.94199	16.282	0.795	M1.6	N	Y	3.406	0.04	...	...	...	...	...	...	...	...
2053296664471049472	292.84317	40.09897	18.542	0.977	M4.1	N	N	3.465	0.139	...	...	...	...	...	...	...	...
2099294153599724544	288.50723	37.84410	16.011	3.773	M0.8	N	N	2.727	0.035	...	...	...	...	...	...	...	...
2072661405022124800	299.48102	39.03476	19.939	4.484	K5.1	N	N	3.147	0.455	...	...	...	...	...	...	...	...
2045287134585007360	293.34757	32.04168	19.827	4.690	M2.0	N	N	2.977	0.332	...	...	...	...	...	...	...	...
2072520323928187648	298.71801	38.23241	18.132	0.323	K2.7	N	N	3.25	0.385	...	...	...	...	...	...	...	...
2047599618012175360	297.55071	35.18792	17.654	4.798	M2.5	N	N	2.931	0.077	...	...	...	...	...	...	...	...
2039799716869484416	289.91451	31.36283	15.724	4.657	M0.5	N	N	3.064	0.028	0.161	0.016	4	...	...	...	...	...
2078763385296160768	296.61843	43.05853	15.36	3.854	K7.2	N	Y	2.92	0.022	17.148	0.286	1, 3	...	...	...	...	...
2072730669936461440	298.98991	39.37798	14.554	1.028	K5.0	N	N	3.228	0.017	...	...	...	...	...	...	...	...
2099752100192430464	287.72965	39.37987	15.046	4.459	K5.3	N	Y	2.733	0.022	20.418	0.059	1, 2, 3	...	...	...	...	...
2044187627253001984	287.01851	33.82199	16.108	1.190	M0.4	N	N	2.835	0.032	...	...	...	...	...	...	...	...
2098549268829941632	281.46583	40.64636	12.737	3.672	G5.2	Y	N	3.084	0.009	...	...	...	...	...	-4.49	2.77	7
2078817016545461248	296.50652	43.67947	16.151	3.798	M1.1	N	N	2.962	0.033	...	...	...	...	...	...	...	...
2097382583914478080	281.92084	38.93346	18.219	3.388	M3.4	N	N	3.24	0.108	...	...	...	...	...	...	...	...
2072305335056539648	299.41744	38.03346	16.662	2.205	M1.7	N	N	2.993	0.047	...	...	...	...	...	...	...	...
2093063942759941376	282.86685	34.66101	11.299	4.938	K1.7	Y	N	3.13	0.011	...	...	...	...	...	-61.11	1.36	7
2044898152309449600	293.02978	31.58477	16.945	3.464	M2.5	N	N	3.071	0.271	...	...	...	...	...	...	...	...
2044978176124042112	292.14996	31.47703	15.331	3.934	K7.7	N	N	3.138	0.022	0.274	0.027	4	...	...	...	...	...
2045893656988832256	291.04380	32.55423	18.225	4.522	M4.1	N	N	3.311	0.117	...	...	...	...	...	...	...	...
2046259897436426624	290.80335	33.40280	17.268	3.934	G7.2	Y	N	2.816	0.1	1.214	0.121	4	...	...	...	...	...
2035376003622121216	297.52144	34.09891	19.859	1.711	K5.9	N	N	3.126	0.462	...	...	...	...	...	...	...	...
2072925489643044352	297.53018	38.09948	19.823	3.007	M3.9	N	N	2.84	0.446	...	...	...	...	...	...	...	...
2071696785402166400	298.31598	36.22598	17.714	2.572	M3.7	N	N	3.242	0.076	...	...	...	...	...	...	...	...
2035597039844643968	298.10990	35.15153	19.487	2.717	...	N	N	3.19	0.381	...	...	...	...	...	...	...	...
2047478774822890496	296.76477	34.76113	18.316	4.547	K2.2	N	N	3.283	0.495	...	...	...	...	...	...	...	...
2034948220580957440	296.60873	33.22972	17.239	2.431	K3.9	N	N	3.093	0.428	...	...	...	...	...	...	...	...
2035507189142669696	297.98842	34.56174	19.523	2.117	K7.1	N	N	3.04	0.465	...	...	...	...	...	...	...	...
2043012455481906432	288.50129	32.24126	14.423	2.820	K5.6	N	N	3.266	0.016	...	...	...	...	...	...	...	...
2072614121704209792	298.81958	38.99560	19.365	1.711	M4.4	N	N	3.258	0.24	...	...	...	...	...	...	...	...
2106183384220719488	287.99326	44.98196	12.131	1.609	G6.7	Y	N	3.24	0.009	...	...	...	...	...	-51.07	1.15	7
2072305335042508800	299.41917	38.03228	20.201	1.945	WD	N	N	3.182	0.472	...	...	...	...	...	...	...	...
2050872314350242176	290.20636	36.34314	16.103	1.734	M3.4	N	N	3.481	0.035	...	...	...	...	...	...	...	...
2127336574891550336	288.47307	45.69380	19.021	0.785	M4.2	N	N	3.075	0.17	...	...	...	...	...	...	...	...
2078738813782006784	297.40467	43.37885	20.096	4.927	K4.0	N	N	2.999	0.491	...	...	...	...	...	...	...	...
2043449408265789824	288.20607	33.49053	18.953	0.892	M4.0	N	N	2.823	0.168	...	...	...	...	...	...	...	...
2100719631764623744	285.77174	39.94869	17.854	0.455	M4.5	N	N	3.436	0.116	...	...	...	...	...	...	...	...
2071898962416384256	298.36706	37.34976	18.997	4.902	M1.6	N	N	3.285	0.279	...	...	...	...	...	...	...	...

Table 5 *continued*

Table 5 *(continued)*

Gaia EDR3	α	δ	Gmag	$V_{\rm off}$	Spectral[a]	TESS[b]	Kepler[b]	π	σ_π	$P_{\rm rot}$	$\sigma_{P_{\rm rot}}$	$P_{\rm rot}$[c]	Li	$\sigma_{\rm li}$	RV	$\sigma_{\rm RV}$	RV[d]
	(J2016)	(J2016)	(mag)	(km/s)	Class			(mas)	(mas)	(days)	(days)	ref	(mÅ)	(mÅ)	(km/s)	(km/s)	ref
2101479982717916672	289.48109	41.44275	18.272	4.852	M4.2	N	N	3.464	0.289	...	...	...	...	...	...	...	...
2072210845763476352	298.16065	38.39876	20.258	4.955	M2.6	N	N	3.314	0.464	...	...	...	...	...	...	...	...
2073261802762236672	296.87252	39.44676	17.838	3.565	M3.6	N	N	2.809	0.087	...	...	...	...	...	...	...	...
2099293294606209920	288.48725	37.76804	16.096	3.641	M2.4	N	N	2.72	0.044	5.967	0.597	4	...	...	...	...	...
2103996386874495616	285.94709	42.03265	12.128	2.130	G3.6	Y	N	3.391	0.011	5.366	0.537	4	...	...	-24.44	1.11	7
2099413347532157184	288.82577	38.49219	17.194	1.836	M2.4	N	N	2.715	0.057	...	...	...	...	...	...	...	...
2127034518431825152	290.54972	45.27463	19.937	3.041	M3.9	N	N	2.928	0.363	...	...	...	...	...	...	...	...
2050661070679148416	287.71023	35.98050	16.821	1.146	M2.9	N	N	3.457	0.055	4.26	0.426	4	...	...	...	...	...
2059785088748864896	299.12010	36.45836	18.83	3.599	M3.6	N	N	2.994	0.175	...	...	...	...	...	...	...	...
2048630818156165120	295.62153	36.43720	12.535	4.235	G8.7	N	N	3.409	0.01	7.259	0.726	4	...	...	...	...	...
2072775749914283136	299.65459	40.01545	19.83	2.811	M3.7	N	N	3.145	0.318	...	...	...	...	...	...	...	...
2044470644114758016	286.41475	34.60318	19.668	3.497	M4.1	N	N	3.385	0.296	...	...	...	...	...	...	...	...
2072866734503491840	296.38371	37.92367	19.803	2.036	K5.0	N	N	3.405	0.435	...	...	...	...	...	...	...	...
2046276871147153664	290.47978	33.58992	17.372	1.480	M2.7	N	N	2.799	0.065	...	...	...	...	...	...	...	...
2049062037184535936	295.69908	38.08524	19.615	3.239	K2.2	N	N	2.769	0.438	...	...	...	...	...	...	...	...
2098380562514570240	281.85958	40.53395	18.547	4.991	M3.7	N	N	3.228	0.123	...	...	...	...	...	...	...	...
2060208576838804736	299.65196	37.17216	20.325	3.491	M2.8	N	N	3.101	0.49	...	...	...	...	...	...	...	...
2100538628963464960	287.50769	40.01520	12.471	2.774	G9.0	Y	N	3.477	0.056	3.157	0.316	4	...	...	-28.38	5.37	7
2043571247906297088	285.79107	32.19080	17.444	4.919	M1.1	N	N	3.048	0.196	...	...	...	...	...	...	...	...
2035558213355165440	297.74898	34.70382	14.728	3.201	G6.2	N	N	2.954	0.385	...	...	...	...	...	...	...	...
2051530367766907392	293.20562	36.43482	19.333	4.359	M3.6	N	N	2.738	0.233	...	...	...	...	...	...	...	...
2126384672702589184	292.81078	44.73571	17.12	3.505	M2.1	N	N	2.893	0.06	...	...	...	...	...	...	...	...
2096873918048932096	281.09371	37.69378	19.486	3.715	M4.1	N	N	3.053	0.272	...	...	...	...	...	...	...	...
2072724072867622656	299.43374	39.48065	20.166	3.710	M3.2	N	N	3.209	0.489	...	...	...	...	...	...	...	...
2043235140944669056	287.58780	32.37512	16.496	0.698	M1.7	N	N	2.901	0.048	...	...	...	...	...	...	...	...
2044999066845940224	291.67975	31.43535	17.718	4.548	K1.6	N	N	2.977	0.315	...	...	...	...	...	...	...	...
2072140786263744128	298.42093	37.99581	16.28	3.759	G6.8	N	N	2.875	0.401	...	...	...	...	...	...	...	...
2049777406933975424	290.66660	34.82208	19.284	4.606	M4.6	N	N	3.451	0.212	...	...	...	...	...	...	...	...
2046227629335778048	291.58657	33.41772	17.721	3.472	M4.3	N	N	3.385	0.086	...	...	...	...	...	...	...	...
2092879430966059136	284.79175	35.94635	13.223	4.810	K0.5	N	N	2.807	0.011	9.616	0.962	4	...	...	-21.93	3.24	7
2099588891435130752	287.88510	38.91648	12.525	1.238	G6.0	Y	Y	2.719	0.01	...	...	...	...	...	-19.92	0.98	7
2099547621093774464	287.34979	38.41880	20.354	2.291	M2.5	N	N	3.488	0.473	...	...	...	...	...	...	...	...
2045830916096719104	290.73966	31.79759	18.64	3.541	M3.9	N	N	3.262	0.134	...	...	...	...	...	...	...	...
2042628176160001792	287.22643	31.66133	20.086	1.961	M3.6	N	N	3.156	0.359	...	...	...	...	...	...	...	...
2039745802130541184	290.82928	31.12864	18.453	0.561	M4.0	N	N	3.029	0.137	...	...	...	...	...	...	...	...
2106634179689109888	283.75282	44.00022	18.633	2.782	M3.6	N	N	3.04	0.128	...	...	...	...	...	...	...	...
2045076822913720576	292.47729	31.71641	19.337	3.366	K4.8	N	N	2.946	0.396	...	...	...	...	...	...	...	...
2049723290341467008	290.82439	34.58277	13.277	4.221	K0.4	N	N	2.759	0.011	5.967	0.597	4	...	...	-27.57	9.05	7
2034853151521982336	295.69956	32.47904	10.01	3.385	F3.7	N	N	3.027	0.149	...	...	...	...	...	...	...	...

Table 5 *continued*

Table 5 *(continued)*

Gaia EDR3	α	δ	Gmag	$V_{\rm off}$	Spectral[a]	TESS[b]	Kepler[b]	π	σ_π	$P_{\rm rot}$	$\sigma_{P_{\rm rot}}$	$P_{\rm rot}$[c]	Li	$\sigma_{\rm li}$	RV	$\sigma_{\rm RV}$	RV[d]
	(J2016)	(J2016)	(mag)	(km/s)	Class			(mas)	(mas)	(days)	(days)	ref	(mÅ)	(mÅ)	(km/s)	(km/s)	ref
2097481054627089536	283.02156	39.82116	19.478	4.067	M3.6	N	N	2.844	0.26	...	...	...	...	...	...	...	...
2035620473184524928	298.22146	35.43991	19.955	3.979	WD	N	N	3.238	0.354	...	...	...	...	...	...	...	...
2059719294186348416	299.34518	36.18797	17.716	2.202	K5.6	N	N	3.121	0.423	...	...	...	...	...	...	...	...
2102876259404857472	289.66673	43.80526	15.587	4.325	M0.5	N	Y	3.381	0.027	15.8	0.701	1, 2, 3	...	...	...	...	...
2045837994204287616	290.75823	31.99780	19.495	4.593	K7.2	N	N	2.891	0.481	...	...	...	...	...	...	...	...
2127081320692480640	290.25348	45.28784	17.318	4.273	...	N	N	3.263	0.094	...	...	...	...	...	-21.94	3.42	6
2102347493091019008	287.77319	41.38558	17.389	1.553	M3.0	N	N	2.745	0.063	...	...	...	...	...	...	...	...
2101433047314568960	289.61931	40.97999	14.862	4.703	K5.2	N	Y	2.724	0.019	12.409	0.073	1, 2, 3	...	...	...	...	...
2035572262163581696	297.95806	34.99376	18.403	2.701	M3.6	N	N	3.236	0.125	...	...	...	...	...	...	...	...
2098139872547430144	281.02508	39.15513	18.344	3.571	M3.5	N	N	3.003	0.14	...	...	...	...	...	...	...	...
2099571982147097984	288.02075	38.71572	18.277	0.347	M4.2	N	N	3.502	0.113	...	...	...	...	...	...	...	...
2072663844556645888	299.29924	39.05782	15.421	3.865	M0.7	N	N	2.927	0.023	...	...	...	...	...	...	...	...
2039764326337748736	290.68345	31.40132	17.332	4.209	M3.3	N	N	2.953	0.069	...	...	...	...	...	...	...	...
2059610579970201600	298.96284	35.70534	19.176	1.819	K4.5	N	N	2.992	0.372	...	...	...	...	...	...	...	...
2035373804634502912	297.43159	34.00156	19.825	2.937	M3.7	N	N	2.966	0.366	...	...	...	...	...	...	...	...
2099411835704664960	289.05677	38.56415	17.714	1.285	M4.2	N	N	3.515	0.152	...	...	...	...	...	...	...	...
2035036490752882688	296.77431	33.80260	17.117	3.778	M2.8	N	N	2.926	0.06	...	...	...	...	...	...	...	...
2093357546725698048	281.95522	35.45154	20.031	3.485	M2.7	N	N	3.007	0.36	...	...	...	...	...	...	...	...
2045346306370823936	294.63208	32.39451	16.22	1.861	G9.6	N	N	2.933	0.414	...	...	...	...	...	...	...	...
2097748961804097664	280.80478	38.70191	17.809	4.918	M3.6	N	N	3.036	0.091	...	...	...	...	...	...	...	...
2127058192292076416	289.65996	44.94166	19.789	3.693	M3.6	N	N	2.875	0.311	...	...	...	...	...	...	...	...
2050699931542300672	288.44096	36.06236	15.193	1.719	M0.0	N	N	3.486	0.022	...	...	...	...	...	...	...	...
2072867456050222592	296.45443	38.01354	17.968	4.178	M3.7	N	N	2.78	0.089	...	...	...	...	...	...	...	...
2102841173813071360	289.54320	43.42839	18.307	2.372	M3.2	N	N	2.788	0.103	...	...	...	...	...	...	...	...
2072490254847590912	300.10633	39.18293	17.116	3.750	K5.3	N	N	3.131	0.412	...	...	...	...	...	...	...	...
2103882411324553728	285.39928	41.68599	19.768	3.729	M3.9	N	N	2.789	0.328	...	...	...	...	...	...	...	...
2042606976199603968	287.34430	31.35263	20.17	2.700	M3.1	N	N	3.077	0.472	...	...	...	...	...	...	...	...
2101328245814804608	289.30151	40.63521	19.489	0.693	M3.8	N	N	3.501	0.23	...	...	...	...	...	...	...	...
2127988623947420416	294.22506	45.55388	15.607	3.352	K7.9	N	N	3.04	0.025	...	...	...	...	...	...	...	...
2048753143137250944	296.47658	36.92023	16.901	2.468	M3.2	N	N	2.79	0.056	...	...	...	...	...	...	...	...
2040032259274049536	290.09547	31.98329	16.52	4.267	M2.5	N	N	3.302	0.042	...	...	...	...	...	...	...	...
2092301878124319232	282.95443	34.35270	17.754	3.976	M3.2	N	N	2.971	0.084	...	...	...	...	...	...	...	...
2093615897596762496	284.01214	35.85026	16.282	2.769	M1.0	N	N	2.826	0.037	...	...	...	...	...	...	...	...
2098557893123715968	281.10840	40.61281	19.662	1.303	M3.7	N	N	3.165	0.249	...	...	...	...	...	...	...	...
2046886309812806528	295.28239	32.83306	19.109	1.359	K5.7	N	N	3.264	0.487	...	...	...	...	...	...	...	...
2035397577239823872	297.87828	34.32187	12.443	2.882	G5.3	N	N	2.967	0.054	...	...	...	...	...	-5.32	1.97	7
2092234906692408576	283.31241	34.02642	19.218	3.824	M4.0	N	N	2.963	0.227	...	...	...	...	...	...	...	...
2034931629122810880	296.72066	33.08620	19.202	4.217	K5.4	N	N	2.992	0.471	...	...	...	...	...	...	...	...
2060239706786224512	300.01493	37.42834	19.29	1.192	K5.3	N	N	3.054	0.348	...	...	...	...	...	...	...	...

Table 5 *continued*

Table 5 *(continued)*

Gaia EDR3	α	δ	Gmag	$V_{\rm off}$	Spectral[a]	TESS[b]	Kepler[b]	π	σ_π	$P_{\rm rot}$	$\sigma_{P_{\rm rot}}$	$P_{\rm rot}$[c]	Li	$\sigma_{\rm li}$	RV	$\sigma_{\rm RV}$	RV[d]
	(J2016)	(J2016)	(mag)	(km/s)	Class			(mas)	(mas)	(days)	(days)	ref	(mÅ)	(mÅ)	(km/s)	(km/s)	ref
2103772876775835264	285.54115	40.77368	15.135	2.903	M0.0	N	N	3.441	0.02	1.434	0.143	4	...	...	...	...	...
2039796551464880768	289.88657	31.25833	17.087	4.595	M2.7	N	N	2.959	0.057	...	...	...	...	...	...	...	...
2101328215753018368	289.29886	40.63557	18.234	0.939	M3.9	N	N	3.505	0.1	...	...	...	...	...	...	...	...
2076376276839108992	295.55755	40.03728	18.579	1.873	M0.4	N	N	2.758	0.426	...	...	...	...	...	...	...	...
2106152082498649472	287.66489	44.64575	17.762	4.979	M2.5	N	N	2.869	0.077	...	...	...	...	...	...	...	...
2076528451810442624	294.46058	40.36860	18.206	4.905	M4.2	N	N	2.739	0.114	...	...	...	...	...	...	...	...
2093556038634002432	282.50290	36.46374	18.594	1.590	M3.8	N	N	3.302	0.133	...	...	...	...	...	...	...	...
2105573120908549760	286.01179	43.34544	13.55	4.763	K2.9	N	Y	3.365	0.01	15.382	0.078	1, 2, 3	...	...	-46.91	5.08	6
2075528347215214208	299.11378	42.32946	15.437	3.984	K7.7	N	N	3.026	0.024	7.5	0.75	4	...	...	...	...	...
2072137762607078016	298.27053	37.96493	18.18	4.224	K3.5	N	N	2.846	0.429	...	...	...	...	...	...	...	...
2047593020949598976	297.46239	35.10038	18.615	2.589	K5.9	N	N	3.307	0.322	...	...	...	...	...	...	...	...
2060252591673833472	300.15456	37.73963	19.513	2.696	M4.5	N	N	3.117	0.262	...	...	...	...	...	...	...	...
2079675941287005312	295.53771	44.83787	20.226	1.114	M3.5	N	N	3.208	0.478	...	...	...	...	...	...	...	...
2038994255884014336	290.91980	31.12276	19.189	3.160	M4.4	N	N	3.201	0.252	...	...	...	...	...	...	...	...
2047553266713842944	296.39199	35.24569	18.549	1.310	...	N	N	2.82	0.464	...	...	...	...	...	...	...	...
2098726839954943360	287.35450	36.44961	18.423	1.067	...	N	N	3.488	0.149	...	...	...	...	...	...	...	...
2104168524863869312	285.49364	41.94926	16.877	1.279	M3.3	N	N	3.414	0.045	...	...	...	...	...	...	...	...
2059602471065286912	299.27439	35.70451	15.788	4.674	M0.4	N	N	3.166	0.027	3.164	0.316	4	...	...	...	...	...
2049974799334830720	291.76891	36.15311	18.884	1.381	M3.8	N	N	2.715	0.184	...	...	...	...	...	...	...	...
2034787868025390208	295.95424	32.27033	18.105	3.323	K4.2	N	N	3.045	0.468	...	...	...	...	...	...	...	...
2126951956280730368	289.62077	44.61998	15.904	4.114	M0.8	N	Y	2.839	0.03	26.048	0.406	1, 2, 3	...	...	...	...	...
2034934481034201984	297.00242	33.10459	19.259	4.341	K5.4	N	N	3.168	0.406	...	...	...	...	...	...	...	...
2042555191783228416	287.46982	31.19689	20.098	3.502	M3.5	N	N	3.052	0.388	...	...	...	...	...	...	...	...
2046227118244683904	291.68198	33.43576	16.465	2.950	M1.6	N	N	2.789	0.041	...	...	...	...	...	...	...	...
2077208504056339200	296.84890	42.75081	18.499	4.470	M3.7	N	N	2.86	0.124	...	...	...	...	...	...	...	...
2047886036479782016	296.80283	36.06192	17.679	4.904	K5.3	N	N	2.81	0.241	...	...	...	...	...	...	...	...
2046538069577311104	292.94782	34.07791	11.603	2.583	F9.7	N	N	3.428	0.011	...	...	...	...	...	16.64	1.81	7
2092055067824008192	284.01412	33.91946	18.868	4.427	M4.1	N	N	2.902	0.208	...	...	...	...	...	...	...	...
2035465437740187776	297.47541	34.56564	18.273	4.936	M2.9	N	N	3.284	0.3	...	...	...	...	...	...	...	...
2105997768616675584	287.29819	43.56297	18.226	1.107	M3.3	N	N	3.392	0.1	...	...	...	...	...	...	...	...
2046470866234008704	293.21553	33.75437	16.754	4.912	M1.8	N	N	2.791	0.048	...	...	...	...	...	...	...	...
2072163154458766976	297.82822	37.95078	17.721	1.913	K0.5	N	N	3.376	0.383	...	...	...	...	...	...	...	...
2050270331734089984	288.28314	34.42156	18.441	2.555	M4.5	N	N	3.449	0.195	...	...	...	...	...	...	...	...
2072301005733702912	299.48061	37.91540	17.901	2.808	K2.6	N	N	3.258	0.419	...	...	...	...	...	...	...	...
2044040150954670336	285.56732	33.72475	19.955	4.931	M3.6	N	N	2.841	0.4	...	...	...	...	...	...	...	...
2075384203803462784	299.10758	42.14583	19.623	4.861	K5.8	N	N	2.979	0.491	...	...	...	...	...	...	...	...
2125958341367719680	292.53423	43.86558	12.586	3.537	G9.1	N	N	2.804	0.032	7.5	0.75	4	...	...	-15.41	1.85	7
2045763399203433600	291.22718	31.59969	17.611	3.778	M3.3	N	N	3.281	0.078	...	...	...	...	...	...	...	...
2093308270559797760	283.48666	36.05048	18.149	1.331	M4.6	N	N	3.362	0.115	...	...	...	...	...	...	...	...

Table 5 *continued*

Table 5 *(continued)*

Gaia EDR3	α	δ	Gmag	$V_{\rm off}$	Spectral[a]	TESS[b]	Kepler[b]	π	σ_π	$P_{\rm rot}$	$\sigma_{P_{\rm rot}}$	$P_{\rm rot}$[c]	Li	$\sigma_{\rm li}$	RV	$\sigma_{\rm RV}$	RV[d]
	(J2016)	(J2016)	(mag)	(km/s)	Class			(mas)	(mas)	(days)	(days)	ref	(mÅ)	(mÅ)	(km/s)	(km/s)	ref
2075249547991542912	299.79226	41.60502	17.846	4.720	M3.4	N	N	3.108	0.209	...	...	...	...	...	...	...	...
2073753323131546368	297.36348	40.66992	17.007	4.154	M2.3	N	N	2.813	0.053	...	...	...	...	...	...	...	...
2045337544643659904	293.93527	32.75205	18.994	4.105	...	N	N	2.855	0.417	...	...	...	...	...	...	...	...
2060149787349407616	300.15641	37.07456	19.76	1.018	K7.8	N	N	3.064	0.451	...	...	...	...	...	...	...	...
2090707478882159488	283.14144	33.61014	18.239	4.033	M3.7	N	N	3.004	0.111	...	...	...	...	...	...	...	...
2101910991275973504	290.05235	42.43998	11.687	0.834	F9.5	Y	N	3.473	0.01	3.233	0.323	4	109.0	12.0	-26.28	0.05	5
2047759734386631680	296.17032	35.49087	18.77	1.870	K4.2	N	N	2.798	0.452	...	...	...	...	...	...	...	...
2099480349022624512	288.70765	38.81454	17.095	0.775	M3.8	N	N	3.531	0.055	...	...	...	...	...	...	...	...
2034860500173190144	295.68823	32.71778	18.905	0.607	K5.2	N	N	2.923	0.434	...	...	...	...	...	...	...	...
2071813922084206976	298.98998	36.92730	18.103	4.480	K1.9	N	N	2.895	0.351	...	...	...	...	...	...	...	...
2078683082288392320	297.89393	43.89533	19.98	2.804	M3.0	N	N	3.021	0.347	...	...	...	...	...	...	...	...
2099576792509340416	287.75880	38.66803	20.206	0.688	M3.5	N	N	2.703	0.483	...	...	...	...	...	...	...	...
2101358997780341248	289.72856	40.53936	18.851	0.636	M3.9	N	N	3.523	0.184	...	...	...	...	...	...	...	...
2093973032712421248	283.14504	37.08744	18.412	4.203	M3.6	N	N	3.377	0.145	...	...	...	...	...	...	...	...
2044848193247250304	292.98450	31.19493	14.717	4.249	K5.2	N	N	2.981	0.019	...	...	...	...	...	...	...	...
2050661070679148672	287.71128	35.98069	16.097	1.093	M1.6	N	N	3.497	0.04	4.26	0.426	4	...	...	...	...	...
2033178492231704064	294.29095	31.36889	19.009	4.704	K2.9	N	N	3.147	0.491	...	...	...	...	...	...	...	...
2077208504056331136	296.84284	42.74459	14.264	4.057	K4.2	N	Y	2.848	0.015	43.993	0.334	1, 3	...	...	...	...	...
2090440336220493184	283.63016	32.95219	19.676	4.863	M3.6	N	N	3.035	0.331	...	...	...	...	...	...	...	...
2102522044860511232	288.52603	42.51048	19.218	4.565	M4.5	N	N	3.468	0.213	...	...	...	...	...	...	...	...
2078465967394310656	298.04637	42.55501	19.874	1.619	M4.0	N	N	2.897	0.328	...	...	...	...	...	...	...	...
2035436820378759296	296.94229	34.19335	19.84	3.477	...	N	N	3.314	0.491	...	...	...	...	...	...	...	...
2047881470939011072	296.81868	35.97319	11.837	2.301	G5.3	N	N	3.399	0.021	4.709	0.471	4	...	...	...	...	...
2106741626889502336	284.68087	44.85847	17.258	4.948	M3.1	N	N	3.198	0.057	...	...	...	...	...	...	...	...
2101052646350595456	289.49047	39.66965	20.362	3.307	M2.1	N	N	3.539	0.474	...	...	...	...	...	...	...	...
2035199562080802176	298.19398	34.05595	19.011	1.972	M0.2	N	N	3.196	0.374	...	...	...	...	...	...	...	...
2102876259404859264	289.66784	43.80672	16.196	4.509	M2.9	N	Y	3.421	0.035	...	...	...	...	...	...	...	...
2078632199816869248	298.19007	43.33899	16.587	4.581	M3.0	N	N	2.96	0.05	...	...	...	...	...	...	...	...
2048740739255456000	295.86030	36.90845	19.88	3.499	M4.5	N	N	3.458	0.338	...	...	...	...	...	...	...	...
2046538069581432448	292.94615	34.07777	11.027	3.480	F8.4	Y	N	3.444	0.012	...	...	...	...	...	13.51	1.42	7
2034934304887810304	296.89664	33.14149	18.757	4.204	M3.9	N	N	2.948	0.154	...	...	...	...	...	...	...	...
2090422434794530944	283.82474	32.73802	18.085	3.684	M3.8	N	N	3.037	0.108	...	...	...	...	...	...	...	...
2072569973734233088	299.14997	38.99325	17.869	2.509	...	N	N	3.316	0.102	...	...	...	...	...	...	...	...
2042361372796678784	284.17522	32.45230	16.819	3.288	M3.1	N	N	3.051	0.21	...	...	...	...	...	...	...	...
2091986932462007168	284.47276	33.66584	17.275	4.705	M2.0	N	N	2.874	0.062	...	...	...	...	...	...	...	...
2060142434322913536	300.30324	36.87244	17.282	4.933	K5.0	N	N	3.093	0.344	...	...	...	...	...	...	...	...
2104259719908757888	284.34008	42.57702	12.777	1.905	K0.6	Y	Y	3.373	0.017	6.545	0.058	1, 2, 3	...	...	-21.8	3.17	7
2045013905936304128	291.36733	31.47303	18.535	4.268	M4.0	N	N	3.29	0.151	...	...	...	...	...	...	...	...
2096693911675730560	281.69385	37.45572	18.491	4.882	M3.8	N	N	3.303	0.134	...	...	...	...	...	...	...	...

Table 5 *continued*

Table 5 *(continued)*

Gaia EDR3	α	δ	Gmag	$V_{\rm off}$	Spectral[a]	TESS[b]	Kepler[b]	π	σ_π	$P_{\rm rot}$	$\sigma_{P_{\rm rot}}$	$P_{\rm rot}$[c]	Li	$\sigma_{\rm li}$	RV	$\sigma_{\rm RV}$	RV[d]
	(J2016)	(J2016)	(mag)	(km/s)	Class			(mas)	(mas)	(days)	(days)	ref	(mÅ)	(mÅ)	(km/s)	(km/s)	ref
2043550009284291968	285.73561	31.98056	18.292	4.359	M3.8	N	N	3.224	0.195	...	...	...	...	...	...	...	...
2049355263185449344	289.92373	34.07863	10.111	4.654	F5.5	Y	N	3.466	0.013	...	...	...	...	...	...	...	...
2045118913619083008	292.86208	32.17623	17.824	4.875	K4.3	N	N	2.856	0.471	...	...	...	...	...	...	...	...
2043529363382642944	285.35317	31.73225	17.666	3.395	M3.1	N	N	3.121	0.079	...	...	...	...	...	...	...	...
2075276181101557120	299.78423	42.01218	12.608	4.395	G9.1	N	N	3.033	0.176	...	...	...	...	...	-19.64	3.99	6
2090434048386865536	283.59322	32.88582	13.934	3.030	K3.5	N	N	3.149	0.017	...	...	...	...	...	...	...	...
2044852488197038208	292.90208	31.26488	20.252	3.457	M2.1	N	N	3.235	0.454	...	...	...	...	...	...	...	...
2078075503326188800	295.26780	43.50625	19.294	3.008	M4.4	N	N	2.823	0.23	...	...	...	...	...	...	...	...
2092421690531387648	283.70831	34.83900	17.322	4.837	M3.3	N	N	3.347	0.067	...	...	...	...	...	...	...	...
2101356768694676736	289.62914	40.43800	16.606	0.998	M2.8	N	N	3.535	0.041	...	...	...	...	...	...	...	...
2034878058020104960	295.49353	32.88730	18.874	4.038	M4.5	N	N	2.881	0.21	...	...	...	...	...	...	...	...
2043606462337292928	285.04705	32.17350	18.542	0.424	M4.2	N	N	2.973	0.164	...	...	...	...	...	...	...	...
2078955662392859776	297.29191	44.69382	14.112	3.350	K4.6	N	N	3.076	0.103	...	...	...	...	...	-30.44	15.96	7
2101080104074781824	290.54820	39.76054	20.127	4.329	M3.1	N	N	2.687	0.404	...	...	4	...	...	...	...	...
2039635442949156096	289.97361	30.90389	17.065	3.327	M3.2	N	N	3.225	0.073	...	...	...	...	...	...	...	...
2076944827425916928	297.29982	41.76893	15.653	2.226	M0.2	N	N	3.378	0.027	...	...	...	...	...	...	...	...
2045679492751565184	294.15352	33.59444	18.941	3.898	K1.2	N	N	3.404	0.439	...	...	...	...	...	...	...	...
2045462231812414592	294.37781	33.05085	19.167	1.100	M3.7	N	N	2.831	0.203	...	...	...	...	...	...	...	...
2044924334394933120	291.77174	31.00374	18.683	3.556	M3.3	N	N	2.948	0.153	...	...	...	...	...	...	...	...
2078955662388392832	297.29164	44.69377	14.427	3.923	...	N	N	3.128	0.048	...	...	...	...	...	...	...	...
2034930667049652736	296.78949	33.06394	18.473	4.510	K5.2	N	N	2.933	0.335	...	...	...	...	...	...	...	...
2093973032717697920	283.14585	37.08764	16.159	4.778	M1.3	N	N	3.396	0.033	...	...	...	...	...	...	...	...
2046768554694492672	292.22566	34.59368	18.336	4.379	M4.1	N	N	3.482	0.114	...	...	...	...	...	...	...	...
2053613190676007424	292.46650	41.27008	19.513	2.175	M3.9	N	N	2.711	0.264	...	...	...	...	...	...	...	...
2097423472002729856	282.92684	39.08662	18.968	3.805	M3.4	N	N	2.803	0.166	...	...	...	...	...	...	...	...
2090793313811517312	282.51145	34.07706	14.75	4.766	K5.2	N	N	2.976	0.018	9.266	0.927	4	...	...	...	...	...
2075580535348810496	299.01715	42.91809	19.603	3.702	M3.9	N	N	3.19	0.27	...	...	...	...	...	...	...	...
2071832510703880192	299.23496	36.88326	19.041	2.697	K2.5	N	N	2.892	0.428	...	...	...	...	...	...	...	...
2078318559819774976	294.98418	44.26687	11.816	4.777	F8.5	Y	Y	2.851	0.01	9.463	0.946	4	...	...	-9.63	2.63	7
2078933221177778176	296.96982	44.39704	18.335	1.577	M3.8	N	N	3.233	0.104	...	...	...	...	...	...	...	...
2101393602335156224	290.01815	40.88419	16.222	2.359	M0.9	N	N	3.534	0.156	...	...	...	...	...	...	...	...
2053613220739715072	292.48154	41.27155	18.35	2.593	M3.9	N	N	2.71	0.112	...	...	...	...	...	...	...	...
2039621694757984000	289.84573	30.59365	19.247	3.711	M4.3	N	N	3.007	0.254	...	...	...	...	...	...	...	...
2105260584727347584	282.22896	43.61609	13.23	4.890	K1.9	N	Y	3.149	0.009	14.706	0.115	1, 2, 3	...	...	-26.18	4.7	7
2091563487345509632	282.31633	34.39512	14.458	4.570	K4.6	N	N	2.959	0.017	5.479	0.548	4	...	...	...	...	...
2035494991436488832	298.13180	34.57362	17.813	3.453	K7.7	N	N	2.906	0.495	...	...	...	...	...	...	...	...
2073891444974578304	297.89092	41.32039	20.178	4.998	WD	N	N	2.827	0.42	...	...	...	...	...	...	...	...
2075250857971184896	299.82500	41.65593	14.661	1.129	K5.4	N	N	3.203	0.018	...	...	...	...	...	...	...	...
2075496427020761472	299.58227	42.37392	17.73	3.681	K5.1	N	N	3.0	0.294	...	...	...	...	...	...	...	...

Table 5 *continued*

Table 5 *(continued)*

Gaia EDR3	α	δ	Gmag	$V_{\rm off}$	Spectral[a]	TESS[b]	Kepler[b]	π	σ_π	$P_{\rm rot}$	$\sigma_{P_{\rm rot}}$	$P_{\rm rot}$[c]	Li	$\sigma_{\rm li}$	RV	$\sigma_{\rm RV}$	RV[d]
	(J2016)	(J2016)	(mag)	(km/s)	Class			(mas)	(mas)	(days)	(days)	ref	(mÅ)	(mÅ)	(km/s)	(km/s)	ref
2034608785053215872	296.73045	32.23678	19.31	2.388	M0.1	N	N	3.067	0.496	...	...	4	...	...	...	...	...
2077289386878257920	294.00214	40.47831	19.09	4.485	M3.8	N	N	2.713	0.189	...	...	...	...	...	...	...	...
2074286891201244800	299.91857	40.34210	18.047	4.733	M3.0	N	N	3.256	0.105	...	...	...	...	...	...	...	...
2060127900191203456	300.46905	36.81684	16.972	4.383	K3.1	N	N	3.112	0.435	...	...	...	...	...	...	...	...
2073430685195146624	297.96599	39.51389	17.656	2.739	M3.4	N	N	3.403	0.078	...	...	...	...	...	...	...	...
2098473398229061888	280.18768	40.10855	19.22	3.603	M3.6	N	N	3.042	0.211	...	...	...	...	...	...	...	...
2079999854839810048	295.55300	45.59855	19.502	3.081	K3.2	N	N	3.159	0.48	...	...	...	...	...	...	...	...
2034948942137058560	296.49440	33.24572	18.766	4.156	K5.4	N	N	3.299	0.466	...	...	...	...	...	...	...	...
2043366700083996160	287.54272	33.42792	20.073	1.253	M1.5	N	N	2.785	0.392	...	...	...	...	...	...	...	...
2097210441625883648	283.16822	38.63566	16.188	3.462	M1.7	N	N	3.419	0.034	...	...	...	...	...	...	...	...
2050547305583981184	287.59559	35.11381	14.964	4.151	...	N	N	2.73	0.025	...	...	...	...	...	...	...	...
2049390584996835712	290.30935	34.46992	11.372	4.299	F8.9	Y	N	3.494	0.015	2.555	0.256	4	...	...	-25.64	2.24	7
2077589343090087040	292.97439	41.37548	16.974	4.625	M3.3	N	N	3.514	0.047	...	...	4	...	...	...	...	...
2079052518193127552	298.37255	44.09580	19.024	3.944	M3.8	N	N	3.104	0.176	...	...	...	...	...	...	...	...
2045334379224810624	293.85108	32.61599	18.069	4.480	M3.9	N	N	2.834	0.11	...	...	...	...	...	...	...	...
2049525172090954752	288.96670	34.27429	12.826	2.118	K1.1	N	N	3.482	0.011	8.2	0.82	4	...	...	-8.64	0.85	7
2039991409845427328	289.64118	31.48069	16.683	4.589	M2.7	N	N	3.316	0.046	...	...	...	...	...	...	...	...
2059760354073210752	299.76928	36.59283	13.183	2.921	K1.2	N	N	3.247	0.016	...	...	...	...	...	-30.6	2.59	7
2078006852574214144	295.45483	42.87965	15.424	2.104	K7.7	N	Y	2.791	0.025	18.332	0.093	1, 2, 3	...	...	...	...	...
2102905048563740672	288.34384	42.77780	20.245	3.010	M2.3	N	N	2.742	0.454	...	...	...	...	...	...	...	...
2044943056160410240	291.84485	31.13095	18.493	3.968	WD	N	N	3.271	0.131	...	...	...	...	...	...	...	...
2128109707666691456	294.14905	46.04038	17.787	2.726	K1.8	N	N	3.18	0.409	...	...	...	...	...	...	...	...
2059364632941028992	298.88376	34.96452	19.919	2.940	K7.3	N	N	2.934	0.472	...	...	...	...	...	...	...	...
2099507695076654464	288.87620	39.05392	18.848	1.708	M4.1	N	N	3.557	0.153	...	...	...	...	...	...	...	...
2044760094878757120	292.41965	31.02918	19.145	1.571	K5.5	N	N	2.937	0.437	...	...	...	...	...	...	...	...
2043340625343891840	287.53003	33.09318	14.175	1.389	K3.5	N	N	2.797	0.015	...	...	...	...	...	...	...	...
2046954273417307648	295.65322	33.71349	18.217	1.512	G8.8	N	N	3.378	0.477	...	...	...	...	...	...	...	...
2128272809044885120	292.90773	46.37716	18.969	3.124	M4.3	N	N	3.167	0.184	...	...	...	...	...	...	...	...
2043515477746272384	285.51076	31.61563	18.455	0.699	M3.8	N	N	3.185	0.153	...	...	...	...	...	...	...	...
2100669672705335552	286.07882	39.91231	20.053	2.590	M1.8	N	N	3.511	0.458	...	...	...	...	...	...	...	...
2103214908983951360	284.07612	39.36259	14.24	2.914	K5.8	N	N	3.459	0.019	2.181	0.218	4	...	...	...	...	...
2105918917314419584	285.87841	44.33451	14.797	4.109	K5.3	N	N	2.846	0.019	...	...	...	...	...	...	...	...
2042376555501554176	284.23116	32.62074	18.814	1.643	M4.0	N	N	2.947	0.164	...	...	...	...	...	...	...	...
2092254770922633472	283.95015	34.31580	13.945	4.372	K4.8	N	N	2.842	0.012	9.266	0.927	4	...	...	...	...	...
2071840688290572416	299.38466	37.01625	19.381	4.237	G6.8	N	N	2.884	0.373	...	...	...	...	...	...	...	...
2078629451037625344	297.97912	43.30283	16.434	1.744	M2.0	N	N	3.284	0.038	3.889	0.389	4	...	...	...	...	...
2079725075708677248	296.92349	45.01725	19.836	2.050	WD	N	N	3.167	0.292	...	...	...	...	...	...	...	...
2071968880171921536	297.40115	36.99908	11.804	4.183	G1.4	N	N	3.426	0.085	...	...	...	...	...	...	...	...
2079332034661555072	297.30106	44.82463	18.741	4.727	M3.4	N	N	3.163	0.149	...	...	...	...	...	...	...	...

Table 5 *continued*

Table 5 *(continued)*

Gaia EDR3	α	δ	Gmag	$V_{\rm off}$	Spectral[a]	TESS[b]	Kepler[b]	π	σ_π	$P_{\rm rot}$	$\sigma_{P_{\rm rot}}$	$P_{\rm rot}$[c]	Li	$\sigma_{\rm li}$	RV	$\sigma_{\rm RV}$	RV[d]
	(J2016)	(J2016)	(mag)	(km/s)	Class			(mas)	(mas)	(days)	(days)	ref	(mÅ)	(mÅ)	(km/s)	(km/s)	ref
2078884950051870336	297.83573	44.30739	19.316	3.932	K4.1	N	N	3.197	0.494	...	...	...	...	...	...	...	...
2078582962313182336	298.30495	43.15487	17.527	3.854	K5.4	N	N	3.276	0.273	...	...	...	...	...	...	...	...
2034726462850693632	297.18739	32.81216	19.423	2.734	M0.5	N	N	2.964	0.481	...	...	...	...	...	...	...	...
2032794968837203840	293.70589	30.90144	19.218	4.646	...	N	N	2.998	0.308	...	...	...	...	...	...	...	...
2035394283013302144	297.83058	34.19047	18.007	0.730	M1.0	N	N	2.892	0.5	...	...	...	...	...	...	...	...
2044802838397149440	293.14012	31.14334	18.571	1.953	K2.7	N	N	3.254	0.442	...	...	...	...	...	...	...	...
2090453805230646656	283.25563	32.70549	20.315	2.292	M1.2	N	N	3.126	0.474	...	...	...	...	...	...	...	...
2051997046029841664	294.42149	37.79702	18.095	4.326	M3.7	N	N	3.529	0.099	...	...	...	...	...	...	...	...
2097350045242066176	281.80122	38.58132	16.811	0.607	M1.7	N	N	2.841	0.044	...	...	...	...	...	...	...	...
2034702861998369664	297.56191	32.91666	19.797	3.225	K5.4	N	N	3.194	0.466	...	...	...	...	...	...	...	...
2039628502283521920	289.78476	30.77700	20.053	3.984	M1.2	N	N	2.938	0.48	...	...	...	...	...	...	...	...
2035247773085894656	299.12764	34.11427	18.99	1.742	K5.6	N	N	3.11	0.419	...	...	...	...	...	...	...	...
2072017091188480640	297.27253	37.05375	18.937	3.473	M1.2	N	N	2.776	0.286	...	...	...	...	...	...	...	...
2078663742057126656	298.16842	43.64593	14.224	4.975	K4.2	N	N	2.935	0.014	...	...	...	...	...	-17.65	2.37	6
2074417050206133760	300.68226	41.11641	19.8	3.909	K1.7	N	N	3.097	0.491	...	...	...	...	...	...	...	...
2043229226768610432	287.69628	32.23021	17.085	4.929	M3.0	N	N	2.835	0.061	...	...	...	...	...	...	...	...
2096541113922857856	281.40019	36.67998	15.036	4.031	K7.2	N	N	3.297	0.019	...	...	...	...	...	...	...	...
2059912292833185664	300.50237	36.32908	18.102	2.091	K5.5	N	N	3.093	0.369	...	...	...	...	...	...	...	...
2091613549484765952	281.90191	34.51857	17.937	3.669	M3.5	N	N	3.219	0.093	...	...	...	...	...	...	...	...
2042602642580508544	287.39272	31.26417	19.106	1.306	M3.5	N	N	2.924	0.228	...	...	...	...	...	...	...	...
2091797167925612416	281.41774	34.66648	10.662	4.809	F5.1	Y	N	3.154	0.011	...	...	...	...	...	-19.51	2.01	7
2034623868995446016	296.91701	32.55592	8.254	4.647	F9.4	N	N	2.965	0.2	...	...	...	...	...	...	...	...
2093494642080134784	282.46117	36.10249	15.783	1.123	M0.6	N	N	3.358	0.028	...	...	...	...	...	...	...	...
2099411835701970432	289.05670	38.56448	18.389	1.043	...	N	N	3.568	0.161	...	...	...	...	...	...	...	...
2059298073811697152	299.58712	34.68978	18.345	4.853	M2.8	N	N	3.125	0.253	...	...	...	...	...	...	...	...
2034576108930945024	296.28630	31.87506	18.834	3.037	M0.9	N	N	3.167	0.359	...	...	...	...	...	...	...	...
2039576168108731904	289.71211	30.32060	19.803	2.754	M3.7	N	N	3.154	0.344	...	...	...	...	...	...	...	...
2059667617133782784	299.03709	35.96966	19.772	1.558	K4.1	N	N	2.881	0.477	...	...	...	...	...	...	...	...
2050930554107640832	289.34285	36.68737	13.673	2.175	K1.9	N	N	2.682	0.073	...	...	...	...	...	...	...	...
2099008997832012032	286.59945	37.19531	18.42	1.314	M4.6	N	N	3.531	0.122	...	...	...	...	...	...	...	...
2059537599877637632	300.20115	36.03678	18.674	1.613	K5.3	N	N	3.181	0.433	...	...	...	...	...	...	...	...
2073934983089169792	300.98165	39.17015	18.185	1.874	K4.7	N	N	3.158	0.458	...	...	...	...	...	...	...	...
2047029589927135232	296.13283	33.66966	19.754	2.492	...	N	N	2.832	0.459	...	...	4	...	...	...	...	...
2043793005656747904	284.90412	32.29185	16.564	2.878	K5.4	N	N	2.921	0.331	...	...	...	...	...	...	...	...
2034834288030677888	296.49375	32.85779	18.621	2.787	K5.6	N	N	3.292	0.323	...	...	4	...	...	...	...	...
2034571917042958336	296.36557	31.78795	19.916	3.037	M2.8	N	N	3.043	0.422	...	...	...	...	...	...	...	...
2059326729841621376	299.81826	34.93828	19.774	2.585	M4.1	N	N	3.058	0.314	...	...	...	...	...	...	...	...
2107193835406075904	284.30484	45.51869	11.659	3.682	F9.5	Y	Y	3.098	0.01	9.647	0.965	4	...	...	10.5	0.95	7
2071977027747227904	297.71002	36.92586	17.333	4.669	M3.6	N	N	3.423	0.064	...	...	...	...	...	...	...	...

Table 5 *continued*

Table 5 *(continued)*

Gaia EDR3	α	δ	Gmag	$V_{\rm off}$	Spectral[a]	TESS[b]	Kepler[b]	π	σ_π	$P_{\rm rot}$	$\sigma_{P_{\rm rot}}$	$P_{\rm rot}$[c]	Li	$\sigma_{\rm li}$	RV	$\sigma_{\rm RV}$	RV[d]
	(J2016)	(J2016)	(mag)	(km/s)	Class			(mas)	(mas)	(days)	(days)	ref	(mÅ)	(mÅ)	(km/s)	(km/s)	ref
2039260268972721280	289.16773	30.23041	19.207	1.166	M5.3	N	N	3.091	0.215	...	...	...	...	...	...	...	...
2073364504023353088	298.04826	38.98652	19.039	3.044	M5.0	N	N	3.425	0.169	...	...	...	...	...	...	...	...
2102079010389058944	288.03639	40.67302	19.881	1.166	...	N	N	3.546	0.387	...	...	...	...	...	...	...	...
2042497055103777664	287.02825	30.89620	17.646	3.933	M2.9	N	N	2.983	0.083	...	...	...	...	...	...	...	...
2091578910568540544	281.59593	34.20902	19.78	3.733	WD	N	N	3.141	0.266	...	...	...	...	...	...	...	...
2128101869344360192	294.42091	46.09158	18.445	3.114	M4.0	N	Y	2.98	0.127	...	...	...	...	...	...	...	...
2049191362926461184	289.91842	33.41555	12.229	3.158	G8.3	N	N	3.47	0.009	3.313	0.331	4	...	...	-26.62	2.3	7
2073143158588073984	295.90599	38.58887	17.906	4.889	M3.4	N	N	2.723	0.095	...	...	...	...	...	...	...	...
2045513878791512576	293.56263	32.46788	20.162	4.392	M3.7	N	N	2.82	0.432	...	...	...	...	...	...	...	...
2038698001912176512	291.93730	30.23209	13.736	3.848	K3.0	N	N	3.108	0.013	7.742	0.774	4	...	...	-25.23	3.02	7
2047762483144548736	295.89967	35.48840	19.911	3.110	K5.7	N	N	2.757	0.441	...	...	...	...	...	...	...	...
2047903736027531264	296.62864	36.27227	17.539	2.940	K2.3	N	N	3.457	0.344	...	...	...	...	...	...	...	...
2045099770930205696	292.81519	32.02238	17.738	1.144	M0.6	N	N	2.833	0.41	...	...	...	...	...	...	...	...
2130431704422841600	287.32913	46.43624	13.559	3.741	K1.7	N	Y	3.003	0.018	26.038	0.393	1, 3	...	...	-2.88	0.03	8
2052954750711586048	291.22209	39.20029	18.115	4.897	M3.1	N	N	2.669	0.106	...	...	...	...	...	...	...	...
2047626418615459968	297.72901	35.42836	19.714	2.411	K3.6	N	N	2.82	0.449	...	...	...	...	...	...	...	...
2042356523773209728	284.22224	32.33175	17.993	0.157	M3.6	N	N	2.952	0.092	...	...	...	...	...	...	...	...
2074252982458281216	300.67055	40.36646	19.315	2.465	...	N	N	2.971	0.341	...	...	...	...	...	...	...	...
2075254534452611584	300.01273	41.67015	19.514	1.848	K7.7	N	N	3.239	0.434	...	...	...	...	...	...	...	...
2049628972855982208	290.08763	35.22950	20.16	1.492	M3.8	N	N	2.698	0.451	...	...	...	...	...	...	...	...
2046192140029849088	291.32173	33.08442	11.704	2.701	F9.9	N	N	2.763	0.029	...	...	...	...	...	-50.22	1.07	7
2043931234882955392	285.54094	32.87507	16.462	3.961	M1.5	N	N	3.362	0.042	...	...	...	...	...	...	...	...
2035235231805086080	298.94791	34.09861	12.738	3.245	G9.1	N	N	3.206	0.01	5.712	0.571	4	...	...	-24.7	4.42	7
2052874795604401536	290.06164	38.57568	20.27	0.951	M3.9	N	N	3.581	0.49	...	...	...	...	...	...	...	...
2075098575613530240	299.95832	41.21660	18.178	3.412	K5.3	N	N	3.271	0.499	...	...	...	...	...	...	...	...
2042737852451295360	285.83931	31.20725	15.431	3.991	K7.5	N	N	2.991	0.028	...	...	...	...	...	...	...	...
2077262105249669120	296.59125	43.02488	9.518	2.278	F5.9	Y	Y	3.398	0.057	1.806	0.014	1, 2, 3	...	...	7.98	1.43	7
2035501515450229760	298.19060	34.64302	18.508	2.603	K5.9	N	N	3.326	0.39	...	...	...	...	...	...	...	...
2106664244459171840	283.39062	44.58236	18.539	4.680	M4.1	N	N	2.951	0.127	...	...	...	...	...	...	...	...
2073973637768027136	301.21342	39.58126	18.398	2.628	K4.4	N	N	3.126	0.36	...	...	...	...	...	...	...	...
2034902045418615040	296.17342	33.13867	19.617	2.753	K3.6	N	N	2.852	0.394	...	...	...	...	...	...	...	...
2060327873840119552	300.52930	37.64385	19.074	4.257	M4.2	N	N	2.942	0.215	...	...	...	...	...	...	...	...
2074016243867293440	301.04997	39.64361	17.799	4.996	K5.2	N	N	3.0	0.459	...	...	...	...	...	...	...	...
2072467031971999872	300.22569	38.81877	19.453	1.976	M3.3	N	N	2.897	0.296	...	...	...	...	...	...	...	...
2073086568097576960	295.68673	38.29656	15.397	2.644	M0.1	N	N	3.52	0.022	...	...	...	...	...	...	...	...
2039208003508637824	289.38654	30.09435	16.157	4.825	M1.3	N	N	3.123	0.034	...	...	...	...	...	...	...	...
2034533949553936640	296.61255	31.96595	15.977	2.137	M3.0	N	N	3.2	0.04	...	...	...	...	...	...	...	...
2034947640765981696	296.54950	33.19053	18.368	2.392	K2.0	N	N	3.339	0.497	...	...	...	...	...	...	...	...
2127705053024405120	289.95108	46.26279	12.991	4.078	G7.5	N	Y	2.906	0.012	25.166	0.432	1, 3	...	...	-6.59	2.52	7

Table 5 *continued*

Table 5 *(continued)*

Gaia EDR3	α	δ	Gmag	$V_{\rm off}$	Spectral[a]	TESS[b]	Kepler[b]	π	σ_π	$P_{\rm rot}$	$\sigma_{P_{\rm rot}}$	$P_{\rm rot}$[c]	Li	$\sigma_{\rm li}$	RV	$\sigma_{\rm RV}$	RV[d]
	(J2016)	(J2016)	(mag)	(km/s)	Class			(mas)	(mas)	(days)	(days)	ref	(mÅ)	(mÅ)	(km/s)	(km/s)	ref
2127024214810722688	290.28077	44.97479	18.182	4.001	K0.9	N	N	3.406	0.45	...	...	...	...	...	...	...	...
2079362099431143808	297.72284	45.08701	13.172	2.713	K1.2	N	Y	3.096	0.01	12.856	0.105	1, 2, 3	...	...	-26.76	5.47	7
2038921585039935360	291.17173	30.65963	10.348	4.775	WD	N	N	3.269	0.469	...	...	...	...	...	...	...	...
2060071240955404032	301.10980	37.32475	17.65	2.105	K5.3	N	N	3.12	0.495	...	...	...	...	...	...	...	...
2076781854882648832	296.89440	41.04771	19.462	4.850	M4.2	N	N	3.46	0.236	...	...	...	...	...	...	...	...
2042439846138132352	286.97978	30.66187	18.639	2.926	M4.4	N	N	3.18	0.147	...	...	...	...	...	...	...	...
2042079859157623040	284.86412	31.73260	16.308	0.356	M1.9	N	N	3.223	0.04	...	...	...	...	...	...	...	...
2126559499348114432	292.13939	44.67274	8.444	1.765	A7.1	Y	Y	2.794	0.023	1.871	0.187	4	...	...	18.36	0.28	8
2034575662285071488	296.43974	31.95277	18.091	2.910	K5.3	N	N	3.221	0.383	...	...	...	...	...	...	...	...
2040073387874754944	289.58881	32.15377	12.685	2.635	G8.4	N	N	2.8	0.011	...	...	...	...	...	-14.95	3.11	7
2110520334817128320	279.70037	40.59862	14.161	4.352	K4.1	N	N	3.096	0.014	5.874	0.587	4	...	...	...	...	...
2050887020318420736	289.90342	36.53347	14.159	1.237	K3.0	N	N	2.673	0.013	...	...	...	...	...	...	...	...
2073991917153481728	300.75767	39.44785	19.724	4.351	M4.1	N	N	3.245	0.379	...	...	...	...	...	...	...	...
2075209557565365376	300.58122	41.45200	19.6	3.986	M4.1	N	N	2.984	0.3	...	...	...	...	...	...	...	...
2033232230870666496	294.51256	31.98844	18.789	4.417	M3.3	N	N	3.337	0.157	...	...	...	...	...	...	...	...
2051282054228339328	289.72565	37.77974	14.75	4.072	K4.9	N	N	2.664	0.017	...	...	...	...	...	-50.47	2.52	6
2104970382376984576	283.13187	42.83491	13.167	1.721	K1.9	N	Y	3.366	0.009	6.842	0.045	1, 3	...	...	-27.15	1.45	7
2127811293335040256	290.07305	46.65657	17.335	3.753	M2.5	N	N	2.953	0.055	...	...	...	...	...	...	...	...
2051391008967184000	292.43279	35.75986	19.135	2.113	K1.7	N	N	2.69	0.355	...	...	...	...	...	...	...	...
2052331568144316672	292.90456	38.78222	18.883	4.456	M4.5	N	N	3.576	0.168	...	...	...	...	...	...	...	...
2076162146945730176	295.40360	38.85625	15.776	2.174	M2.2	Y	Y	3.532	0.03	44.424	0.53	1, 3	...	...	...	...	...
2039196428587083520	289.49300	30.05919	13.801	4.898	M0.2	N	N	3.038	0.475	...	...	...	...	...	...	...	...
2033140490365517568	295.27212	31.35036	11.517	1.224	F9.1	N	N	3.229	0.013	2.254	0.225	4	101.0	16.0	-27.15	0.06	5
2058528935397195520	299.77801	34.40480	19.794	4.567	M1.2	N	N	3.109	0.485	...	...	...	...	...	...	...	...
2126719680147408896	292.65811	45.43596	18.778	4.482	M3.9	N	N	2.842	0.148	...	...	...	...	...	...	...	...
2043131271455838208	289.45557	32.68960	14.47	3.063	M0.2	N	N	3.448	0.221	...	...	...	...	...	...	...	...
2032907393921661824	294.82731	30.75338	19.076	0.455	K3.1	N	N	3.07	0.474	...	...	...	...	...	...	...	...
2035134901379274112	297.78203	33.21726	11.427	1.703	F7.4	N	N	2.923	0.016	...	...	...	...	...	...	...	...
2059866216423717632	300.81695	36.26046	16.789	3.205	M2.3	N	N	3.046	0.056	...	...	...	...	...	...	...	...
2103900042167615872	286.24914	41.47616	14.014	4.802	K3.0	N	N	2.716	0.014	9.45	0.945	4	...	...	-34.07	9.07	6
2090796062590610432	282.64946	34.20038	16.727	4.069	M2.3	N	N	2.884	0.045	...	...	...	...	...	...	...	...
2050768955955966848	288.20157	36.43343	19.012	3.386	M4.4	N	N	3.565	0.179	...	...	...	...	...	...	...	...
2032985218712943488	295.87731	31.21408	14.067	0.799	K3.4	N	N	3.132	0.016	...	...	...	...	...	...	...	...
2126090866877971456	290.88050	43.55913	15.512	3.696	K7.6	N	Y	2.737	0.026	16.461	0.163	1, 2, 3	...	...	...	...	...
2060258845151434880	301.06594	37.32113	18.656	4.652	K4.9	N	N	3.011	0.435	...	...	...	...	...	...	...	...
2100313057280470784	285.30264	39.58430	17.723	4.558	M3.0	N	N	2.709	0.075	...	...	...	...	...	...	...	...
2073415292031904256	297.80110	39.12328	16.71	3.034	M1.1	N	N	2.764	0.061	...	...	...	...	...	...	...	...
2034695401634216064	297.65084	32.71316	18.987	1.950	K5.6	N	N	3.226	0.438	...	...	...	...	...	...	...	...
2047126346964378368	295.78106	34.39312	20.13	2.788	M3.2	N	N	2.773	0.424	...	...	...	...	...	...	...	...

Table 5 *continued*

Table 5 *(continued)*

Gaia EDR3	α	δ	Gmag	$V_{\rm off}$	Spectral[a]	TESS[b]	Kepler[b]	π	σ_π	$P_{\rm rot}$	$\sigma_{P_{\rm rot}}$	$P_{\rm rot}$[c]	Li	$\sigma_{\rm li}$	RV	$\sigma_{\rm RV}$	RV[d]
	(J2016)	(J2016)	(mag)	(km/s)	Class			(mas)	(mas)	(days)	(days)	ref	(mÅ)	(mÅ)	(km/s)	(km/s)	ref
2072360649903759360	300.20284	38.00141	18.984	4.593	K5.6	N	N	2.888	0.332	...	...	...	...	...	...	...	...
2074026861029362688	301.01105	39.81659	17.014	4.478	K3.2	N	N	2.968	0.426	...	...	...	...	...	...	...	...
2104521158860140160	283.11639	41.63353	17.742	0.281	M1.9	N	N	2.795	0.092	...	...	...	...	...	...	...	...
2042689194762106496	285.94421	31.09083	19.557	3.131	M3.6	N	N	3.219	0.302	...	...	...	...	...	...	...	...
2033107023985549824	294.68365	30.97360	19.515	3.067	K3.2	N	N	2.971	0.441	...	...	...	...	...	...	...	...
2034732720649313664	297.05013	32.78381	18.939	0.829	K5.6	N	N	2.905	0.406	...	...	...	...	...	...	...	...
2078641300848295040	297.73818	43.29115	19.645	1.919	M4.4	N	N	2.852	0.283	...	...	...	...	...	...	...	...
2049583167026993280	289.39887	34.57021	17.344	4.447	M4.1	N	N	3.533	0.061	...	...	...	...	...	...	...	...
2032983122768999424	296.06274	31.22507	10.846	4.026	F4.9	Y	N	3.101	0.066	0.371	0.037	4	...	...	...	...	...
2091553213783598976	282.15768	34.11114	18.05	3.163	M3.1	N	N	3.274	0.097	...	...	...	...	...	...	...	...
2032642549032668544	293.14288	30.20536	17.188	1.789	K2.0	N	N	3.128	0.297	...	...	...	...	...	...	...	...
2093450279359321344	282.02727	36.11518	19.452	2.647	M3.9	N	N	3.369	0.254	...	...	...	...	...	...	...	...
2046951284120062336	295.67801	33.69973	18.484	4.593	K4.5	N	N	3.421	0.397	...	...	...	...	...	...	...	...
2045029818815071872	291.78388	31.69152	16.596	4.455	K5.2	N	N	2.823	0.264	...	...	...	...	...	...	...	...
2077505402251102080	294.46636	41.66853	16.456	2.364	M0.8	N	N	2.714	0.039	...	...	...	...	...	...	...	...
2050543762233656704	289.03850	36.32766	20.267	0.247	M3.4	N	N	3.575	0.477	...	...	...	...	...	...	...	...
2059489801154960768	299.82401	35.56417	19.384	3.866	M1.2	N	N	2.924	0.422	...	...	...	...	...	...	...	...
2073986106064541952	300.53830	39.36156	19.791	1.867	K4.5	N	N	3.29	0.469	...	...	...	...	...	...	...	...
2042027945895281664	285.02263	31.59402	16.953	0.661	M3.6	N	N	3.242	0.063	...	...	...	...	...	...	...	...
2035236503121083520	298.74363	34.05011	20.3	2.246	M3.0	N	N	3.271	0.497	...	...	...	...	...	...	...	...
2045111869868403968	292.77362	32.06682	17.81	3.733	M4.3	N	N	3.402	0.083	...	...	...	...	...	...	...	...
2035264570697242880	298.97836	34.27874	16.378	2.028	M3.1	N	N	3.268	0.039	...	...	...	...	...	...	...	...
2044265619555725824	287.77605	34.12463	19.981	2.242	M4.0	N	N	3.505	0.425	...	...	...	...	...	...	...	...
2033140490333678464	295.27257	31.35020	14.776	0.558	...	N	N	3.25	0.041	...	...	...	...	...	...	...	...
2092240374191428224	283.71603	33.98094	7.67	4.454	B8.9	Y	N	2.831	0.031	...	...	...	...	...	...	...	...
2072223627593305984	299.45079	37.33273	17.372	2.446	M3.0	N	N	2.841	0.066	...	...	...	...	...	...	...	...
2035443108234760576	297.12787	34.32959	17.941	2.710	K3.1	N	N	3.397	0.34	...	...	...	...	...	...	...	...
2125747647451556736	292.62719	42.57975	20.242	2.935	M1.5	N	N	2.712	0.418	...	...	...	...	...	...	...	...
2079111758680537600	298.44946	44.78114	19.76	4.584	M4.2	N	N	3.132	0.326	...	...	...	...	...	...	...	...
2051929632221539200	292.74556	38.29484	17.726	3.015	M3.0	N	N	2.664	0.073	...	...	...	...	...	...	...	...
2077754102333782784	294.19030	42.56506	19.26	3.675	M4.3	N	N	3.504	0.235	...	...	...	...	...	...	...	...
2039634820177170304	289.89537	30.83658	19.868	4.152	M3.9	N	N	2.881	0.4	...	...	...	...	...	...	...	...
2103392067795211136	285.10996	40.59768	17.84	2.234	M3.6	N	N	2.717	0.091	...	...	...	...	...	...	...	...
2042534060544124928	287.76004	31.02070	20.292	3.361	M0.9	N	N	3.306	0.444	...	...	...	...	...	...	...	...
2047068382102503680	296.25543	34.10309	18.772	1.136	K7.0	N	N	2.791	0.354	...	...	...	...	...	...	...	...
2091529780441954048	281.97371	34.04269	13.002	4.032	K0.0	N	N	2.933	0.017	6.244	0.624	4	...	...	...	...	...
2046143727160895744	289.99375	32.99228	16.931	4.980	M2.8	N	N	3.478	0.063	...	...	...	...	...	...	...	...
2076412354557634048	296.02233	40.44533	19.668	4.903	...	N	N	3.515	0.429	...	...	...	...	...	...	...	...
2106386136737753984	285.70782	45.16344	19.427	2.521	M3.9	N	N	3.34	0.248	...	...	...	...	...	...	...	...

Table 5 *continued*

Table 5 *(continued)*

Gaia EDR3	α	δ	Gmag	$V_{\rm off}$	Spectral[a]	TESS[b]	Kepler[b]	π	σ_π	$P_{\rm rot}$	$\sigma_{P_{\rm rot}}$	$P_{\rm rot}$[c]	Li	$\sigma_{\rm li}$	RV	$\sigma_{\rm RV}$	RV[d]
	(J2016)	(J2016)	(mag)	(km/s)	Class			(mas)	(mas)	(days)	(days)	ref	(mÅ)	(mÅ)	(km/s)	(km/s)	ref
2049003041495144320	295.19249	37.37874	17.453	4.949	M3.2	N	N	2.698	0.204	...	...	...	...	...	...	...	...
2076570546796133632	294.35533	40.70323	16.568	3.668	M2.7	N	N	3.55	0.041	...	...	...	...	...	...	...	...
2039507452931612800	288.08062	30.61740	18.049	4.070	M3.7	N	N	2.929	0.099	...	...	...	...	...	...	...	...
2092351901603818752	284.10039	34.53254	20.079	4.076	M3.7	N	N	3.425	0.385	...	...	...	...	...	...	...	...
2073018741978769920	296.89069	38.80418	18.529	1.319	M3.9	N	N	2.73	0.251	...	...	...	...	...	...	...	...
2032919660346450048	295.34835	30.81735	17.443	4.243	K5.2	N	N	3.125	0.366	...	...	...	...	...	...	...	...
2034846069081417728	296.38788	32.95123	12.394	3.207	G0.3	N	N	2.85	0.011	...	...	4	...	...	...	...	...
2105388742253587456	281.87633	44.37533	19.1	2.701	M4.1	N	N	3.048	0.182	...	...	...	...	...	...	...	...
2032931819344467456	295.46585	31.04501	18.682	3.300	K2.6	N	N	3.191	0.245	...	...	...	...	...	...	...	...
2059839244020998656	300.88773	35.88355	19.02	3.937	M3.8	N	N	3.114	0.179	...	...	...	...	...	...	...	...
2059300036635759232	299.62157	34.76655	18.317	1.282	M2.4	N	N	2.943	0.484	...	...	...	...	...	...	...	...
2093127744494585600	282.51934	34.84625	18.773	3.695	M3.5	N	N	2.846	0.139	...	...	...	...	...	...	...	...
2092334137618691200	283.20048	34.67695	17.779	3.787	M3.3	N	N	2.819	0.077	...	...	...	...	...	...	...	...
2102262590177839232	289.20893	42.00130	19.178	2.667	M3.6	N	N	2.69	0.191	...	...	...	...	...	...	...	...
2034849883009060480	296.24925	32.97883	11.934	4.174	F8.9	N	N	2.84	0.013	...	...	...	...	...	...	...	...
2052841367874931584	290.89364	38.54935	19.934	3.454	M2.7	N	N	3.605	0.426	...	...	...	...	...	...	...	...
2052385036194166016	294.01015	38.97397	14.577	4.758	K4.9	N	N	2.675	0.015	...	...	4	...	...	...	...	...
2042007467491387776	285.41986	31.41662	17.38	4.217	M3.5	N	N	3.262	0.072	...	...	...	...	...	...	...	...
2096748818540009984	280.79590	37.05196	18.738	4.572	M3.6	N	N	2.88	0.134	...	...	...	...	...	...	...	...
2101632986631893120	291.78376	41.04022	18.183	3.832	M3.5	N	N	2.673	0.118	...	...	...	...	...	...	...	...
2053562574485095552	292.84695	41.06672	18.202	3.457	M3.4	N	N	2.68	0.112	...	...	...	...	...	...	...	...
2042246710046921856	284.00298	31.53735	19.679	4.426	M4.2	N	N	3.062	0.34	...	...	...	...	...	...	...	...
2073719616218643584	296.75652	40.19203	17.61	2.933	K5.0	N	N	2.731	0.308	...	...	...	...	...	...	...	...
2042719568769267712	286.50399	31.37024	19.407	3.058	K4.8	N	N	2.888	0.45	...	...	...	...	...	...	...	...
2045591634897440768	293.22561	33.05746	17.616	1.957	M1.9	N	N	2.761	0.324	...	...	...	...	...	...	...	...
2032524179759317632	294.60533	30.50159	19.755	2.012	K3.4	N	N	3.04	0.48	...	...	...	...	...	...	...	...
2033174747029548032	294.46367	31.34423	16.632	3.046	K4.7	N	N	2.892	0.345	...	...	...	...	...	...	...	...
2033793462836481024	297.32633	31.88177	19.768	4.100	M0.3	N	N	3.029	0.434	...	...	...	...	...	...	...	...
2072722530993534720	299.46824	39.40104	16.216	4.928	M2.5	N	N	2.823	0.067	1.296	0.13	4	...	...	...	...	...
2059651566802258944	298.57762	35.81934	17.419	4.168	K4.2	N	N	2.82	0.463	...	...	...	...	...	...	...	...
2060058940186416000	301.42912	37.16230	19.948	4.205	K5.7	N	N	3.108	0.475	...	...	...	...	...	...	...	...
2034473751304792960	299.48808	33.76045	19.776	1.911	M0.5	N	N	3.155	0.41	...	...	...	...	...	...	...	...
2042095875095349120	284.80311	31.92339	17.441	3.498	M2.9	N	N	2.907	0.196	...	...	...	...	...	...	...	...

Table 5 *continued*

Table 5 *(continued)*

Gaia EDR3	α	δ	Gmag	V_{off}	Spectral[a]	TESS[b]	Kepler[b]	π	σ_π	P_{rot}	$\sigma_{P_{\mathrm{rot}}}$	P_{rot}[c]	Li	σ_{li}	RV	σ_{RV}	RV[d]
	(J2016)	(J2016)	(mag)	(km/s)	Class			(mas)	(mas)	(days)	(days)	ref	(mÅ)	(mÅ)	(km/s)	(km/s)	ref

Note—Table 5 is truncated. The full version will be available online.

[a] Spectral types are assigned based on the star's $B_P - R_P$ color and the table from Pecaut & Mamajek (2013).

[b] Indicates if the target had a light curve in *TESS* or *Kepler* of sufficient quality for running the Notch transit-search pipeline.

[c] Key for rotation period references: 1 = (McQuillan et al. 2013, 2014), 2 = (Nielsen et al. 2013), 3 = Santos et al. (2021, 2019), 4 = This work

[d] Key for radial velocity references: 5 = Coude, 6 = LAMOSTDR5 (Luo et al. 2019), 7 = Gaia DR2 (Katz et al. 2019), 8 = APOGEE DR16 (Jönsson et al. 2020), 9 = CKS (Petigura et al. 2022)